MODELING THE BIODEGRADABILITY AND PHYSICOCHEMICAL PROPERTIES OF POLYCYCLIC AROMATIC HYDROCARBONS

A Dissertation

by

PETROS DIMITRIOU-CHRISTIDIS

Submitted to the Office of Graduate Studies of
Texas A&M University
in partial fulfillment of the requirements for the degree of

DOCTOR OF PHILOSOPHY

August 2005

Major Subject: Civil Engineering

MODELING THE BIODEGRADABILITY AND PHYSICOCHEMICAL PROPERTIES OF POLYCYCLIC AROMATIC HYDROCARBONS

A Dissertation

by

PETROS DIMITRIOU-CHRISTIDIS

Submitted to the Office of Graduate Studies of
Texas A&M University
in partial fulfillment of the requirements for the degree of

DOCTOR OF PHILOSOPHY

Approved by:

Chair of Committee,	Robin L. Autenrieth
Committee Members,	Bill Batchelor
	Kirby C. Donnelly
	Thomas J. McDonald
Head of Department,	David V. Rosowsky

August 2005

Major Subject: Civil Engineering

ABSTRACT

Modeling the Biodegradability and Physicochemical Properties
of Polycyclic Aromatic Hydrocarbons. (August 2005)
Petros Dimitriou-Christidis, B.S., University of the Aegean;
M.S., University of California, Berkeley
Chair of Advisory Committee: Dr. Robin L. Autenrieth

The biodegradability and physicochemical properties of unsubstituted and methylated polycyclic aromatic hydrocarbons (PAHs) were investigated. The focus was on the development of models expressing the influence of molecular structure and properties on observed behavior.

Linear free energy relationships (LFERs) were developed for the estimation of aqueous solubilities, octanol/water partition coefficients, and vapor pressures as functions of chromatographic retention time. LFERs were tested in the estimation of physicochemical properties for twenty methylated naphthalenes containing up to four methyl substituents. It was determined that LFERs can accurately estimate physicochemical properties for methylated naphthalenes.

Twenty unsubstituted and methylated PAHs containing up to four aromatic rings were biodegraded individually by *Sphingomonas paucimobilis* strain EPA505, and Monod-type kinetic coefficients were estimated for each PAH using the integral method. Estimated extant kinetic parameters included the maximal specific biodegradation rate, the affinity coefficient, and the inhibition coefficient. The generic Andrews model adequately simulated kinetic data. The ability of PAHs to serve as sole energy and carbon sources was also evaluated.

Quantitative structure-biodegradability relationships (QSBRs) were developed based on the estimates of the kinetic and growth parameters. A genetic algorithm was used for QSBR development. Statistical analysis and validation demonstrated the

predictive value of the QSBRs. Spatial and topological molecular descriptors were essential in explaining biodegradability. Mechanistic interpretation of the kinetic data and the QSBRs provided evidence that simple or facilitated diffusion through the cell membranes is the rate-determining step in PAH biodegradation by strain EPA505.

A kinetic experiment was conducted to investigate biodegradation of PAH mixtures by strain EPA505. The investigation focused on 2-methylphenanthrene, fluoranthene, and pyrene, and their mixtures. Integrated material balance equations describing different interaction types were fitted to the depletion data and evaluated on a statistical and probabilistic basis. Mixture degradation was most adequately described by a pure competitive interaction model with mutual substrate exclusivity, a fully predictive model utilizing parameters estimated in the sole-PAH experiments only.

The models developed in this research provide insight into how molecular structure and properties influence physicochemical properties and biodegradability of PAHs. The models have considerable predictive value and could reduce the need for laboratory testing.

DEDICATION

To Makis, Maryio, Evi, and Hannah

ACKNOWLEDGEMENTS

I thank my committee members: Dr. Robin Autenrieth, my committee chair, for her guidance, advice, criticism, encouragement, and generosity; Dr. Tom McDonald for his support and counsel, and for being so readily available; and Drs. Bill Batchelor and K.C. Donnelly for their suggestions, availability, and commitment.

I thank the Superfund Basic Research Program of Texas A&M University and the NIEHS, the State Scholarship Foundation of Greece, and the Department of Civil Engineering of Texas A&M University for their financial support, and Dr. Robin Autenrieth for ensuring that support was always available.

I thank Dr. Tom McDonald, Donnie Golden, Dr. Cord Harris, Hannah Wilner, Sarah Sterman, Anthony Skach, and Anu Desai for their help in the laboratory; also, Dr. Lisa Perez of Texas A&M University and Dr. Michael Abraham of University College London for their help and suggestions on QSAR.

I thank the fellow students and co-workers of the 128 group for their help, support, and friendship.

A special thanks goes to my family for their love, support, encouragement, and patience; and to Hannah Wilner for her significant contribution, direct and indirect.

TABLE OF CONTENTS

Page

CHAPTER Page

CHAPTER Page

LIST OF FIGURES

LIST OF TABLES

CHAPTER I
INTRODUCTION

STATEMENT OF PURPOSE

Polycyclic aromatic hydrocarbons (PAHs) are ubiquitous pollutants of significant public health and environmental concern. The health effect of particular concern associated with PAHs is cancer. Several PAHs exhibit acute and chronic toxicity, microbial recalcitrance, bioaccumulation potential, and low removal efficiency in traditional detoxification processes (Herbes and Schwall, 1978). PAHs rank number 8 on the 2003 CERCLA Priority List of Hazardous Substances (ATSDR, 2003). PAHs are often present as complex mixtures characterized by a broad range of properties and behavior.

The risk assessment/management methodology provides a quantitative framework for the calculation and reduction of risk posed to humans and ecosystems by pollutants. Knowledge of physicochemical behavior, bioavailability, and fate of PAHs is necessary for accurate exposure assessment and implementation of effective detoxification strategies for wastes and contaminated sites. Considerable uncertainties are introduced to risk assessment/management involving complex mixtures of PAHs because a very limited number of individual PAHs are fully characterized for their physical, chemical, and biological activities. In addition, chemical interactions and their effects on the activities of the compounds are largely unknown.

This research focuses on physicochemical properties and biodegradability of PAHs. Physicochemical properties determine environmental partitioning and bioavailability of organic pollutants; biodegradation is the primary mechanism of PAH removal from the environment (NRC, 2003) and a valuable clean-up technology. Due to the enormous number and diversity of PAHs, it is impossible to experimentally test every compound for properties and behavior. Alternatively, models can be trained on experimental data, which can provide quantitative information on the physicochemical

---

This thesis follows the style of *Chemosphere*.

properties and biodegradability. Models include linear free energy relationships (LFERs), quantitative structure-activity relationships (QSARs), and interaction kinetic models. The importance of these models is twofold: (i) they explain properties and behavior on a quantitative and mechanistic basis; and (ii) they predict properties and behavior without requiring full laboratory testing. These and other similar models can be integrated into the risk assessment/management methodology for a more accurate evaluation of exposures and provide guidance for appropriate detoxification strategies. The research approach followed in this dissertation is an adaptation of the risk assessment/management paradigm proposed by the National Research Council recommending the development of extrapolation methods based on experimental data and development of regulatory options for risk management (NRC, 1983).

Table 1.1
PAHs used in the four experiments discussed in this dissertation. PAHs included parent compounds, as well as methylated versions of naphthalene, fluorene, phenanthrene, anthracene, and pyrene - a total of 40 PAHs.

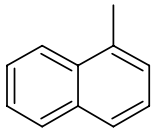 naphthalene and methylnaphthalenes	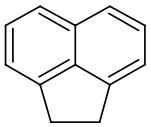 acenaphthene	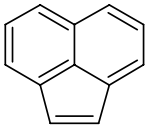 acenaphthylene	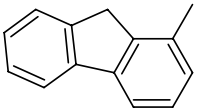 fluorene and methylfluorenes
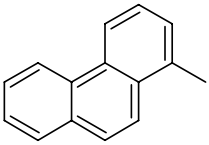 phenanthrene and methylphenanthrenes	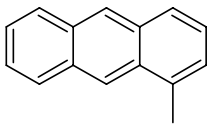 anthracene and methylanthracenes	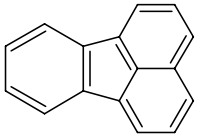 fluoranthene	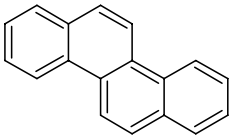 chrysene
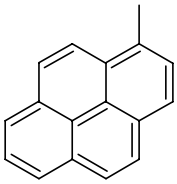 pyrene and methylpyrenes	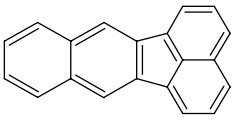 benzo[k]fluoranthene	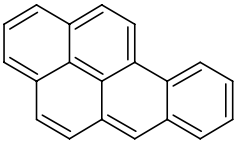 benzo[a]pyrene	

BACKGROUND

PAHs

PAHs constitute an enormously large and diverse class of organic compounds (Harvey, 1997). It is believed that PAHs are the most abundant organic compounds in the universe (Allamandola, et al., 1987) and that they may have played a role in biogenesis and evolution. For example, UV photolysis of naphthalene in ice produces 1,4-naphthoquinone, which is a precursor to key biomolecules (Bernstein et al., 2002). PAHs are composed of two or more fused rings (Table 1.1). PAHs can be classified as alternant, containing only six-membered rings, and nonalternant, with six-membered rings and rings with an odd number of members. Aromatic rings are planar or nearly planar circular configurations of sp^2 hybridized atoms with overlapping p-orbitals that form π-molecular orbitals occupied by $4n + 2$ electrons. PAHs with 24 or more aromatic ring carbons are named large PAHs and are characterized by significantly different properties and behavior than smaller PAHs (Fetzer, 2000). PAHs are thermodynamically and chemically stable, which distinguishes them from aliphatic hydrocarbons.

PAHs are released into the environment by a number of sources, anthropogenic and natural. Creosote, with a PAH mass fraction of 85% (Mueller et al., 1989), is an obvious source. Coal tar creosote is the most common wood preservative in the United States. Various kinds of creosote are used for road paving, roofing, coking, and aluminum smelting (ATSDR, 1997). Petroleum is another significant source. Petroleum is a complex mixture containing thousands of hydrocarbons including PAHs. It is estimated that the annual global input of petroleum hydrocarbons to the environment is 1.7 – 8.8 million metric tons with anthropogenic sources responsible for the majority of it (NRC, 2003). PAHs are emitted into the atmosphere by both natural and anthropogenic processes. Examples include combustion of fossil fuels, forest fires, and volcanic activity. It is believed that anthropogenic sources are predominant. For example, it was found that concentration patterns in soil and sediments are closely related to the degree of urbanization (U.S. EPA, 2000). The type of source and, more specifically, the temperature of generation determines the composition of a PAH

mixture. Pyrogenic mixtures generated at low temperatures consist primarily of alkylated PAHs, while those generated at high temperatures consist of unsubstituted PAHs (Harvey, 1997). Petroleum contains mostly methylated PAHs (Youngblood and Blumer, 1975). The composition of a mixture is also affected by the maturity and the degree of degradation that a mixture undergoes.

Several PAHs have the potential to cause harmful effects to humans and ecosystems. Detailed information on the toxicity of PAHs can be found in a number of sources including IARC (1987), ATSDR, (1995), WHO (1998), and U.S. EPA (2005), and the references therein. The health effect of particular concern associated with PAHs is cancer. PAHs have caused tumors in laboratory animals via different routes of exposure, i.e., inhalation, ingestion, and dermal contact (ATSDR, 1995). Studies on humans showed that individuals exposed to PAHs via inhalation or dermal contact for extended periods develop cancer (WHO, 1998). Mutagenicity and carcinogenicity of a number of PAHs have been associated to the degree of nonplanarity, which can be caused by methylation or steric interference between rings (Dabestani and Ivanov, 1999). Mutagenicity is expressed through covalent binding of a PAH or its metabolites to DNA, potentially leading to tumor initiation.

This research focuses on the list of 17 nonheterocyclic PAHs considered by the ATSDR (1995) and the similar list of 16 PAHs regulated by the U.S. EPA as priority pollutants (Hodgeson et al., 1990). As explained in the Toxicological Profile by the ATSDR (1995), these compounds were chosen based on their toxicity, occurrence in contaminated sites, potential for exposure, and extent of available information. In addition to these compounds, methylated homologues of naphthalene, fluorene, phenanthrene, anthracene, and pyrene were used in this research based on their abundance in petroleum and their commercial availability as pure compounds. Jointly, 40 PAHs were involved in the four experimental chapters (Chapters II through V) of this research, including 29 methylated PAHs.

Physicochemical properties

The distribution and partitioning of organic pollutants in the environment (air,

water, soil/sediment, and biota) is determined by the physicochemical properties of the pollutants. Physicochemical properties are widely used in transport and fate modeling, as well as risk assessment. For example, the octanol/water partition coefficient, an indicator of hydrophobicity, is used to estimate bioconcentration factors (Veith et al., 1979). Similarly, physicochemical properties determine the bioavailability of PAHs to target populations or microorganisms. Also, the rates of biodegradation of organic substrates in aqueous suspensions are affected by the aqueous solubility of the substrates (Leahy and Colwell, 1990). Other significant physicochemical properties include the Henry's law constants and vapor pressure, which determine the potential for air pollution and atmospheric transport. Generally, PAHs are hydrophobic, tending to sorb to solid phases and are characterized by low volatility. Values of physicochemical properties of PAHs are available from a number of individual studies or compilations including Howard and Meylan (1997) and its on-line database version (SRC, 2005), Mackay et al. (1992), Karcher (1985), LaGrega et al. (2001), and WHO (1998). However, information is generally limited to the most common PAHs, as identified by the ATSDR and U.S. EPA, while it is scarce for substituted versions and high-molecular-weight PAHs. Physicochemical properties can be measured directly using pure compounds and analytical methods dictated by the definition of a property. However, for hydrophobic compounds, some limitations, e.g., low aqueous phase concentrations and slow equilibration between phases, are thought to be responsible for widespread discrepancies in reported values (Karickhoff and Brown, 1979). Indeed, a literature review, e.g., as presented by Mackay et al. (1992), reveals wide ranges, often of 1-2 orders of magnitude, in reported values. This research investigates the accuracy of indirect methods requiring less experimentation and allowing for prediction of physicochemical properties.

Biodegradation

Biodegradation greatly influences the persistence, fate, and toxicity potential of most organic pollutants. Biodegradation is a complex process involving action of microbial consortia on multi-component substrates. Biodegradation by natural microbial

populations is one of the main mechanisms by which PAHs are eliminated from the environment (NRC, 2003). Also, biodegradation is an important clean-up technology applicable to organic wastes and contaminated sites. Better knowledge of the kinetics and extent to which PAHs are biodegraded, as well as the ecology of PAH-degrading microorganisms, could enhance our understanding of the environmental fate of PAHs and lead to the implementation of effective detoxification strategies.

Many microorganisms are capable of degrading PAHs as energy and carbon sources or cometabolically (Atlas, 1995). A step necessary in all catabolic pathways is the cleavage of aromatic rings. Aerobic catabolism of PAHs by bacteria begins with the oxygenation of an aromatic ring or alkyl-side chain. In most cases these reactions are catalyzed by dioxygenases (Gibson and Parales, 2000). Dioxygenases are versatile in catalyzing a wide range of catabolic reactions and are utilized by a variety of microorganisms, as presented in the University of Minnesota Biocatalysis /Biodegradation Database (UMBBD, 2005).

While biochemical reactions are crucial, biodegradation of PAHs in nature or engineered systems is also governed by a number of environmental conditions including the presence of electron acceptors and microorganisms capable of degrading PAHs. Anaerobic biodegradation of PAHs is possible (Coates et al., 1997), but uncommon and slow compared to aerobic degradation. Under aerobic conditions oxygen acts as direct reactant in ring destabilization and as terminal electron acceptor. This research addresses aerobic degradation only. Certain microorganisms are particularly competent in degrading PAHs. Members of the genus *Sphingomonas* have been recognized for their ability to degrade a wide range of aromatic hydrocarbons including certain five-ring PAHs (Mueller et al., 1990). A phylogenetic comparison of PAH-degrading bacteria from geographically diverse soils indicated that sphingomonads are common in creosote- and fuel oil-contaminated soils (Mueller et al., 1997). Despite their unique abilities and ubiquity, sphingomonads have been barely characterized in terms of biodegradation kinetics. The kinetics of PAH biodegradation by *Sphingomonas*

paucimobilis strain EPA505 and its ability to utilize individual PAHs as sole energy and carbon sources are investigated in this research.

Microbial kinetics relate the rates of substrate uptake to the rates of microbial growth. Microbial kinetics are important in determining the persistence of PAHs in the environment and the extent of their removal in engineered systems. Despite their importance, a review of the literature reveals the following inadequacies: (i) testing often excludes alkylated PAHs; (ii) kinetic measurements are often limited to the calculation of simplistic and system-specific quantities, e.g., percent degradation or first-order degradation coefficients; and (iii) measurement of kinetics in complex mixtures, e.g., creosote or petroleum, neglects interaction effects, whereas mathematical modeling of mixture degradation is very limited for specified mixtures. In addition, kinetic experiments are often performed under undefined kinetic conditions (Kovárová-Kovar and Egli, 1998) or do not account for other potential rate-determining processes, e.g., bioavailability and mass transfer from solid phases, resulting in wide ranges in reported kinetic parameter values (for example, see Aronson et al., 1998). This research addresses the above issues by: testing degradation of both parent and methylated PAHs; applying standard microbial kinetic models, e.g., the Monod and Andrews models and calculating the uncertainties in the estimates of the kinetic coefficients; applying mechanistic interaction models, e.g., competitive interaction model, among others; conducting kinetic experiments under extant conditions (Grady et al., 1996); and eliminating or accounting for bioavailability constraints influencing biodegradation kinetics. This approach has resulted in a consistent and reproducible set of biokinetic coefficients reflecting the effects of substrate molecular structure on the rates of PAH biotransformation and allowing for the development of quantitative structure biodegradability relationships (QSBRs). In addition, use of standard interaction models and well-defined PAH mixtures can allow for a mechanistic and quantitative explanation of mixture effects.

LFERs and QSARs

Due to the existence of a large number of PAHs it is impossible to experimentally test properties and behavior for all PAHs of concern. Thus, developing predictive models would be very beneficial. LFERs and QSARs can predict physicochemical properties and biological activities of PAHs based on limited experimental data. They can also offer insight into the molecular characteristics, properties, and processes that are responsible for the observed properties and behavior of PAHs.

An LFER is a relationship describing the change in the shapes of the potential energy surfaces of a reaction as a function of the change in a similar standard process (Williams, 2003). In terms of the Gibbs free energy, this relationship can be written as:

$$\Delta G = a\Delta G_s + b \tag{1.1}$$

where ΔG is the Gibbs free energy change for the process of interest, ΔG_s is the Gibbs free energy change for a similar standard process, and a and b are linear regression coefficients. The slope a is also known as the similarity coefficient. Note that the relationship refers to a single compound but the regression can be applicable to more than one homologue. Given the relationship between ΔG of a reaction and the equilibrium constant, K, Eq. 1.1 can be written as follows:

$$\log K = a_1 \log K_s + b_1 \tag{1.2}$$

where K_s is the equilibrium constant of the standard process. Other classes of LFERs include (Williams, 2003):

$$\log k = a_2 \log K_s + b_2 \tag{1.3}$$

$$\log k = a_3 \log k_s + b_3 \tag{1.4}$$

where k is a rate coefficient and k_s is the rate coefficient for a standard process. LFERs are routinely used for the estimation of physicochemical properties by establishing relationships between the retention time in a chromatographic column and a physicochemical property based on a set of reference compounds. The suitability of high-pressure liquid chromatography (HPLC) for the estimation of physicochemical properties involving liquid phases, e.g., the octanol/water partition coefficient and

solubility, has been demonstrated (Veith and Morris, 1978; Finizio et al., 1997). Gas chromatography (GC) has been used to estimate physicochemical properties for the gaseous phase, e.g., the vapor pressure (Fischer et al., 1992; Kurz and Ballschmiter, 1999). The same approach is tested in this research in estimating physicochemical properties for methylated naphthalenes. LFERs are closely related to QSARs. The Hammett equation, of the form of Eq. 1.2, provided the mechanistic basis for the development of the QSAR methodology by Hansch and Fujita (1964).

A QSAR is a multivariate relationship between a set of *n* 2D and 3D molecular descriptors, *D*, and a biological activity, *BA*. In most cases QSARs are linear:

$$BA = d_0 + d_1D_1 + d_2D_2 + \ldots + d_nD_n \qquad (1.5)$$

where coefficients *d* represent multiple regression coefficients. Molecular descriptors quantify the structure, properties, and other features of molecules. The general QSAR theory introduced three major descriptor types: electronic, steric, and hydrophobic (Hansch and Leo, 1995). Biological activity pertains to an aspect of a specific and uniform biological function that is quantifiable and related to ΔG, i.e., standard equilibrium constants and rate constants. Examples include Michaelis-Menten coefficients, inhibition coefficients, biochemical equilibrium constants, and toxicity coefficients. QSAR development is based on a set of reference compounds, or a training set, with accurately known biological activity values. The essence of QSAR is the prediction of biological activity based on the values of molecular descriptors, allowing quantitative and mechanistic interpretation of the underlying biological process. Attempts to construct QSBRs have been made as early as 1966 (Alexander and Lustigman, 1966); however, QSBRs are scarce compared to other types of QSAR, e.g., for toxicity. No QSBRs could be found for PAHs in the literature; therefore, this research examines their feasibility.

RESEARCH OBJECTIVES

The overall goal of this research was to develop models describing physicochemical properties and biodegradability of PAHs. The specific objectives, corresponding to the four experimental chapters of this dissertation, were the following:

1. To develop and evaluate LFERs for the aqueous solubilities, octanol/water partition coefficients, and vapor pressures of methylated naphthalenes based on chromatographic retention data.
2. To measure extant biodegradation rate coefficients for individual unsubstituted and methylated PAHs in a consistent manner capturing the effects of substrate molecular structure on kinetics; to determine which of the PAHs can serve as sole energy and carbon sources.
3. To develop QSBRs for biodegradation rate and microbial growth coefficients and to evaluate the relationships on a statistical and mechanistic basis; to determine the most important molecular descriptors explaining kinetics and to identify the rate-limiting process in biodegradation.
4. To investigate biodegradation kinetics in binary and ternary mixtures of PAHs; to apply standard mechanistic models to kinetic data and to make inferences about receptor-ligand interactions based on model fit.

CHAPTER II
ESTIMATION OF SELECTED PHYSICOCHEMICAL PROPERTIES FOR METHYLATED NAPHTHALENES*

OVERVIEW

Liquid aqueous solubility, $S_{w,L}$, octanol/water partition coefficients, K_{ow}, liquid vapor pressure, $P_{v,L}$, and Henry's law constants, H_c, were estimated for 20 methylated naphthalenes consisting of monomethyl to tetramethyl homologues. Linear free energy relationships (LFERs) were developed for the estimation. Chromatographic retention measurements were conducted for eleven reference polycyclic aromatic hydrocarbons (PAHs) and regressions were fit between the retention indices and the physicochemical properties. A high-pressure liquid chromatography (HPLC) octadecylsilyl column with acetonitrile/water eluent was used for the estimation of $S_{w,L}$ and K_{ow}. Two gas chromatography (GC) columns, the HP5-MS and the more hydrophobic HP-1, were tested for the estimation of $P_{v,L}$. Measured retention indices for the methylated naphthalenes were entered to the regression equations to calculate the physicochemical properties of these compounds. Available literature values were used for comparison and validation. The method accurately estimated physicochemical properties. Estimated $S_{w,L}$ and $P_{v,L}$ decreased with the number of methyl groups, while K_{ow} increased. There was no obvious relation between H_c and the number of methyl groups. Log$S_{w,L}$ ranged from 0.88 for 1,2,5,6-tetramethylnaphthalene to 2.27 for 1-methylnaphthalene (mmol m^{-3}). LogK_{ow} ranged from 3.89 for 1-methylnaphthalene to 4.95 for 1,2,5,6-tetramethylnaphthalene. Log$P_{v,L}$ ranged from -0.98 for 1,2,5,6-tetramethylnaphthalene to 0.79 for 2-methylnaphthalene (Pa). LogH_c ranged from 1.03 for 1,4,5-trimethylnaphthalene to 1.73 for 2,6-dimethylnaphthalene (Pa m^3 mol^{-1}). There were no apparent effects of GC column hydrophobicity on the accuracy of the estimates. Estimates of $S_{w,L}$ and K_{ow} based on GC retention indices were not as accurate as those based on HPLC. Comparison of

*Reprinted from *Chemosphere*, Vol. 52, P. Dimitriou-Christidis, B.C. Harris, T.J. McDonald, E. Reese, R.L. Autenrieth, Estimation of selected physicochemical properties for methylated naphthalene compounds, Pages 869-881, Copyright 2003, with permission from Elsevier.

the estimated values with values predicted by EPIWIN indicated that this software is useful in performing order-of-magnitude predictions of physicochemical properties.

INTRODUCTION

Physicochemical properties provide an understanding of the transport and fate of organic pollutants and allow a variety of environmental models to predict media-specific distribution of the pollutants in the environment (air, water, soil/sediment, and biota). Physicochemical properties are important in pollutant transport and fate modeling, risk assessment, and biodegradation studies. For example, the octanol/water partition coefficient, an indicator of hydrophobicity, is used to estimate bioconcentration factors (Veith et al., 1979). Furthermore, aqueous solubility greatly affects biodegradability of organic compounds in the environment (Leahy and Colwell, 1990).

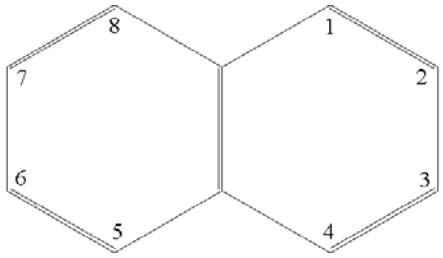

Fig. 2.1. Structure and ring numbering of naphthalene.

Naphthalene is an aromatic hydrocarbon consisting of two fused rings with a total of ten carbon atoms. Fig. 2.1 shows the planar structure of naphthalene and its ring numbering. Naphthalene and its family of methylated homologues are common components of complex mixtures of PAHs such as crude oil, coal tar, gasoline, cigarette smoke, diesel engine exhaust, among other sources. Methylated naphthalenes are reported to occur in crude oil with up to six methyl substituents and are ubiquitous constituents of sedimentary organic matter (van Aarssen et al., 1999). Production capacity of naphthalene in the United States was estimated at 159,000 metric tons in 1992 (SRI International, 1992). Naphthalene has been identified in at least 536 of the

1408 hazardous waste sites proposed for inclusion in the National Priority List (ATSDR, 1994). The two monomethylated naphthalenes, 2-methylnaphthalene and 1-methylnaphthalene, have been identified in at least 328 of the sites. Naphthalene contamination of up to 46,000 mg/kg is reported in the soils and sediments at these sites. Naphthalene has a relatively high volatility compared to other PAHs, which may explain its widespread distribution in the environment.

There is considerable toxicological interest in naphthalene and its substituted homologues because of widespread human exposure and the potential formation of toxic and carcinogenic metabolites (Wilson et al., 1996). Naphthalene toxicity to humans can be expressed as hemolytic anemia in children and adults. Higher incidence of both cataracts and laryngeal tumors has been reported in workers in the naphthalene chemical industry (Wilson et al., 1996). Little to no toxicity data is available on substituted naphthalene compounds.

In this paper the aqueous solubilities, octanol/water partition coefficients, vapor pressures, and Henry's law constants were estimated for 20 members of the naphthalene family including mono- through tetramethylated homologues. These four physicochemical properties describe partitioning of the compounds of interest in air, water, and biota. Among other applications, they can be used to quantify risk of exposure and optimize detoxification efforts, such as bioremediation.

Physicochemical properties can be measured directly using pure compounds and analytical methods dictated by the definition of a property. For example, the shake-flask and slow-stirring methods are commonly used for measurement of K_{ow}. However, some characteristics of hydrophobic compounds, e.g., low aqueous phase concentrations and slow equilibration between phases, have been reported to be responsible for widespread discrepancies in reported values (Karickhoff and Brown, 1979). A literature review of on some well-studied compounds reveals wide ranges, often of 1-2 orders of magnitude, in reported values. Chromatographic methods use mixtures of compounds of much lower concentrations to estimate physicochemical properties. These methods are generally accurate and, because they are indirect, fast, and inexpensive.

The chromatographic approach establishes LFERs between the retention time and physicochemical properties. The approach is based on the assumption that transfer between the stationary and mobile phases can be expressed as a chemical equilibrium and the free energy of the equilibrium is related to the retention time (Snow, 1996). Chromatographic retention measurements are conducted for a set of reference compounds with known physicochemical properties and linear regressions are fitted between the retention times and the values of the physicochemical properties. The resulting LFERs can then be used to estimate physicochemical properties of other similar compounds given their measured retention times. The suitability of HPLC has been demonstrated for the estimation of physicochemical properties involving liquid phases, e.g., K_{ow} and $S_{w,L}$ (Veith and Morris, 1978; Finizio et al., 1997). GC has been used for the estimation of physicochemical properties involving gaseous phases, e.g., $P_{v,L}$ (Fischer et al., 1992; Kurz and Ballschmiter, 1999). In this study, HPLC was used to estimate K_{ow} and $S_{w,L}$, while GC to estimate $P_{v,L}$. The chromatographic technique holds promise for determining physicochemical behavior in the absence of direct measurements. For complex mixtures consisting of many chemicals, some of which may not be fully characterized for physicochemical, biological, and toxicological behavior, this approach provides an easy and accurate alternative for estimating properties.

MATERIALS AND METHODS

Chemicals

Naphthalene is abbreviated as NAP. Methylated naphthalenes with 1, 2, 3, and 4 methyl substituents are abbreviated as MNAP, DMNAP, TMNAP, and TeMNAP, respectively. The number in front of the acronym specifies the position of the methyl groups on the carbon skeleton (Fig. 2.1). For example, 146TMNAP corresponds to 1,4,6-trimethylnaphthalene. NAP, 1MNAP, 15DMNAP, 16DMNAP, 17DMNAP, 23DMNAP, 26DMNAP, and 27DMNAP were purchased from Alfa Aesar (Ward Hill, MA). 2MNAP, 12DMNAP, 13DMNAP, 14DMNAP, 18DMNAP, 124TMNAP, 137TMNAP, 145TMNAP, 146TMNAP, 236TMNAP, 245TMNAP, 1256TeMNAP, and 1467TeMNAP were purchased from Chiron AS (Trondheim, Norway). The EPA 610

PAH Mix, used as the mixture containing the reference PAHs, was purchased from Supelco (Bellefonte, PA). *N*-phenylalkanes (C1-C10) were purchased from Sigma Aldrich (St. Louis, MO); C11 (Undecylbenzene) and C12 (Dodecylbenzene) phenylalkanes were purchased from VWR (West Chester, PA). Arabian medium crude oil was used as the source of *n*-alkanes (C11-C33).

Chromatographic analyses

GC measurements were conducted on a HP 5890 Series II chromatograph interfaced with a HP 5972 mass selective detector (Agilent Technologies Inc., Palo Alto, CA). Two non-polar columns were used: the HP-5MS ((5%-Phenyl)-Methylpolysiloxane, 0.25 mm × 30 m × 0.25 μm, J&W Scientific (Palo Alto, CA)), and the HP-1 (Polydimethylsiloxane, 0.25 mm × 30 m × 0.25 μm, J&W Scientific (Palo Alto, CA)). The following temperature program was used for both columns: 60 ºC, 7.0 ºC/min, 225 ºC, 15.0 ºC/min, 300 ºC (11.43 min). The mass spectrometer was operated in the selective ion mode (SIM) for the naphthalene compounds. *N*-alkanes were detected in full scan mode using the same temperature program. The compounds were injected three times and the retention index for each compound was calculated for each run. The mean values from the three runs were used in the regression analyses.

HPLC analysis was performed on a Finnigan Mat Spectra System (Thermo Electron Corporation, San Jose, CA) with an octadecylsilyl SUPELCOSIL LC-PAH column (4.6 mm × 25 cm × 5 μm, Supelco (Bellefonte, PA)). The UV6000LP photodiode array detector measured peak response at a wavelength of 254 nm. A mixture of acetonitrile (ACN) and water at a flow rate of 2.0 mL/min constituted the eluent. The percentage of ACN in the mix ramped from 40% to 100% between minutes 5 and 30 and then stayed at 100% for 20 minutes. Triplicate analyses were performed on the compounds and a retention index for each compound was calculated for each run. The mean values from the three runs were used in the regression analyses.

Regression analysis and retention indices

LFERs can be constructed between the chromatographic retention index (*RI*) and the logarithm of a physicochemical property:

Table 2.1
Measured mean retention indices (*RI*) on the three chromatography columns (LC-PAH, HP-5MS, and HP-1), and logarithmic values of $S_{w,L}$, K_{ow}, and $P_{v,L}$ of the 11 reference PAHs. Reference compounds are listed from low to high molecular weight (MW). Uncertainty in *RI* is expressed as one standard deviation from the mean. Physicochemical property values are reported at 25 ºC.

Reference Compound	**MW**	$RI_{HPLC,LC\text{-}PAH}$	$RI_{GC,HP\text{-}5MS}$	$RI_{GC,HP\text{-}1}$	$\log S_{w,L}$ [a,b] **(mmol/m^3)**	$\log K_{ow}$ [a,b]	$\log P_{v,L}$ [a,b] **(Pa)**
Naphthalene	128.18	210.16 ± 2.06	1184.04 ± 0.24	1159.35 ± 0.56	2.91	3.30	1.58
Acenaphthylene	152.20	266.85 ± 0.80	1453.37 ± 0.62	1418.54 ± 0.71	2.68	3.94	-0.26
Acenaphthene	154.21	333.62 ± 0.48	1488.20 ± 0.18	1455.06 ± 1.28	2.10	3.92	0.22
Fluorene	166.22	363.89 ± 0.78	1586.39 ± 0.72	1552.98 ± 1.90	1.85	4.18	-0.23
Phenanthrene	178.24	423.36 ± 1.02	1784.21 ± 1.48	1744.37 ± 0.52	1.38	4.46	-1.26
Anthracene	178.24	483.55 ± 0.70	1793.42 ± 1.40	1754.97 ± 0.46	1.39	4.45	-0.64
Fluoranthene	202.26	543.73 ± 0.65	2068.42 ± 1.24	2020.45 ± 0.23	0.83	5.16	-2.19
Pyrene	202.26	590.09 ± 0.23	2120.64 ± 1.04	2069.70 ± 0.16	0.71	4.88	-2.34
Chrysene	228.29	792.55 ± 1.45	2471.68 ± 2.97	2409.82 ± 1.24	-0.04	5.81	-4.07
Benzo[k]fluoranthene	252.32	982.40 ± 1.13	2789.11 ± 2.13	2722.00 ± 1.17	-0.61	6.11	-5.38[c]
Benzo[a]pyrene	252.32	1026.95 ± 0.43	2872.45 ± 3.49	2798.00 ± 1.27	-0.67	6.13	-4.67[c]

[a] From Howard and Meylan (1997).
[b] From SRC (2005).
[c] From Mackay et al. (1992).

$$\log K = aRI + b \tag{2.1}$$

where *K* is a physicochemical property of interest. The values of the linear coefficients *a* and *b* are obtained from the regression with the reference compounds, a set of compounds with known *K* values and experimentally measured *RI* values. Estimation of $P_{v,L}$ as a linear function of a retention parameter on a GC column, as described by Eq. 2.1, was introduced by Fischer et al. (1992). This approach is one of several suggested for nonpolar columns. Five of these methods, including the one used in this study, are compared in Koutek et al. (2001) for a range of compounds. The method by Fisher et al. (1992) and two other methods resulted in the lowest average percent error when the accuracy of the five models was tested against literature values. Another reason for using this method in this study was uniformity, since Eq. 2.1 is also used for the estimation of $S_{w,L}$ and K_{ow}. Table 2.1 provides a list of the 11 reference compounds used in this study and their calculated *RI* values on the HPLC (LC-PAH) and the two GC columns (HP-5-

MS and HP-1). The physicochemical properties of the reference compounds are reported at 25 ºC.

Development and validation of LFERs required accuracy in physicochemical property values for the reference compounds and for methylated naphthalenes, where available. Compilations considered and evaluated for reliability as sources of physicochemical property values included Howard and Meylan (1997) and its on-line database version SRC (2005), Mackay et al. (1992), Karcher (1985), LaGrega et al. (2001), and WHO (1998). Howard and Meylan (1997) and SRC (2005), and Mackay et al. (1992) contained the most extensive collection of values for the compounds of interest. Howard and Meylan (1997) and SRC (2005) provide values for a larger number of methylated naphthalenes. The disadvantage of these sources is that they provide one value for each property and the literature reference but no information on the exact technique used to determine the property value. Nevertheless, they make a distinction between experimentally determined and estimated or extrapolated values. Mackay et al. (1992) reports values for a smaller number of compounds of interest, yet it provides a series of values by different studies as well as the technique used for the determination of each value. Accurate values are easily discernible when different techniques resulted in similar values. Single values from Howard and Meylan (1997) and SRC (2005) were compared with accurate values from Mackay et al. (1992) and the differences were found to be minimal. For reasons of consistency, physicochemical property values for the reference compounds and the naphthalene compounds, when available, were all obtained from Howard and Meylan (1997) and SRC (2005), unless otherwise stated. Only experimental values were considered; extrapolated or estimated values were disregarded. Aqueous solubilities and vapor pressures were converted to liquid aqueous solubilities and liquid vapor pressures respectively, as a common basis for calculations and comparison. Conversion was necessary because a solid solute has lower solubility and vapor pressure than the same solute in a hypothetical liquid state under the same conditions. Solid-liquid fugacity factors f^s/f^l were used for the conversion. Fugacity factors were calculated using the following equation (Prausnitz et al., 1986):

$$\ln \frac{f^l}{f^s} = \frac{\Delta h^{fus}}{R_g T_m}\left(\frac{T_m}{T} - 1\right) \tag{2.2}$$

where Δh^{fus} is the enthalpy of fusion at the melting temperature, T_m, T is the system temperature, and R_g is the ideal gas constant. No conversion was required for liquid solutes, since the fugacity factor for liquids is 1. Fugacity factors were computed using data from Daubert and Danner (1989) when available; otherwise fugacity factors from Mackay et al. (1992) were used.

Retention time can be expressed in a normalized manner as the retention index, *RI*. RI_{GC}, the retention index in temperature programmed GC, was calculated as (van den Dool and Kratz 1963):

$$RI_{GC} = \frac{t_{n+1} - t_x}{t_{n+1} - t_n} \cdot 100 + 100n \tag{2.3}$$

where t_x is the retention time of x, the compound of interest, and t_n and t_{n+1} are the retention times of the two n-alkanes bracketing x with carbon numbers n and $n+1$, respectively. The n-alkanes were used as the retention index markers for GC measurements. To calculate *RI* from HPLC measurements, a similar equation was used (Kurz and Ballschmiter 1999):

$$RI_{HPLC} = \frac{\log t_{n+1} - \log t_x}{\log t_{n+1} - \log t_n} \cdot 100 + 100n \tag{2.4}$$

A mixture of n-phenylalkanes was selected as retention index markers for HPLC measurements.

RESULTS

RI generally increased with the molecular weight of the reference compounds. Average *RI* values for each reference compound on each chromatography column are presented in Table 2.1. For the analysis, 10 n-phenylalkanes, from C1 (toluene) to C10 (decylbenzene), were used as the retention index markers for the HPLC-based *RI*s. Nineteen (19) n-alkanes, from n-undecane to n-heneicosane, were used to calculate the GC-based *RI*s. LFERs between *RI*s and the logarithm of physicochemical properties are depicted in Fig. 2.2 for the reference compounds. Naphthalenes with known literature

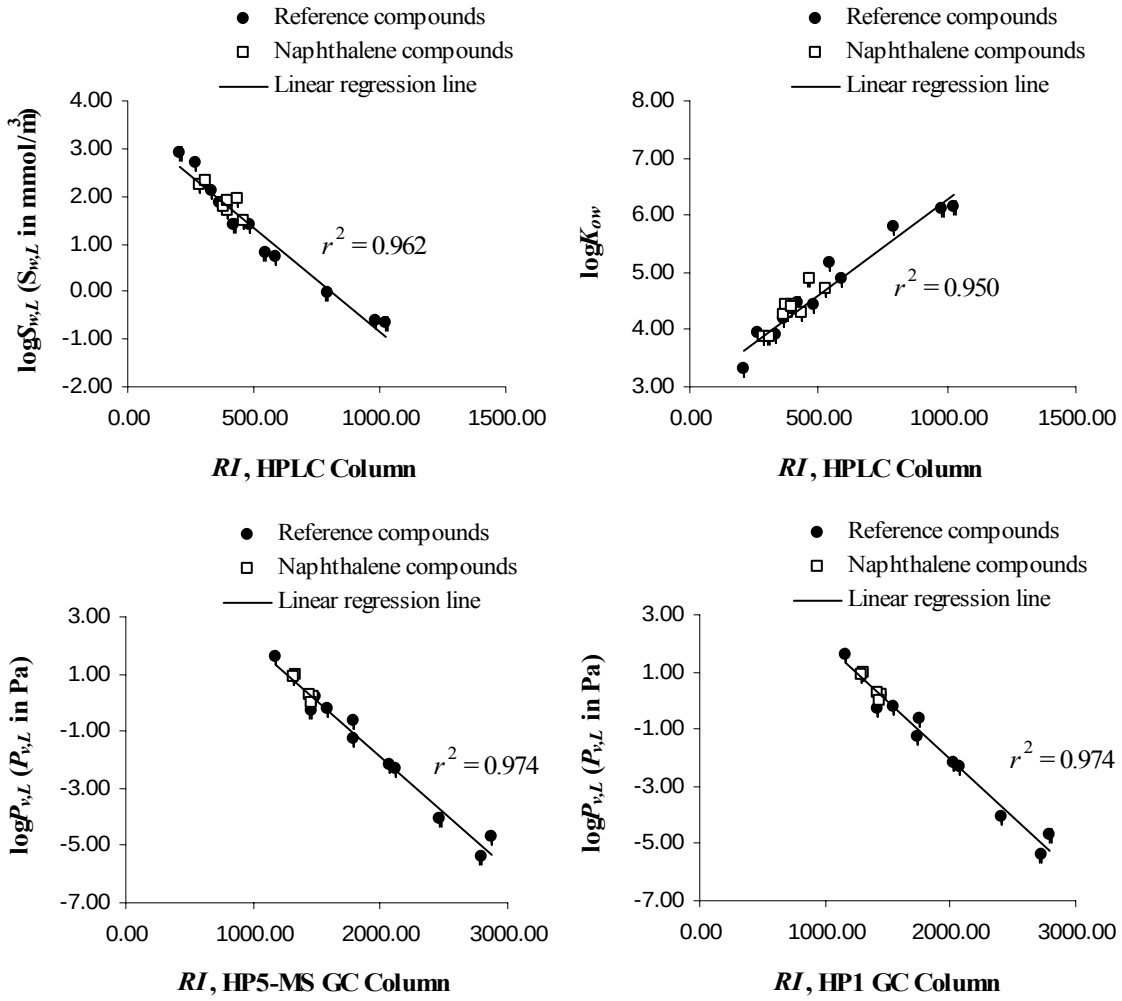

Fig. 2.2. Linear regressions between the retention indices of the reference compounds and the logarithm of their physicochemical properties. The reference compounds (●) were used to establish the linear models; literature values for methylated naphthalenes (□) were superimposed for evaluation of the models. Horizontal error bars appear in the graphs but they are narrower than the symbols.

values are also depicted for model evaluation. Horizontal error bars generated from triplicate chromatographic measurements are depicted but they are insignificantly small. LFERs regression equations are presented below. Uncertainties in regression coefficients correspond to the margins of error at the 95% confidence level. The correlation

coefficient, r, and the coefficient of determination, r^2, were calculated for each equation as measures of fit. The F-statistic was used to test the significance of r^2.

$$\log S_{w,L} = (- 0.00433 \pm 0.00052) \cdot RI_{HPLC,LC\text{-}PAH} + (3.510 \pm 0.393) \quad (2.5)$$

$n = 11$, $r = - 0.981$, $r^2 = 0.962$, $F = 230.0$

$$\log K_{ow} = (0.00333 \pm 0.00072) \cdot RI_{HPLC,LC\text{-}PAH} + (2.938 \pm 0.351) \quad (2.6)$$

$n = 11$, $r = 0.975$, $r^2 = 0.950$, $F = 170.2$

$$\log P_{v,L} = (- 0.00391 \pm 0.00068) \cdot RI_{GC,HP5\text{-}MS} + (5.934 \pm 0.981) \quad (2.7)$$

$n = 11$, $r = - 0.987$, $r^2 = 0.974$, $F = 336.5$

$$\log P_{v,L} = (- 0.00402 \pm 0.00070) \cdot RI_{GC,HP\text{-}1} + (5.972 \pm 0.987) \quad (2.8)$$

$n = 11$, $r = - 0.987$, $r^2 = 0.974$, $F = 335.7$

The values of r indicate valid linear relationships between *RI*s and the physicochemical parameters of interest. The high r^2 values (0.950 – 0.974) and their significance indicate the validity of the linear relationship between the *RI*s and physicochemical properties. Given the compound diversity in the training set and the wide range of *RI* observed, Eq. 2.5 through 2.8 can be used for the estimation of unknown physicochemical properties for various PAHs; in this study they were used for the estimation methylated naphthalenes. To estimate Henry's law constants the following equation was used (Mackay et al., 1992):

$$H_c = P_{v,L} / S_{w,L} \quad (2.9)$$

This equation is valid only for sparingly-soluble chemicals, e.g., PAHs.

Estimated physicochemical property values are presented in Table 2.2 with uncertainties expressed as the 95% margins of error, $E_{95\%}$, from the regression analysis. Literature values for naphthalenes, when available, are also provided for comparison. Calculation of $P_{v,L}$ and H_c, used only the data from the HP5-MS column, as it generated values closer to literature values than the HP-1 column. Selection of HP5-MS over the HP-1 column is further justified in the DISCUSSION section. Generally, $S_{w,L}$ and $P_{v,L}$ decreased with the number of methyl groups. Log$S_{w,L}$ ranged from 0.88 for

Table 2.2
Estimated physicochemical property values of 20 methylated naphthalenes. Uncertainties are expressed as the margin of error at the 95% confidence level. Literature values, Lit., are provided for comparison. Non-available literature values are marked as *NA*. Solubility and vapor pressure are expressed as liquid solubility and liquid vapor pressure. All physicochemical properties are reported at 25 ºC.

	log$S_{w,L}$ (mmol/m^3)		logK_{ow}		log$P_{v,L}$ (Pa)		logH_c (Pa m^{-3} mol^{-1})	
Compound	**Estim.**	**Lit.[a, b]**	**Estim.**	**Lit.[a, b]**	**Estim.**	**Lit.[a, b]**	**Estim.**	**Lit.[a, b]**
1MNAP	**2.27** ± 0.24	2.26	**3.89** ± 0.21	3.87	**0.72** ± 0.40	0.95	**1.45** ± 1.87	1.72
2MNAP	**2.18** ± 0.23	2.30	**3.96** ± 0.21	3.86	**0.79** ± 0.40	0.93	**1.61** ± 1.77	1.72
12DMNAP	**1.85** ± 0.20	*NA*	**4.21** ± 0.18	4.31	**0.15** ± 0.35	0.23	**1.29** ± 1.51	*NA*
13DMNAP	**1.78** ± 0.20	1.71	**4.27** ± 0.18	4.42	**0.29** ± 0.36	*NA*	**1.51** ± 1.42	*NA*
14DMNAP	**1.83** ± 0.20	1.86	**4.22** ± 0.18	4.37	**0.20** ± 0.35	*NA*	**1.37** ± 1.48	*NA*
15DMNAP	**1.84** ± 0.20	1.80	**4.22** ± 0.18	4.38	**0.20** ± 0.35	*NA*	**1.35** ± 1.49	1.55
16DMNAP	**1.77** ± 0.20	*NA*	**4.27** ± 0.17	*NA*	**0.25** ± 0.36	0.29	**1.50** ± 1.41	*NA*
17DMNAP	**1.88** ± 0.20	*NA*	**4.19** ± 0.18	4.44	**0.29** ± 0.36	*NA*	**1.41** ± 1.52	*NA*
18DMNAP	**1.92** ± 0.21	*NA*	**4.16** ± 0.18	4.26	**0.06** ± 0.34	*NA*	**1.14** ± 1.58	*NA*
23DMNAP	**1.81** ± 0.20	1.90	**4.25** ± 0.18	4.40	**0.20** ± 0.35	-0.04	**1.40** ± 1.45	1.97
26DMNAP	**1.62** ± 0.19	1.93	**4.39** ± 0.17	4.31	**0.35** ± 0.36	*NA*	**1.73** ± 1.26	*NA*
27DMNAP	**1.64** ± 0.19	*NA*	**4.37** ± 0.17	*NA*	**0.34** ± 0.36	*NA*	**1.70** ± 1.28	*NA*
124TMNAP	**1.49** ± 0.18	*NA*	**4.49** ± 0.16	*NA*	**-0.36** ± 0.31	*NA*	**1.15** ± 1.18	*NA*
137TMNAP	**1.63** ± 0.19	*NA*	**4.38** ± 0.17	*NA*	**-0.14** ± 0.32	*NA*	**1.22** ± 1.31	*NA*
145TMNAP	**1.51** ± 0.18	1.46[c]	**4.48** ± 0.16	4.90	**-0.46** ± 0.30	*NA*	**1.03** ± 1.20	*NA*
146TMNAP	**1.41** ± 0.18	*NA*	**4.55** ± 0.16	*NA*	**-0.22** ± 0.32	*NA*	**1.36** ± 1.10	*NA*
236TMNAP	**1.21** ± 0.17	*NA*	**4.70** ± 0.15	4.73	**-0.24** ± 0.32	*NA*	**1.55** ± 0.89	*NA*
245TMNAP	**1.45** ± 0.18	*NA*	**4.52** ± 0.16	*NA*	**-0.37** ± 0.31	*NA*	**1.17** ± 1.14	*NA*
1256TeMNAP	**0.88** ± 0.17	*NA*	**4.95** ± 0.16	*NA*	**-0.98** ± 0.27	*NA*	**1.13** ± 0.61	*NA*
1467TeMNAP	**1.16** ± 0.17	*NA*	**4.74** ± 0.15	*NA*	**-0.78** ± 0.28	*NA*	**1.06** ± 0.87	*NA*

[a] From Howard and Meylan (1997).
[b] From SRC (2005).
[c] From Mackay et al. (1992).

1256TeMNAP to 2.27 for 1MNAP. Log$P_{v,L}$ ranged from –0.98 for 1256TeMNAP to 0.79 for 2MNAP. In contrast, K_{ow} increased with the number of methyl groups. LogK_{ow} ranged from 3.89 for 1MNAP to 4.95 for 1256TeMNAP. No relation was evident between H_c and *RI*, or the number of methyl groups. For example logH_c was 1.61 for 2MNAP and 1.55 for 236TMNAP. Additionally, logH_c varied only 0.70 units between

the minimum (1.03 for 145 TMNAP) and the maximum value (1.73 for 26DMNAP). $E_{95\%}$ values were small for $S_{w,L}$ and K_{ow}, larger for $P_{v,L}$, and significantly larger for H_c. Values varied from 0.17 to 0.24 units for log$S_{w,L}$ and from 0.15 to 0.21 units for logK_{ow}. $E_{95\%}$ was larger for log$P_{v,L}$ ranging from 0.27 to 0.40 units. $E_{95\%}$ for logH_c exceeded those for $P_{v,L}$, ranging from 0.61 to 1.87 log units. This is due to propagation of both $S_{w,L}$ and $P_{v,L}$ errors. The available literature values were contained within the 95% confidence intervals for the estimated values. The only exceptions were 26DMNAP for $S_{w,L}$ and 17 DMNAP and 145TMNAP for K_{ow}. Generally, the mean estimated values were comparable to the literature values. The average absolute difference between estimated and predicted values and the maximum difference (in parentheses) for log$S_{w,L}$, logK_{ow}, log$P_{v,L}$, and logH_c were 0.09 (–0.31), 0.14 (–0.42), 0.14 (0.24), and 0.29 (–0.57), respectively. The low average absolute difference from the literature values indicates that the models accurately estimated physicochemical properties.

DISCUSSION

Validation of physicochemical property estimates

A similar study (Abraham et al., 2005) used the Abraham linear solvation energy relationships (LSERs) (Eq. 2.10 and 2.11) to predict physicochemical properties for the naphthalenes investigated in this research and other alkylated naphthalenes. The two solvation equations were of the form (Abraham et al., 2005):

$$K_1 = c_1 + e_1E_s + s_1S_s + a_1A_s + b_1B_s + vV_s \quad (2.10)$$

$$K_2 = c_2 + e_2E_s + s_2S_s + a_2A_s + b_2B_s + lL_s \quad (2.11)$$

where K_1 and K_2 represent a set of solute properties in a condensed and gas-condensed systems, respectively, E_s, S_s, A_s, B_s, V_s, and L_s are chemical descriptors, and c, e, s, a, b, v, and l are multiple regression coefficient determined from a set of reference compounds. It was found that the estimates from Eq. 2.10 and 2.11 were essentially identical to those found in this study, even for H_c, and with experimental observations, where available. In general, predictions by Eq. 2.10 and 2.11 were characterized by lower uncertainties compared to the estimates from the chromatographic method because they included only predictive and not experimental error (Abraham et al., 2005).

Selection of reference compounds

Accuracy in estimated values using chromatographic LFERs depends on appropriate selection of reference compounds. A set of non-heterocyclic, unsubstituted PAHs used in EPA Method 550.1 for the determination of PAH concentrations in drinking water (Hodgeson et al., 1990) were selected as the reference compounds. The set was selected because it is readily available as a standard mixture and because it contains a broad range of PAHs from naphthalene to benzo[g,h,i]perylene. Despite the fact that compounds of interest were substituted naphthalenes, selection of unsubstituted compounds for the reference set was justified by the suitable selection of the chromatography columns. Separation in a chromatography column is determined by the Gibbs free energy. The quantity, enthalpy or entropy, having the largest contribution to the free energy of solute transfer to the stationary phase is the driving force of the separation. Alkylated PAHs have moieties that have rotational degrees of freedom. Thus, their entropies of transfer are different from those of unsubstituted PAHs. However, it is believed that the nonpolar character of the three columns used in this study favored enthalpic-driven partitioning. Separation was based on the size and geometry of the solutes (enthalpic contribution) and not on entropies of mixing/dissolution (entropic contribution). Wysocki (2001) investigated the thermodynamic force of separation of alkylbenzenes on a C18 liquid chromatography stationary phase with acetonitrile and water as the mobile phase. It was found that the partitioning was enthalpically driven.

Of the 16 PAHs in the EPA method, 11 were selected as reference compounds. Indeno[1,2,3-cd]pyrene was excluded because literature data was available only for aqueous solubility and not for any other properties. Benz[a]anthracene, benzo[b]fluoranthene, dibenzo[a,h]anthracene, and benzo[g,h,i]perylene were also excluded as influence points in the regression analysis. Their leverage values and Cook's distances were within acceptable ranges for non-outliers. However, they exhibited considerable unstandardized residuals compared to the other data points resulting in lower coefficients of determination and broad confidence intervals of estimated properties. Further removal of individual data points from the regressions would result in

improved goodness of fit; however, some deviation from the perfect fit was to account for unexpected property variability within the naphthalene family. It is noted that the number of reference compounds used in this study is greater than 6, the minimum number proposed by Finizio et al. (1997). Furthermore, besides structural differences between naphthalenes and larger PAHs, residual analysis and values of influence statistics did not justify removal of compounds such as chrysene, benzo[k]fluoranthene, and benzo[a]pyrene. Due to the broad range of PAH properties described by the models in this study, the same equations can be used for estimation of physicochemical properties of other PAHs or substituted PAH families, e.g. phenanthrene, fluorene, anthracene, and chrysene.

Chromatography performance and column selection

Instrument performance also influences the accuracy of the results. Both chromatography instruments were consistent between runs, resulting in small standard deviations in *RI* (Table 2.1). Measurement precision was also evident by the small horizontal error bars in Fig 2.2. Precision was assured by the use of retention indices instead of retention times or capacity factors used in similar studies. The *RI* can be normalized to any changes that affect the retention time, such as temperature changes and column degradation.

Accuracy in the results also depends on the choice of chromatography column. In HPLC analysis, only the LC-PAH column was used because this is the standard for the separation and quantification of the given set of reference compounds (EPA Method 550.1). Two non-polar columns were used in GC/MS analysis: the HP5-MS column and the more hydrophobic HP-1 column. The second column was chosen to investigate the proposition that accuracy in physicochemical property estimates improves with column hydrophobicity (Kurz and Ballschmiter, 1999). Both columns generated similar relationships between *RI* and $P_{v,L}$ (Eq. 2.7 and 2.8) and the same r^2 of 0.974. A comparison of the estimated values from the two columns with literature values is presented in Table 2.3. The difference from the literature values, expressed as the estimated minus the literature value, is also calculated. Uncertainty values in Table 2.3

Table 2.3
Comparison between estimated vapor pressure values from the two GC columns, HP5-MS and HP-1. Uncertainties represent the margins of error at the 95% confidence level. Literature values (Lit.) are provided as the basis for comparison. Non-available literature values are marked as *NA*. The last two columns calculate the difference from the literature value. All physicochemical properties are reported at 25 ºC.

Compound	HP5-MS column $\log P_{v,L}$ (Pa)	HP-1 column $\log P_{v,L}$ (Pa)	Lit.[a,b] $\log P_{v,L}$ (Pa)	Difference HP5-MS – Lit. (Pa)	Difference HP-1 – Lit. (Pa)
1MNAP	0.72 ± 0.40	0.70 ± 0.40	0.95	-0.23	-0.252
2MNAP	0.79 ± 0.40	0.77 ± 0.40	0.93	-0.14	-0.16
12DMNAP	0.15 ± 0.35	0.11 ± 0.35	0.23	-0.08	-0.12
13DMNAP	0.29 ± 0.36	0.25 ± 0.36	*NA*	*NA*	*NA*
14DMNAP	0.20 ± 0.35	0.18 ± 0.35	*NA*	*NA*	*NA*
15DMNAP	0.20 ± 0.35	0.16 ± 0.35	*NA*	*NA*	*NA*
16DMNAP	0.28 ± 0.36	0.24 ± 0.36	0.29	-0.01	-0.05
17DMNAP	0.29 ± 0.36	0.25 ± 0.36	*NA*	*NA*	*NA*
18DMNAP	0.06 ± 0.34	0.05 ± 0.34	*NA*	*NA*	*NA*
23DMNAP	0.20 ± 0.35	0.18 ± 0.35	-0.04	0.24	0.20
26DMNAP	0.35 ± 0.36	0.32 ± 0.36	*NA*	*NA*	*NA*
27DMNAP	0.34 ± 0.36	0.31 ± 0.36	*NA*	*NA*	*NA*
124TMNAP	-0.36 ± 0.31	-0.40 ± 0.31	*NA*	*NA*	*NA*
137TMNAP	-0.14 ± 0.32	-0.19 ± 0.32	*NA*	*NA*	*NA*
145TMNAP	-0.47 ± 0.30	-0.49 ± 0.30	*NA*	*NA*	*NA*
146TMNAP	-0.23 ± 0.32	-0.27 ± 0.32	*NA*	*NA*	*NA*
236TMNAP	-0.24 ± 0.32	-0.29 ± 0.32	*NA*	*NA*	*NA*
245TMNAP	-0.38 ± 0.31	-0.40 ± 0.31	*NA*	*NA*	*NA*
1256TeMNAP	-0.98 ± 0.27	-1.03 ± 0.27	*NA*	*NA*	*NA*
1467TeMNAP	-0.78 ± 0.28	-0.84 ± 0.28	*NA*	*NA*	*NA*

[a] From Howard and Meylan (1997).
[b] From SRC (2005).
[c] From Mackay et al. (1992).

show that the models developed from the two columns resulted in comparable error values for each naphthalene compound. Therefore, preference of one column over the other could not be based on statistical significance. Nevertheless, the HP5-MS column generated consistently higher $P_{v,L}$ values than the HP-1 column. Differences from literature values are smaller with the HP5-MS column, except for the case of

23DMNAP. Literature data is limited for methylated naphthalenes, therefore, it is not clear which column provided the most accurate results. Nevertheless, HP5-MS results were closer to the literature values and were used in the estimation of $P_{v,L}$ and H_c reported in Table 2.2.

A similar study (Wang and Wong, 2002) used only gas chromatography to estimate vapor pressures, water solubilities, Henry's law constants and octanol/water partition coefficients for polychlorinated-dibenzo-dioxins (PCDDs). Quadratic regressions of the form $\log K = aRI^2 + bRI + c$ were performed, where K is a physicochemical property. This methodology was applied in this research to investigate how well the GC models can estimate $S_{w,L}$ and K_{ow} in addition to P_v. A regression analysis was performed between the RI on HP5-MS and the logarithms of $S_{w,L}$ and K_{ow}. Two types of regressions were used: quadratic regression, as proposed by Wang and Wong (2002), and linear regression, as used in this research. Regression equations are as follows for linear (Eq. 2.10) and quadratic (Eq. 2.12) estimates of $S_{w,L}$, and linear (Eq. 2.11) and quadratic (Eq. 2.13) estimates of K_{ow}.

$$\log S_{w,L} = (-0.00218 \pm 0.00064) \cdot RI_{GC,HP5\text{-}MS} + (5.431 \pm 0.474) \quad (2.10)$$

$n = 11$, $r = -0.990$, $r^2 = 0.980$, $F = 450.6$

$$\log K_{ow} = (0.00169 \pm 0.00031) \cdot RI_{GC,HP5\text{-}MS} + (1.439 \pm 0.353) \quad (2.11)$$

$n = 11$, $r = 0.991$, $r^2 = 0.982$, $F = 485.1$

$$\log S_{w,L} = (3.7 \cdot 10^{-7} \pm 1.9 \cdot 10^{-7}) \cdot RI^2_{GC,HP5-MS} + (-0.00371 \pm 0.00078) \cdot RI_{GC,HP5-MS} + (6.904 \pm 0.772) \quad (2.12)$$

$n = 11$, multiple $r = 0.993$, $r^2 = 0.987$

$$\log K_{ow} = (-2.6 \cdot 10^{-7} \pm 1.4 \cdot 10^{-7}) \cdot RI^2_{GC,HP5-MS} + (0.00277 \pm 0.00060) \cdot RI_{GC,HP5-MS} + (0.400 \pm 0.590) \quad (2.13)$$

$n = 11$, multiple $r = 0.994$, $r^2 = 0.987$

Fits were improved over those of Eq. 2.5 and 2.6. Table 2.4 presents a comparison between literature $S_{w,L}$ and K_{ow} values with those estimated by the GC linear

Table 2.4
Comparison of $S_{w,L}$ and K_{ow} values estimated by the linear and quadratic GC models ($GC_{lin.}$ and $GC_{quad.}$, respectively) with literature values (Lit.).

Compound	log$S_{w,L}$ (mmol/m^3)			Difference (mmol/m^3)		logK_{ow}			Difference	
	$GC_{lin.}$ est.	GC_{quad} est.	Lit.	$GC_{lin.}$ – Lit.	$GC_{quad.}$ – Lit.	GC_{lin} est.	$GC_{quad.}$ est.	Lit.	$GC_{lin.}$ – Lit.	$GC_{quad.}$ – Lit.
1MNAP	2.52	2.61	2.26	0.259	0.352	3.69	3.63	3.87	-0.20	-0.26
2MNAP	2.56	2.66	2.30	0.253	0.355	3.66	3.59	3.86	-0.30	-0.37
12DMNAP	2.20	2.22	*NA*	-	-	3.94	3.93	4.31	-0.27	-0.28
13DMNAP	2.28	2.31	1.71	0.567	0.605	3.88	3.85	4.42	-0.39	-0.42
14DMNAP	2.23	2.26	1.86	0.366	0.393	3.92	3.90	4.37	-0.31	-0.33
15DMNAP	2.23	2.25	1.80	0.428	0.455	3.92	3.90	4.38	-0.30	-0.32
16DMNAP	2.27	2.31	*NA*	-	-	3.88	3.86	*NA*	-	-
17DMNAP	2.28	2.31	*NA*	-	-	3.88	3.85	4.44	-0.31	-0.34
18DMNAP	2.15	2.16	*NA*	-	-	3.98	3.97	4.26	-0.18	-0.19
23DMNAP	2.23	2.26	1.90	0.328	0.355	3.92	3.90	4.40	-0.33	-0.35
26DMNAP	2.31	2.35	1.93	0.378	0.422	3.85	3.82	4.31	-0.53	-0.57
27DMNAP	2.31	2.35	*NA*	-	-	3.86	3.83	*NA*	-	-
124TMNAP	1.91	1.88	*NA*	-	-	4.16	4.18	*NA*	-	-
137TMNAP	2.04	2.03	*NA*	-	-	4.06	4.07	*NA*	-	-
145TMNAP	1.86	1.82	1.46[c]	0.392	0.354	4.20	4.23	4.90	-0.27	-0.25
146TMNAP	1.99	1.97	*NA*	-	-	4.10	4.11	*NA*	-	-
236TMNAP	1.98	1.96	*NA*	-	-	4.11	4.12	4.73	-0.60	-0.59
245TMNAP	1.91	1.88	*NA*	-	-	4.17	4.19	*NA*	-	-
1256TeMNAP	1.57	1.49	*NA*	-	-	4.43	4.48	*NA*	-	-
1467TeMNAP	1.68	1.62	*NA*	-	-	4.34	4.38	*NA*	-	-

and quadratic models. Log$S_{w,L}$ values from both GC models were consistently greater than literature values, as indicated by the positive differences. The mean difference and the standard deviation of the difference for the linear and quadratic GC models were 0.37 ± 0.10 log units and 0.41 ± 0.09 log units, respectively. On the other hand, logK_{ow} values from both GC models were consistently lower than those from the literature, as indicated by the negative difference values. The mean difference and the standard deviation of the difference for the linear and quadratic GC models were –0.41 ± 0.17 log units and –0.47 ± 0.14 log units. To summarize, both GC models consistently overestimated $S_{w,L}$ while underestimating K_{ow}. Therefore, use of GC to estimate physicochemical properties involving liquid phases only is not recommended. In the

case of the SUPELCOSIL LC-PAH column, partitioning takes place between the solute and an octadecylsilyl (liquid) phase bonded on silica surface.

Table 2.5
Physicochemical property values of methylated naphthalenes predicted by EPIWIN (U.S. EPA and SRC, 2000) and their comparison to the estimated values from the present study. Each set of columns reports values predicted by EPIWIN (EPIW.) and those estimated in the present study (Est.). LogH_c was calculated in EPIWIN by both the bond (EPIW.-bond) and the group method (EPIW.-group). All values are reported at 25 ºC.

Compound	**logK_{ow}**		**log$S_{w,L}$ (mmol/m^3)**		**log$P_{v,L}$ (Pa)**		**logH_c (Pa m^3/mol)**		
	EPIW.	**Est.**	**EPIW.**	**Est.**	**EPIW.**	**Est.**	**EPIW.-bond**	**EPIW.-group**	**Est.**
1MNAP	3.72	3.89	2.46	2.27	0.69	0.72	1.77	1.61	1.45
2MNAP	3.72	3.96	2.46	2.18	0.76	0.79	1.77	1.61	1.61
12DMNAP	4.26	4.21	1.98	1.85	0.21	0.15	1.81	1.63	1.29
13DMNAP	4.26	4.27	1.88	1.78	0.26	0.29	1.81	1.63	1.51
14DMNAP	4.26	4.22	1.93	1.83	0.14	0.20	1.81	1.63	1.37
15DMNAP	4.26	4.22	1.92	1.85	0.22	0.20	1.81	1.63	1.35
16DMNAP	4.26	4.27	1.87	1.77	0.23	0.28	1.81	1.63	1.50
17DMNAP	4.26	4.19	1.87	1.88	0.23	0.29	1.81	1.63	1.41
18DMNAP	4.26	4.16	1.92	1.92	0.07	0.06	1.81	1.63	1.14
23DMNAP	4.26	4.25	1.90	1.81	0.15	0.20	1.81	1.63	1.40
26DMNAP	4.26	4.39	1.98	1.62	0.34	0.35	1.81	1.63	1.73
27DMNAP	4.26	4.37	1.98	1.64	0.23	0.34	1.81	1.63	1.70
124TMNAP	4.81	4.49	1.45	1.49	-0.17	-0.36	1.86	1.66	1.15
137TMNAP	4.81	4.38	1.45	1.64	-0.19	-0.14	1.86	1.66	1.22
145TMNAP	4.81	4.48	1.37	1.51	-0.09	-0.47	1.86	1.66	1.03
146TMNAP	4.81	4.55	1.45	1.41	-0.47	-0.23	1.86	1.66	1.36
236TMNAP	4.81	4.70	1.52	1.21	-0.17	-0.24	1.86	1.66	1.55
245TMNAP	4.81	4.52	1.45	1.45	-0.17	-0.38	1.86	1.66	1.17
1256TeMNAP	5.36	4.95	0.88	0.89	-0.52	-0.98	1.90	1.69	1.13
1467TeMNAP	5.36	4.74	0.88	1.16	-0.52	-0.78	1.90	1.69	1.06

Evaluation of the EPIWIN prediction software

A number of computer programs are available that predict physicochemical properties of organic compounds. EPIWIN (Estimations Programs Interface for Windows) v3.10 (U.S. EPA and SRC, 2000) is an interface program that executes 10

prediction algorithms and presents their output. These algorithms can predict physicochemical properties based on simple chemical structure entered as SMILES (Simplified Molecular Input Line Entry System) notation. Property values estimated via the regression relationships of this study were compared to the values predicted by EPIWIN. Of the 10 EPIWIN prediction programs, KOWWIN, WSKOWWIN, MPBWIN, and HENRYWIN predict octanol/water partition coefficients, solubilities, vapor pressures, and Henry's law constants, respectively. KOWWIN uses a methodology in which a structure is divided into fragments, and coefficient values corresponding to each fragment are added together to generate a $\log K_{ow}$ value (Meylan and Howard, 1995). WSKOWWIN uses a simple linear regression equation between the octanol/water partition coefficient and solubility to predict $\log S_w$ (Meylan and Howard, 1994). MPBWIN estimates solid vapor pressures, $P_{v,S}$, through three different methods using the boiling point. The program then picks one estimate based on melting point and chemical class. HENRYWIN predicts Henry's law constants using two different methods: the bond contribution method and the group contribution method (Meylan and Howard, 1991), yielding two separate values.

Table 2.5 summarizes the physicochemical property values predicted by EPIWIN for the methylated naphthalenes. Values estimated in the present study are included to allow comparison. $P_{v,S}$ values from the EPIWIN output were converted to $P_{v,L}$ using fugacity factors. EPIWIN yielded values comparable to the estimates of this study (Table 2.5). A fundamental difference is that EPIWIN predicted a single value of K_{ow} and H_c for all isomers, i.e., naphthalenes with the same number of methyl substituents. EPIWIN does not account for molecular structure in its prediction procedure, as captured by the chromatographic retention indices. The greater variability in the predicted $S_{w,L}$ and $P_{v,L}$ values for isomers was due to differences in melting point and boiling point. Nevertheless, in the cases of 16DMNAP and 17DMNAP, liquids with similar melting points and boiling points, EPIWIN predicted the same value of S_w and P_v for both compounds. Use of melting and boiling points in S_w and P_v predictions can account, in part, for the effects of structural variation on the property values. Finally, it was found

that the H_c values predicted by the group contribution method are closer to the estimated values than those by the bond contribution method.

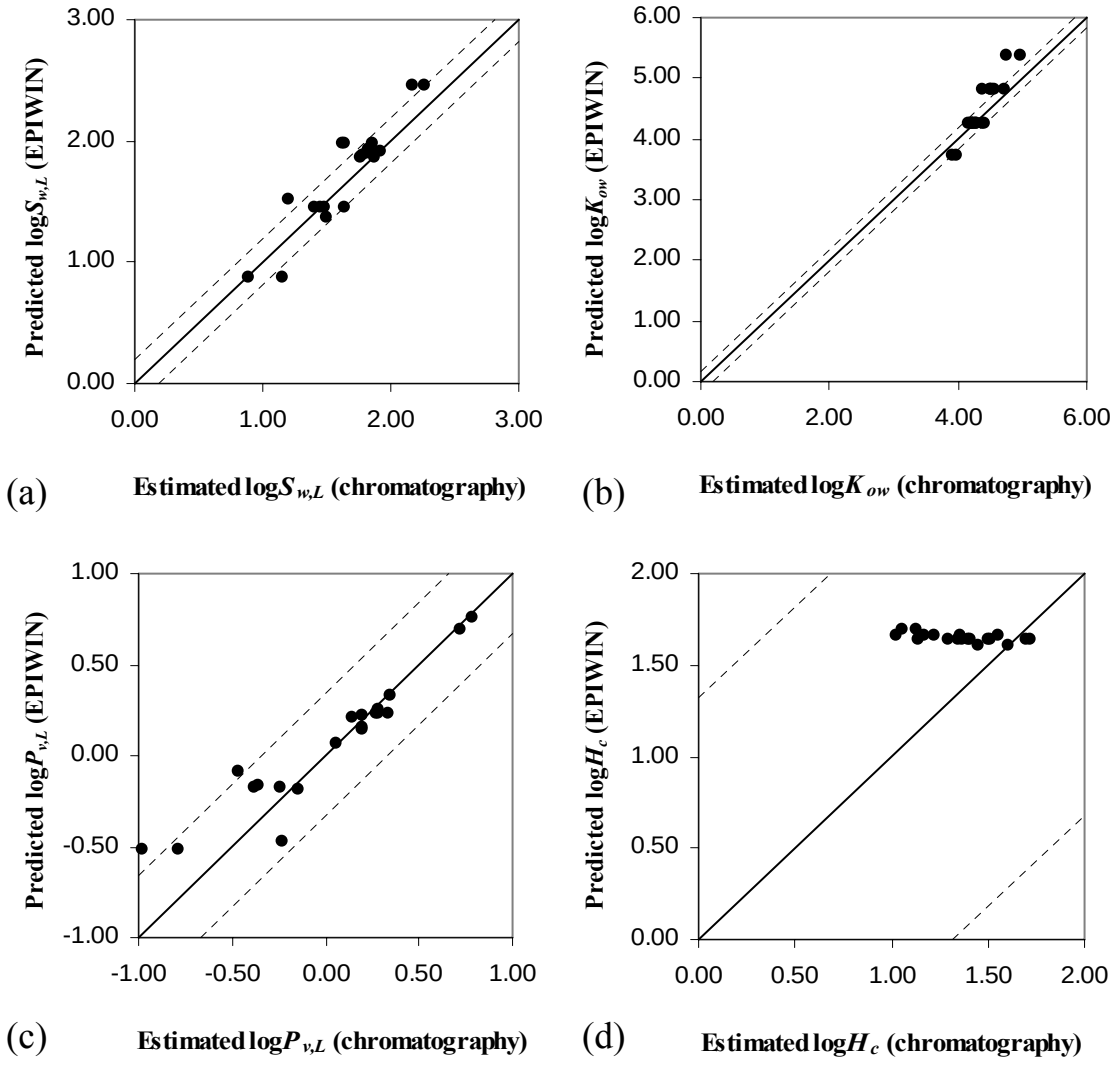

Fig. 2.3. Comparison between property values predicted by EPIWIN and values estimated via the chromatographic LFERs. Graphs (a) through (d) compare the two set of values for log$S_{w,L}$, logK_{ow}, log$P_{v,L}$, and logH_c, respectively. The solid diagonal lines have a slope of 1:1. The distance of the two dashed lines from the 1:1 line is equal to the average margin of error calculated for the estimated property of interest.

A comparison between property values predicted by EPIWIN and those estimated in this study is illustrated in Fig. 2.3. The two sets of values, estimated and predicted, are plotted in each graph (a through d). A straight line with slope of 1:1 represents absolute accordance between the two sets. The distance of the two dashed lines from the 1:1 line is equal to the average margin of error calculated for the estimated property of interest. Average margins of error were calculated from Table 2.2, and were equal to 0.19, 0.17, 0.34, and 1.32 units for $\log S_{w,L}$, $\log K_{ow}$, $\log P_{v,L}$, and $\log H_c$, respectively. Only the H_c values predicted by the group contribution method were compared to the estimated values. EPIWIN adequately predicted aqueous solubility (Fig. 2.3a). Although a perfect match with the estimated values was not observed, only 6 of the 20 predicted values were located outside the confidence bands for the estimated values. Prediction of K_{ow} was not accurate, especially for naphthalenes with high K_{ow} values, containing three and four methyl groups (Fig. 2.3b). EPIWIN successfully predicted vapor pressure as illustrated in Fig. 2.3c. All but two predicted values were located inside the confidence bands for the estimated values. Prediction was more accurate for monomethyl and dimethylnaphthalenes than for the eight trimethyl- and tetramethylnaphthalenes (scattered points). Prediction of H_c was statistically acceptable, but only due to the large uncertainty in the estimated values (Fig. 2.3d). Significant discrepancies from the estimated value were observed, especially with decreasing H_c. To summarize, EPIWIN accurately predicted vapor pressure, particularly for naphthalenes with one and two methyl groups; it adequately predicted aqueous solubility; and it provided order-of-magnitude predictions of octanol/water partition coefficient and Henry's law constants. Overall, EPIWIN provides acceptable approximations of physicochemical properties in the absence of experimental data.

An extension of the chromatographic method for estimation of physicochemical properties would be the prediction of *RI*s for the compounds of interest. The predicted *RI*s could then be entered into chromatographic LFERs like those developed in this study. As a first step, this would eliminate the need for *RI* measurements, the most time-consuming and expensive part in the LFER development. This strategy is indirect and it

could introduce considerable uncertainties. However, it is simple to implement, as it only requires the introduction of a QSRR (Quantitative Structure-Retention Relationship). The development of QSRRs is discussed in detail in Kaliszan (1987). Ledesma and Wornat (2000) used QSRRs to predict chromatographic retention of ethynyl-substituted PAHs. QSPRs (Quantitative Structure-Property Relationships) for the prediction of physicochemical properties is another tool that could eliminate experimentation. QSPR models consider the effects of geometric and spatial molecular structure on properties (Dunnivant et al., 1992). Such models could be supplemental to LFERs or could stand independent when reliable QSPR relationships are available for specific categories of compounds.

CHAPTER III
MEASUREMENT OF BIODEGRADABILITY PARAMETERS FOR UNSUBSTITUTED AND METHYLATED POLYCYCLIC AROMATIC HYDROCARBONS

OVERVIEW

Substrate depletion experiments were conducted to characterize biodegradability of 20 individual polycyclic aromatic hydrocarbons (PAHs) by induced cells of *Sphingomonas paucimobilis* strain EPA505, a potent PAH degrader. PAHs consisted of low-molecular-weight, unsubstituted, and methyl-substituted homologues. A material balance equation containing the Andrews kinetic model, an extension of the Monod model accounting for substrate inhibition, was numerically fitted to batch depletion data to estimate extant kinetic parameters including the maximal specific biodegradation rates, q_{max}, the affinity coefficients, K_S, the specific affinities, q_{max}/K_S, and the inhibition coefficients, K_I. The uncertainties in the best estimates of the kinetic parameters were calculated using a sensitivity method and are reported as the margins of error at the 95% confidence level. Strain EPA505 degraded all PAHs tested. The Monod and Andrews models adequately described biodegradation kinetics. A novel cell proliferation assay involving reduction of the dye WST-1 was used to investigate the ability of strain EPA505 to utilize individual PAHs as sole energy and carbon sources. Of the 22 PAHs tested, 9 supported bacterial growth. The experiments were designed to capture the effects of substrate molecular structure on the kinetic and growth parameters. The generated data is essential for the development of quantitative structure-biodegradability relationships (QSBRs) and for modeling biodegradation of simple mixtures of PAHs.

INTRODUCTION

Polycyclic aromatic hydrocarbons (PAHs) are ubiquitous environmental pollutants (Harvey, 1991). PAHs usually occur in complex mixtures containing parent compounds and substituted homologues (Luthy et al., 1994). The PAH composition of a mixture depends on the type of source; for example, PAHs from petroleum are primarily

present as methylated versions (Youngblood and Blumer, 1975). The health effect of particular concern from exposure to PAHs is cancer (IARC, 1987; U.S. EPA, 2005). It has been found that several methylated PAHs have a greater carcinogenic potential than the parent counterparts (Weis et al., 1998). Knowledge of the extent and rate of the primary removal processes would help assess the threat that these compounds pose to humans and ecosystems and could suggest effective detoxification strategies.

Biodegradation, the primary mechanism of PAH removal from the environment (NRC, 2003), is a complex process that involves action of microbial consortia on multiple substrates. Biodegradation of a specific component of a mixture can be strongly influenced by the other components. Modeling mixture effects requires knowledge of the metabolic role that each substrate plays for the microorganisms. The metabolic role is often expressed in terms of kinetic models relating microbial growth to substrate uptake. Kinetic modeling for microbial transformation of hydrocarbons has typically been based on the Monod model. Development of a sum Monod model, with or without any form of interaction between substrates, usually requires knowledge of the Monod parameters for the individual substrates (Reardon et al., 2002). Measurement of kinetic parameters for all compounds in a complex mixture of PAHs is not feasible due to the complexity of typical PAH mixtures. This chapter and the next (Chapter IV) examine the feasibility of QSBRs (Peijnenburg and Damborsky, 1996), which could reduce the need for experimental determination of biodegradability. QSBRs determine how the molecular structure and properties of PAHs influence their microbial metabolism.

To establish a sufficiently large training set of PAHs for QSBR development, microorganisms are needed that are able to degrade a wide range of PAHs. Kinetic experiments with mixed cultures are often a "black box" approach, in which kinetic parameters are assigned to the total biomass whose composition and activity may vary with time (Kovárová-Kovar and Egli, 1998). To avoid this complication and produce a consistent dataset, a simplistic approach was adopted that implemented the use of a single microorganism. Several microorganisms possess the enzymatic capability of degrading PAHs (Atlas, 1995). Members of the genus *Sphingomonas* have recently been

recognized for their ability to degrade a wide range of aromatic hydrocarbons. *Sphingomonas paucimobilis* strain EPA505, originally isolated from a bacterial community present at a creosote waste site (Mueller et al., 1989), was one of the first microorganisms found to utilize PAHs with more than three rings as the sole source of energy and carbon (Mueller et al., 1990). When induced with fluoranthene, EPA505 was able to metabolize several PAHs, including four- and five-ring forms (Ye et al. 1996; Siddiqi et al., 2002). A detailed discussion on the induction of EPA505 by different aromatic compounds can be found in a study by Story et al. (2000). A phylogenetic comparison of PAH-degrading bacteria from geographically diverse soils indicated that EPA505 is common in creosote- and fuel oil-contaminated soils (Mueller et al., 1997).

A limited number of studies reported the kinetics of PAH degradation by strain EPA505, often in the presence of surfactants (Ye et al., 1996; Lantz et al., 1997; Willumsen and Arvin, 1999; Barkay et al., 1999; Luning Prak and Pritchard, 2002; Siddiqi et al., 2002; Daugulis and McCracken, 2003). Only two (Luning Prak and Pritchard, 2002; Siddiqi et al., 2002) measured the zero- or first-order biodegradation rates for a limited number of PAHs, whereas others observed the percentage disappearance of PAHs. The majority of these studies focused on biodegradation of unsubstituted PAHs.

The objective of this study was to measure Monod-type kinetic parameters describing the biodegradation of select PAHs by *Sphingomonas paucimobilis* strain EPA505 and to determine which of the tested compounds can support growth individually. The focus was on priority PAHs containing up to 4 aromatic rings and commercially available methylated homologues; the larger PAHs, i.e., containing 5 and 6 rings, were not tested due to their low solubilities. A total of 20 PAHs were tested in the kinetic experiments; 22 PAHs were tested in the growth experiment. The kinetic experiments were designed to exclude bioavailability constraints by using initial substrate concentrations below solubility and account for unavailable PAH fractions in material balances. The resulting dataset reflects the influence of substrate molecular

structure on biodegradability and can be used in the development of QSBRs. It can also be used in modeling biodegradation of simple PAH mixtures.

MATERIALS AND METHODS

Chemicals

Acenaphthene (ACE), anthracene (ANT), fluorene (FLE), nutrient media, and Tween 80 were purchased from Sigma Chemical Co. (St Louis, MO). Acenaphthylene (ACY), 1-methylanthracene (1MANT), 1-methylfluorene (1MFLE), 1-methylphenanthrene (1MPHE), and 2-methylphenanthrene (2MPHE) were purchased from Ultra Scientific (North Kingstown, RI). 9-Methylanthracene (9MANT), fluoranthene (FLA), 1-methylnaphthalene (1MNAP), 1,5-dimethylnaphthalene (15DMNAP), 1,6-dimethylnaphthalene (16DMNAP), 2,3-dimethylnaphthalene (23DMNAP), 2,6-dimethylnaphthalene (26DMNAP), and pyrene (PYR) were purchased from Avocado Research Chemicals (Heysham, England). Naphthalene (NAP) and phenanthrene (PHE) were purchased from Alfa Aesar (Ward Hill, MA). 2-Methylnaphthalene (2MNAP) was purchased from Chem Service (West Chester, PA). 2,3,5-Trimethylnaphthalene (235TMNAP), 3,6-dimethylphenanthrene (36DMPHE), and 1-methylpyrene (1MPYR) were purchased from TCI America (Portland, OR). All PAHs were of the highest purity available, generally greater than 98%. The internal standard for PAH quantification via gas chromatography was a 1:1 mix of 20016 and GRH-IS purchased from Absolute Standards, Inc. (Hamden, CT) and AccuStandard, Inc. (New Haven, CT), respectively. The protein assay kit with Bovine Serum Albumin (BSA) as the standard was purchased from Bio-Rad (Hercules, CA). WST-1 was purchased from Roche Diagnostics (Indianapolis, IN).

Bacterium, culture conditions, and preparation of inocula

Sphingomonas paucimobilis DSM 7526 (strain EPA505) was purchased from DSMZ (Braunschweig, Germany). Cells grown on casein-peptone soymeal-peptone (CASO) broth were added to a sterile mineral salts base (MSB) containing 100 mg/L fluoranthene and 200 mg/L Tween 80 (Mueller et al., 1990). Tween 80 is a polyoxyethylene derivative of sorbitan esters used for dispersion of oils. Tween 80 at the

concentration used in this study does not inhibit the growth of EPA505 and does not serve as a carbon source (Story et al., 2000). The culture was incubated in the dark for 72 h at 30 ºC on a horizontal shaker operating at 160 rpm (Ye et al., 1996). Cells were washed once with MSB and resuspended in the same base. Autoclaved glycerol was added (10% by volume) to the suspension and aliquots were stored at -80 ºC until used as the inoculum for the biokinetic experiments. To grow biomass for the biokinetic experiments, 5 mL of the cryopreserved inoculum were added to 0.8 L nutrient broth supplemented with 0.4 g/L glucose (Ye et al., 1996). The culture was incubated at 30 ºC on a horizontal shaker (160 rpm) for 36 h. The suspension was centrifuged (RCF = 7500, 10 min) and cells were washed with Bushnell-Haas (BH) broth three times and then resuspended in 100 mL of the same medium. Biomass was added to batch reactors for biodegradation experiments immediately after measurement of the BSA concentration.

Kinetic modeling

Kinetic modeling of microbial biodegradation of PAHs has typically been based on the Monod equation:

$$-\frac{dC_L}{dt} = \frac{q_{\max} C_L}{K_S + C_L} X \tag{3.1}$$

where C_L is the substrate concentration in the liquid phase (μmol/L), $q_{\max}$ is the maximal specific biodegradation rate (μmol substrate mg^{-1} biomass h^{-1}), K_S is the affinity coefficient (μmol/L), and X is the biomass concentration (mg/L). At increased concentrations, some PAHs may become inhibitory. In this case, biodegradation kinetics can be described by the Andrews equation (Andrews, 1968):

$$-\frac{dC_L}{dt} = \frac{q_{\max} C_L}{K_S + C_L + C_L^2 / K_I} X \tag{3.2}$$

where K_I is an inhibition coefficient (μmol/L). The Andrews model is a generalized form of the Monod model that includes substrate inhibition. For $K_I \rightarrow \infty$, i.e., no inhibition, the two models become equivalent. Kinetic modeling in this study used the generic Andrews from (Eq. 3.2).

Kinetic behavior of a pure culture is not set, but depends in part on the culture history, as well as metabolic adjustments during a kinetic test (Kovárová-Kovar and Egli, 1998). Consistency in kinetic behavior is essential for data reproducibility and comparison of kinetics from different experiments or studies, as well as for the development of a consistent QSBR training set. Kinetic parameters obtained under low initial substrate-to-biomass ratios ($C_L^0 : X < 0.05$ by mass) are termed extant, whereas those obtained under high ratios, intrinsic (Grady et al., 1996). Intrinsic parameters depend on the type of bacterial culture, the nature of the substrate, and the environmental conditions. Extant conditions result in minimal cell growth and multiplication. Extant parameters reflect the physiological state of the biomass specific to the environment from which it originated and can better predict effluent quality of continuous reactors with respect to individual substrates (Ellis et al., 1996). Whether extant or intrinsic kinetics better describe biodegradation and predict the fate of organic compounds in engineered systems and the environment is not yet definitive (Kovárová-Kovar and Egli, 1998). In this study, all biokinetic measurements were conducted under extant conditions, in part because of low aqueous solubilities of most PAHs in the study, which dictate low aqueous substrate concentrations.

Estimation of Monod kinetic parameters follows two approaches. Classical methods directly fit the Monod equation or a linearized form of it to initial rate data at different substrate levels. Apart from the statistical drawbacks of linearization, a major disadvantage is that testing at a wide range of substrate concentrations is required, typically ranging from 0.5 to 10 $\cdot$ K_S (Eisenthal and Danson, 1992), which is not always feasible for sparingly-soluble compounds. The integral method involves integration of the Monod equation and curve fitting on data obtained from batch experiments. This method is appealing particularly when a large number of compounds require testing. The disadvantage of this method emanates from the fact that biokinetic parameters are correlated, resulting in difficulties in the estimation of unique values (Robinson, 1985). Nevertheless, establishing appropriate experimental conditions can result in sufficient

independence between the parameters. This study used the integral method to estimate the kinetic parameters of the Andrews equation.

Given that PAHs are lipophilic, sorption to the biomass can be significant. To evaluate kinetics of different PAHs on a common basis given the differences in lipophilicity, it can be assumed that any sorbed PAH is unavailable for cell uptake, at least in the case of Monod-type kinetic modeling. The total concentration, C_T, of the substrate in a liquid sample taken from a bioreactor is:

$$C_T = C_L + XK_bC_L \tag{3.3}$$

where K_b is the partition coefficient for the linear biosorption model. Abiotic losses can be modeled using a first-order loss coefficient, k_a. Details about biosorption and abiotic loss modeling are discussed in the corresponding paragraphs. Including biosorption and abiotic losses and assuming instantaneous partitioning, the substrate balance in a liquid sample becomes:

$$-\frac{dC_T}{dt} = \frac{q_{\max} C_T X}{K_S + \frac{C_T}{1+XK_b} + \frac{C_T^2}{K_I(1+XK_b)^2}} + k_a C_T \tag{3.4}$$

The biomass concentration is a function of substrate utilization according to:

$$dX = YdC_L - bXdt \tag{3.5}$$

where Y is the yield coefficient and b is the biomass first-order decay rate coefficient. Under extant kinetics and for short durations, the right-hand side of Eq. 3.5 becomes minimal and X in Eq. 3.4 can be assumed constant.

Kinetic parameters for each PAH were determined using best-fit simulations of Eq. 3.4 with a fourth-order Runge-Kutta algorithm. The algorithm performed integration of the equation over a series of time steps corresponding to the sampling events. Nonlinear regression was used to obtain best estimates of C_T^0, $q_{\max}$, K_S, and K_I from two independent duplicate reactors. Specifically, the sum of squared errors (*SSE*) based on n observations was minimized:

$$SSE = \sum_{j=1}^{n} (C_T^j - \hat{C}_T^j)^2 \tag{3.6}$$

where C_T^j is the observed total concentration in the *j*th sample and $\hat{C}_T^j$ is the corresponding concentration predicted by the model. Minimization of *SSE* was accomplished with the Solver function in Microsoft Excel (Microsoft Corporation, Redmond, WA). Uncertainties in the best estimates of C_T^0, $q_{\max}$, K_S, and K_I, expressed as the margins of error at the 95% confidence level, $E_{95\%}$, were calculated using the method of Smith et al. (1998). In brief, uncertainties were calculated using the mean square fitting error, s^2, and the inverse of a $p \times p$ matrix containing sensitivity coefficients quantifying the sensitivity of fit to changes in the best estimate of a parameter. The mean-square fitting error is defined as:

$$s^2 = \frac{SSE}{n - p} \tag{3.7}$$

where p is the number of fitting parameters (3 for non-inhibitory PAHs and 4 for inhibitory PAHs). The $E_{95\%}$ for the specific affinity, $q_{\max}/K_S$, was calculated from the $E_{95\%}$ for $q_{\max}$ and K_S using a propagation of error relationship for ratios.

Batch biokinetic experiments

Stock solutions of 20 PAHs were prepared in hexane to a typical concentration of 10000 mg/L. A volume of the hexane solution was added to a sterile 1-L amber bottle. After evaporation of hexane, 0.5 L of autoclaved BH broth was added to achieve the desired C_T^0 of 2.0 mg/L or 0.9 times the solubility of the PAH, whichever was smaller. The PAH solution was shaken in the dark for three days prior to each experiment to achieve full dissolution and to reach saturation of dissolved oxygen (DO). Duplicate reactors were prepared by transferring 150 mL of the PAH solution to each of two sterile 250 mL amber serum bottles with PFTE-coated caps. Reactors were shaken overnight to achieve equilibration between phases. To initiate biodegradation, approximately 2 mL of the concentrated biomass was added to each reactor to achieve $X \approx 4.0$ mg BSA/L. This was equivalent to approximately 60 mg dry cells per L, which satisfied the extant-kinetics condition for a maximum C_L^0 of 2.0 mg/L. Ten, or in some cases eleven, 7-mL samples were taken from each reactor at designated sampling times. Exact sampling

times and initial substrate and biomass concentrations were determined from preliminary experiments. Samples were added to 16-mL screw cap tubes with Teflon-coated caps containing 3 mL dichloromethane (DCM) and then shaken on a rotary shaker for at least 4 h. One mL of the DCM extract was removed with a glass pipette and added together with 10 μL internal standard to an autosampler vial for gas chromatography/mass spectrometry (GC/MS) analysis. A 5-mL sample was taken from each reactor at the beginning and at the end of each run for BSA measurement. At the end of each run, the dissolved oxygen concentration (DO) was measured in each reactor to check that DO had not been exhausted. Experiments were conducted at 22 °C. For each PAH, a single control reactor receiving autoclaved inoculum was treated identically, but substrate concentration was measured in 3 (beginning, middle, and end of a run) of the 10 samples.

Spectrophotometric phenanthrene uptake rate assay

It was not possible to measure biokinetic parameters for 20 PAHs in the same experiment. Consequently, a variable was necessary to account for variations in the extant activity of the biomass between experiments. For this purpose, a spectrophotometric phenanthrene uptake rate assay measuring the specific uptake rate at a given substrate level was performed with each experimental run. The assay was based on the method of Stringfellow and Aitken (1995). An amount of a PHE solution (4.5 μmol/L) in BH broth was added to a 4-mL quartz cuvette. The solution was inoculated with approximately 50 μL of the same biomass used in the biokinetic experiments to a final volume of 3.0 mL and $X \approx 4.0$ mg BSA/L. The cuvette was capped and immediately placed in an HP 8452 UV-Visible spectrophotometer (Agilent Technologies Inc., Palo Alto, CA). The suspension in the cuvette was mixed by a PTFE stir bar and micromagnetic stirrer. Absorbance at 250 nm (A_{250}) was measured automatically every 9-10 s for 10 min and was converted to phenanthrene concentration by using an extinction coefficient of 6.46 10^{-2} L μmol^{-1} cm^{-1}. At the end of the assay, 2.5 mL were taken from the cuvette for BSA analysis. The assay was performed in triplicate. Blank cuvettes contained a cell suspension as above but without PHE. The extant

activity, q_e, was estimated as the specific uptake rate at 3.6 μmol/L expressed in μmol mg^{-1} BSA min^{-1}. Estimation involved polynomial regression and calculation of the slope of the uptake curve at the selected concentration (Eisenthal and Danson, 1992). Negligible uptake was observed in the presence of a suspension of killed cells. It was found that the assay was sensitive enough to detect differences in activity of biomass harvested at different growth stages. However, no significant correlation could be established between these differences and biokinetic parameter values obtained when using biomass harvested at different stages.

Quantification of bacterial growth on PAHs

An experiment was conducted to test the ability of different PAHs to serve as sole energy and carbon sources. In addition to the 20 PAHs tested in the biokinetic experiments, two extra PAHs, 16DMNAP and 9AMNT, were tested. The procedure was based on a method developed to detect growth of EPA505 and other bacterial strains on various PAHs (Johnsen et al., 2002; Johnsen, 2004). In principle, cells were allowed to grow in a solution containing excess PAH as the sole energy and carbon source and then an assay was used to quantify cell proliferation and viability based on the reduction of 4-[3-(4-Iodophenyl)-2-(4-nitrophenyl)-2H-5-tetrazolio]-1,3-benzene disulfonate (WST-1) by mitochondrial dehydrogenases in viable cells. It has been argued that this method is more suitable for PAHs compared to standard growth assays because it can reliably quantify growth despite the low solubility and bioavailability of the PAHs (Johnsen et al., 2002). Strain EPA505, induced with fluoranthene as described above, was grown to the late exponential phase in phosphate minimal medium (PPM) supplemented with 1.0 g/L glucose and glycerol (Johnsen et al., 2000). Cells were washed once in PPM and resuspended in the same medium to A_{540} = 0.4. A volume of a PAH solution in hexane (typically 10.0 mg/mL) containing 0.7 mg of the PAH was added to a semi-micro methyl acrylate cuvette. Cuvettes receiving pure hexane were used as controls. Hexane was allowed to evaporate in a laminar flow hood. After evaporation, each cuvette received 1.4 mL PPM and 70 μL of the cell suspension. Cuvettes were capped and incubated in the dark at 22 ºC for 10 days. After incubation, cuvettes received 350 μL of an electron

donor solution (16.6 mM of each of glucose, pyruvate, and succinate in 40 mM Tris buffer, pH = 6.5) and 70 μL WST-1 reagent. Absorbance was measured immediately at 450 nm with a reference wavelength of 630 nm (net A_{450}). Cuvettes were capped and incubated on a shaker table (300 rpm) at 22 ºC for 6 h. After 6 h, net A_{450} was measured again and the change in net absorbance, Δ(net A_{450}), was calculated as a measure of cell growth. All PAHs and the control were tested in triplicate. WST-1 reduction in cuvettes receiving PAHs was compared to reduction in the control using a one-tail *t*-test.

Measurement of biosorption partition coefficients

A method developed to measure equilibrium partition coefficients, K_b, for the sorption of PAHs, primarily PHE, to bacterial biomass (Stringfellow and Alvarez-Cohen, 1999) was followed. Partition coefficients were measured for 11 PAHs. Anticipating a relationship between K_b and hydrophobicity (Sikkema et al., 1994), the 11 selected PAHs represented the whole range of the octanol/water partition coefficient, K_{ow}, values observed in the biokinetic experiments. Cells were grown and harvested as described for the biokinetic experiments. After washing with BH broth, the cell suspension was concentrated to 100 mL with $X \approx 1500$ mg BSA/L and treated with 5 mL formalin (37% formaldehyde) to start inactivation of the cells. Stock solutions of the 11 PAHs were prepared in BH broth to a concentration of 2.0 mg/L or 0.9 times the solubility, whichever was smaller. Portions of the stock solutions were diluted five and ten times. A volume of 39 mL from each concentration level was transferred to each of four 40-mL glass EPA vials. Of the four vials, two (duplicate treatments) received 2.1 mL formalin, and 0.7 mL cell suspension, while the others (duplicate controls) were treaded identically but received 0.7 mL of BH broth instead of the cell suspension. Formalin was used to prevent biodegradation by inactivating the cells. The target concentration of formaldehyde in each vial was 1.9%. It was found that use of formaldehyde did not significantly affect sorption of PAHs by different strains (Stringfellow and Alvarez-Cohen, 1999). Duplicate treatments contained biomass at a target concentration of 26.0 mg/L as BSA. The zero-headspace EPA vials were sealed with PTFE-lined caps and shaken at 25 ºC for 72 h. After 72 h, a 5-mL sample from each

EPA vial was transferred to a 16 mL screw cap tube with PTFE-coated cap containing 3 mL DCM for liquid-liquid extraction. Also, approximately 30 mL were transferred from each EPA vial to a solvent-washed, high-strength glass centrifuge tube to zero headspace. Centrifuge tubes were sealed with PTFE-lined caps and were centrifuged at RCF = 13100 for 15 minutes. After centrifugation, a 7-mL sample was taken and extracted in DCM. Liquid-liquid extractions and GC/MS measurements were performed as described for the biokinetic experiments. A 2.5-mL sample was taken from the remaining liquid of each EPA vial for BSA measurement. The difference in PAH concentration before and after centrifugation was a measure of the PAH sorbed on the biomass. Data from the controls were used to account for PAH losses from the liquid phase due to processes other than biosorption. Linear sorption isotherms were fitted to relate the equilibrium concentration on the solid phase, Q_e (mg/g BSA), to the equilibrium concentration in the liquid phase, C_L^e (mg/L). The partition coefficient, K_b (L/g BSA), was calculated as the slope of a linear isotherm. After all partition coefficients were calculated, a linear regression was applied to relate the logarithm of K_b to the logarithm of K_{ow}. The regression equation was used to estimate K_b values for the 9 remaining PAHs of the biokinetic experiments.

A separate experiment was performed to determine whether shorter equilibration periods result in significant differences in partition coefficients. The reason was that the 3-day equilibration period suggested by Stringfellow and Alvarez-Cohen (1999) was significantly longer than the timeframe of the biokinetic experiments described in this study, in which instantaneous sorption was assumed for modeling. The additional biosorption experiment for NAP and PYR, two PAHs at the opposite ends of the hydrophobicity range of interest, allowed equilibration for only 45 minutes.

Measurement of abiotic loss rate coefficients

An independent experiment was performed to quantify abiotic losses from the bioreactors. Abiotic losses were modeled as first-order processes and first-order rate coefficients, k_a (h^{-1}), were determined (Smith et al., 1997; Knightes and Peters, 2000). It was assumed that abiotic losses were mostly due to volatilization; therefore only NAP,

1MNAP, 2MNAP, ACE, and FLE, the most volatile compounds based on their Henry's law constants, were tested. Compounds were tested in duplicate, as in the biokinetic experiments, but without the addition of biomass. From each reactor, 10 samples were taken every hour for 9 hours. Linear regressions between $\ln C_T$ and time were fitted to calculate the rate coefficients.

Analytical procedure

Gas chromatography measurements were conducted on a HP 5890 Series II chromatograph interfaced with an HP 5972 mass selective detector (Agilent Technologies Inc., Palo Alto, CA). The type of the column was HP-5MS ((5%-Phenyl)-Methylpolysiloxane, 0.25 mm × 30 m × 0.25 μm, J&W Scientific (Palo Alto, CA)). The following temperature program was used: 60 ºC, 8.0ºC/min for 30 min to 300 ºC. The mass spectrometer was operated in the selective ion mode (SIM). The quantitation limit of the method was 0.001 mg/L.

RESULTS AND DISCUSSION

Biosorption experiment

The results of the biosorption experiment are illustrated in Fig. 3.1. ANOVA showed that the assumption of a linear isotherm was valid. The partition coefficients ranged from 6.0 ± 0.8 for NAP to 256.5 ± 46.3 for PYR, in units of L/g BSA, with the uncertainty being equal to $E_{95\%}$. A linear relationship was observed between $\log K_{ow}$ and $\log K_b$, which was used to determine K_b for the rest of the PAHs in the study. The relationships had the following expression:

$$\log K_b = 0.98(\pm 0.36) \cdot \log K_{ow} - 2.71(\pm 1.55) \qquad (3.8)$$

with the uncertainty in the coefficients expressed as the $E_{95\%}$. In addition, the partition coefficient for NAP at 45 min and at 72 h was 7.1 ± 1.5 L/g BSA and 6.0 ± 0.8 L/g BSA, respectively. The same values for PYR were 298.6 ± 66.6 and 256.5 ± 46.3 L/g BSA. These results show that the shorter equilibration time did not significantly affect the values of the partition coefficients. Therefore, use of the partition coefficients determined after the 3-day equilibration was appropriate for the kinetic modeling and the assumption of instantaneous partitioning was realistic. A definitive verification of the

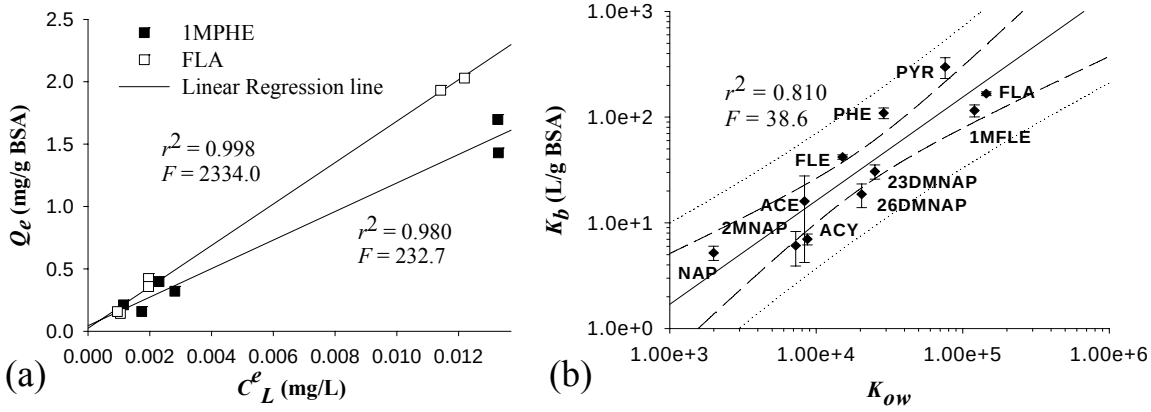

Fig. 3.1. Fitting of linear sorption isotherms for the calculation of the biomass partition coefficients, K_b.(a) A regression was performed between the measured K_b values and the octanol/water partition coefficient, K_{ow}. (b) The dashed lines and the dotted lines represent the 95% confidence intervals and prediction intervals, respectively. Error bars represent standard errors.

instantaneous partitioning assumption would involve measurements of the kinetics of partitioning and their comparison to the biodegradation kinetics. Use of partition coefficients in kinetic modeling significantly decreased the estimates of $q_{\max}$ and K_S while leaving their ratio unaffected. The scale of this effect increased with higher K_b values; for instance, estimates of $q_{\max}$ and K_S for 1MPYR decreased by more than 100% when K_b was included in the kinetic model.

Abiotic losses experiment

ANOVA indicated that the hypothesis of a first-order abiotic loss rate was valid. The first-order abiotic loss coefficient, k_a, was found to be 0.016 ± 0.023 for NAP, 0.031 ± 0.016 for 1MNAP, 0.030 ± 0.022 for 2MNAP, 0.028 ± 0.009 for ACE, and 0.006 ± 0.019 for FLE, all in h^{-1}. As the data shows, k_a was not significantly different from zero for NAP and FLE; therefore, it was not used in the estimation of the biokinetic parameters for those two compounds.

Biokinetic experiments

No significant changes in the biomass concentration, X, were observed during the biokinetic experiments and negligible changes were random and not indicative of

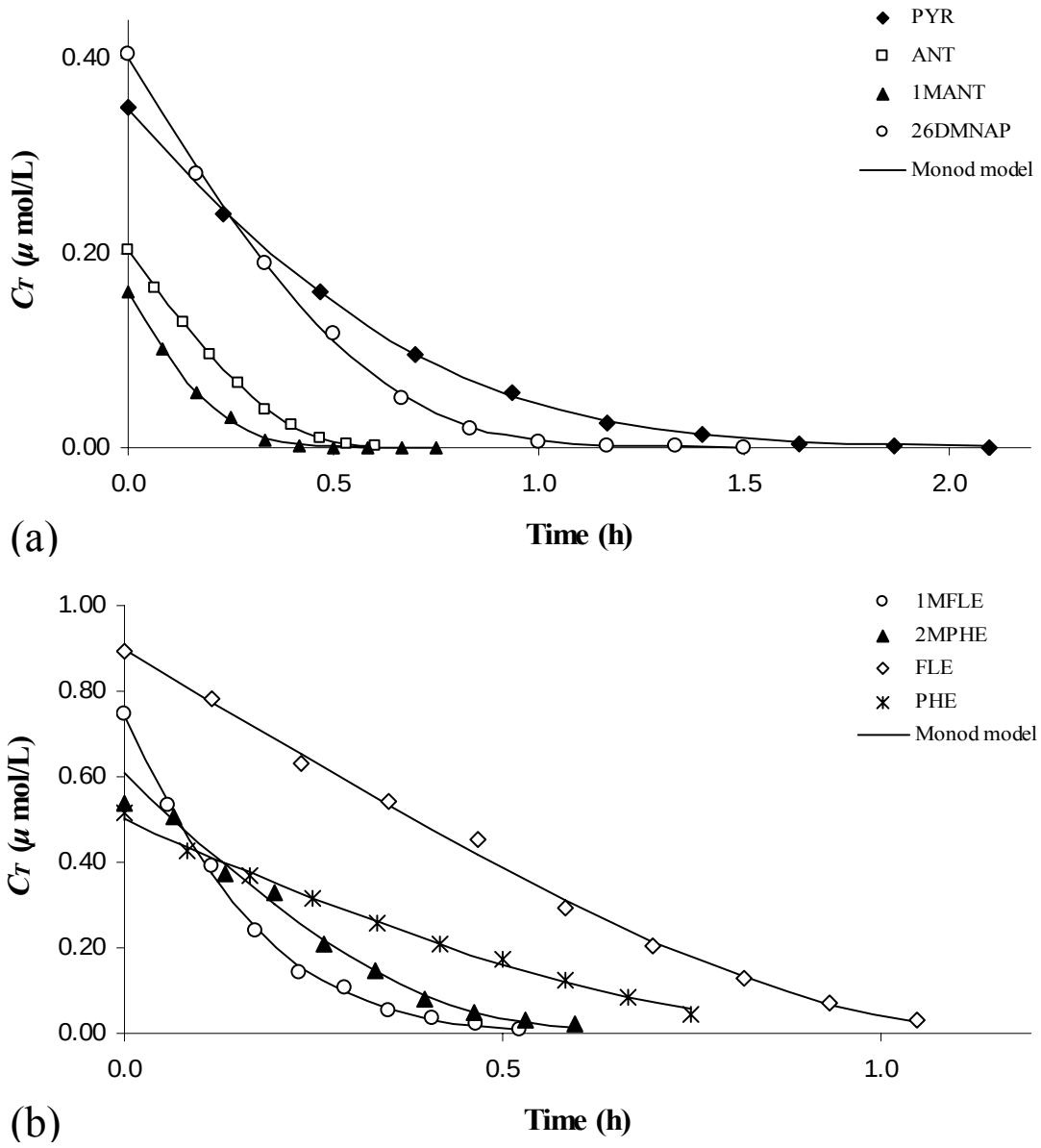

Fig. 3.2. Biodegradation of select PAHs by *Sphingomonas paucimobilis* strain EPA505. Estimation of kinetic parameters was accomplished by fitting an integrated form of the Monod model (curves) to the data (symbols) from batch bioreactors. Compounds are distributed into graphs (a) and (b) according to C_T^0. Compound abbreviations are explained in the Materials and Methods section.

bacterial growth. The lowest DO measured at the end of a run was 6.5 mg/L suggesting that no oxygen limitations occurred that could influence kinetic estimates. Liquid temperature measured in all bioreactors at the end of each run ranged from 22 to 23 °C. No significant degradation was observed in the presence of autoclaved cells.

Strain EPA505 was able to degrade all 20 PAHs, which is consistent with its ability to degrade several four- and five-ring PAHs (Ye et al., 1996; Siddiqi et al., 2002). Biodegradation was also rapid. Assuming first order kinetics for the sake of illustration, the characteristic time of biodegradation ranged from approximately 4 minutes for ANT and 2MPHE to 15 minutes for ACE and 1MPYR with a mean value of 7 minutes. The ability of strain EPA505 to metabolize a wide range of PAHs may be indicative of loose specificity of initial dioxygenases. It may also be related to the fact that strain EPA505 possesses glutathione-*S*-transferase (GST) activity (Lloyd-Jones and Lau, 1997) that may protect it from oxidative damage from PAH metabolites.

The Monod or Andrews model successfully simulated the experimental data. Depletion data and model fitting are illustrated in Fig. 3.2 and Fig. 3.3 for select PAHs. Estimated biokinetic parameters are summarized in Table 3.1. Consistency in depletion curves and parameter estimates between independent duplicate reactors indicated that experimental conditions and parameter estimates were reproducible. Each aspect of the results is discussed separately in the following paragraphs.

The maximal specific biodegradation rate, q_{max}, ranged from 0.01 ± 0.00 for 1MPYR to 2.19 ± 0.07 for 2MNAP in units of μmol mg^{-1} BSA h^{-1}. In the case of NAP, FLE, and PHE and 2MPHE, presence of a methyl group resulted in a higher q_{max} compared to the parent compound. This is consistent with the findings of Siddiqi et al. (2002). However, as illustrated by the NAP and PHE homologues, presence of a second methyl group resulted in a significant decrease in degradation rates. Decreased activity as a result of alkylation is often attributed to steric hindrance of the substrate-enzyme interaction or to decreased flux of the substrate to the cell interior (Bressler and Gray, 2003). However, it is possible for methylation to increase bioavailability of high-molecular-weight PAHs and potentially enhance their biodegradation rates.

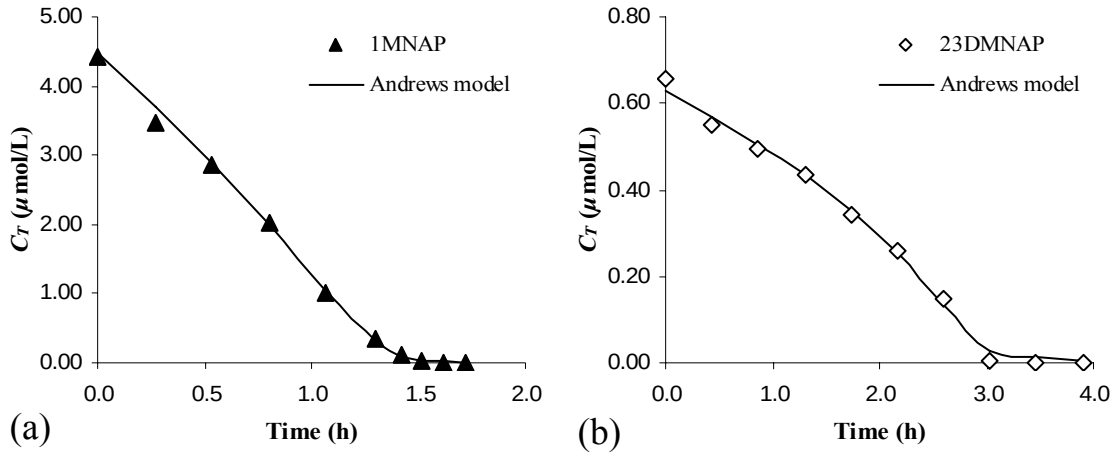

Fig. 3.3. Biodegradation of two PAHs exhibiting substrate inhibition. Of the 20 PAHs tested, only 1-methylnaphthalene (1MNAP, graph A), 2-methylnaphthalene, and 2,3-dimethylnaphthalene (23DMNAP, graph B) exhibited inhibitory behavior, which was manifested as an increase in the slope of the depletion curve with time.

Estimation of the affinity coefficient, K_S, from batch depletion curves often presents considerable challenges. Specifically, when $C_L^0 >> K_S$ model fitting becomes insensitive to changes in K_S. Consequently, estimation of K_S can be inaccurate (Kovárová-Kovar and Egli, 1998). In contrast, for $C_L^0 : K_S < 0.1$, $q_{\max}$ and K_S cannot be estimated uniquely; good separation between the two parameters occurs at $C_L^0 : K_S \geq 1.0$ (Ellis et al., 1996). Good separation also depends on the number of observations and the quality of the data (Knightes and Peters, 2000). Based on results from preliminary runs, kinetic experiments were designed such that C_L^0 was greater than the expected K_S. In addition, data quality was ensured by retesting compounds for which depletion data was insufficient. The experiments described in this study satisfied the above conditions for all PAHs. K_S ranged from 0.01 ± 0.01 μmol/L for 1MPYR to 1.35 ± 0.55 and 1.27 ± 0.28 μmol/L for 2MNAP and 1MNAP, respectively. Data suggests that K_S generally decreases with molecular size and, in the case of methylated naphthalenes, degree of methylation. This can be translated into increased affinity for the substrate with

Table 3.1
Estimated biokinetic parameter values for 20 PAHs. PAHs are grouped into families in order of their MW. Uncertainty is expressed as the margin of error at the 95% confidence level.

Comp.	Sol.[a]	C_T^0	q_{max}	K_S	q_{max}/K_S	K_I
	(μmol/L)	(μmol/L)	(μmol mg^{-1} h^{-1})	(μmol/L)	(L mg^{-1} h^{-1})	(μmol/L)
NAP	241.8	12.11 ± 0.07	1.11 ± 0.02	0.62 ± 0.09	1.80 ± 0.26	
1MNAP	181.4	4.49 ± 0.07	1.84 ± 0.05	1.27 ± 0.28	1.45 ± 0.33	1.40 ± 0.03
2MNAP	173.0	2.39 ± 0.07	2.19 ± 0.07	1.35 ± 0.55	1.64 ± 0.60	0.50 ± 0.02
15DMNAP	17.54	0.56 ± 0.01	0.39 ± 0.06	0.34 ± 0.08	1.16 ± 0.30	
23DMNAP	12.74	0.63 ± 0.01	0.53 ± 0.06	0.31 ± 0.12	1.74 ± 0.67	0.05 ± 0.00
26DMNAP	12.80	0.40 ± 0.01	0.18 ± 0.02	0.12 ± 0.02	1.56 ± 0.35	
235TMNAP	28.07	0.18 ± 0.00	0.07 ± 0.01	0.03 ± 0.01	2.18 ± 0.57	
ACE	25.29	0.37 ± 0.00	0.29 ± 0.02	0.37 ± 0.04	0.79 ± 0.10	
ACY	105.78	13.96 ± 0.15	0.87 ± 0.03	0.70 ± 0.19	1.24 ± 0.34	
FLE	11.37	0.90 ± 0.02	0.32 ± 0.03	0.10 ± 0.04	3.11 ± 1.11	
1MFLE	6.05	0.74 ± 0.01	1.51 ± 0.21	0.53 ± 0.10	2.86 ± 0.66	
ANT	0.24	0.21 ± 0.00	0.19 ± 0.01	0.04 ± 0.01	4.56 ± 0.73	
1MANT	1.28[b]	0.16 ± 0.00	0.14 ± 0.02	0.05 ± 0.01	2.70 ± 0.60	
PHE	6.45	0.50 ± 0.01	0.18 ± 0.02	0.09 ± 0.03	2.09 ± 0.79	
1MPHE	1.40	0.44 ± 0.01	0.14 ± 0.02	0.04 ± 0.02	3.24 ± 1.44	
2MPHE	1.46	0.61 ± 0.02	0.54 ± 0.10	0.15 ± 0.06	3.73 ± 1.56	
36DMPHE	0.35[b]	0.08 ± 0.00	0.05 ± 0.01	0.03 ± 0.01	1.56 ± 0.36	
FLA	1.29	0.70 ± 0.02	0.20 ± 0.02	0.07 ± 0.03	2.96 ± 1.16	
PYR	0.67	0.34 ± 0.01	0.16 ± 0.03	0.15 ± 0.04	1.10 ± 0.31	
1MPYR	0.27[b]	0.08 ± 0.00	0.01 ± 0.00	0.01 ± 0.01	0.82 ± 0.50	

[a] Aqueous solubility values, taken from Howard and Meylan (1997) and converted into μmol/L.
[b] Estimated according to the method of Meylan et al. (1996).

increasing substrate hydrophobicity. Indeed, a significant correlation (r = 0.76) was found between logK_{ow} and log(1/K_S). In other words, a degradative enzyme or another receptor, e.g., a membrane transporter, has an increased affinity for more hydrophobic compounds.

Due to the correlation between $q_{\max}$ and K_S at low concentrations, unique estimates of these parameters are not always accurate. For this reason, the specific affinity, defined as the ratio q_{max}/K_S, was calculated for all PAHs. It has been argued that the specific affinity is a better measure of degradation kinetics (Healy, 1980). Another

advantage of this parameter is that it is independent of biosorption. Numerical analysis showed that estimates of the specific affinity were consistent, even when the algorithm converged to unrealistic estimates for q_{max} and K_S. Specific affinity estimates are presented in Table 3.1. Values ranged from 0.79 ± 0.10 for ACE to 4.56 ± 0.73 for ANT, in units of L mg^{-1} BSA h^{-1}. No trend was evident in the specific affinity variation as a function of molecular size or degree of methylation.

Of the 20 PAHs of the biokinetic experiment only 3 exhibited inhibitory behavior, namely 1MNAP, 2MNAP, and 23DMNAP. Substrate inhibition was manifested as an increase in the depletion rate with decreasing substrate concentrations (Fig. 3.3). Since kinetic modeling used the generic Andrews model, an inhibition coefficient, K_I, was estimated for every PAH in the study. It was found that K_I values above $15 \cdot C_T^0$ did not significantly affect the model fit, and thus these values were omitted. Estimation of K_I is particularly challenging because it is influenced by C_L^0, whose selection depends on K_S. Lack of inhibition evidence does not preclude inhibition (and existence of a K_I) at higher concentrations; however, at low C_L^0, modeling of q_{max} and K_S is insensitive to the presence or absence of a K_I. The value of K_I was 0.05 ± 0.00 for 23DMNAP, 0.50 ± 0.02 for 2MNAP, and 1.40 ± 0.03 for 1MNAP in units of μmol/L. The data may indicate that a methyl substituent on carbon 2 of naphthalene is responsible to substrate inhibition; however, no toxicity was evident for 26DMNAP and 235TMNAP at the concentrations tested.

Spectrophotometric activity assays

A typical uptake curve from the activity assays is presented in Fig. 3.4. There was no statistically significant difference in the biomass extant activity between the six experimental runs. The average extant activity of the biomass, q_e, was 0.015 ± 0.001 μmol PHE mg^{-1} BSA min^{-1} with the uncertainty representing the $E_{95\%}$. Also, biomass stored at room temperature maintained its activity level for at least 3 h. Kinetic parameters for 2MPHE, FLA, and PYR were consistent when measured in separate experiments (see Results in Chapter V). The consistent kinetic behavior does not support the claim that small differences in activity of separate batches of cells degrading

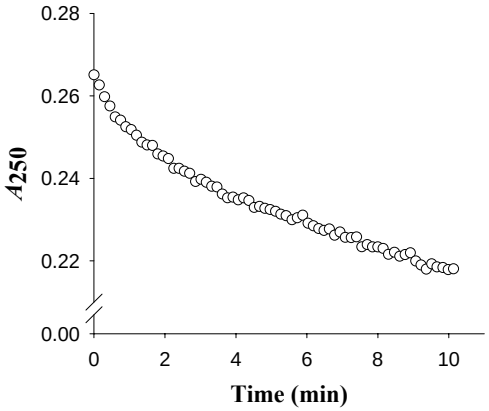

Fig. 3.4. Spectrophotometric phenanthrene uptake rate assay. The assay was performed with each experiment to test the extant activity of the biomass. A_{250} was measured every 9-10 s and converted to concentration using an extinction coefficient. The specific uptake rate at 3.60 μmol/L (equivalent to A_{250} = 0.23) was used as a measure of the biomass activity. The rapid initial uptake rate is believed to be the result of biosorption and intake.

PAHs are an inherent characteristic of strain EPA505 (Luning Prak and Pritchard, 2002). Uptake rates from the activity assays, q_e, were approximately 5 times greater than the PHE $q_{\max}$ estimated in the biokinetic experiments. Biokinetic experiments recorded kinetics of PHE depletion from all phases, including cell interior, governed by the rate-limiting mechanism- cell permeation or enzymatic transformation. Conversely, the spectrophotometric assay recorded kinetics of PHE disappearance from the aqueous phase, which is governed by biosorption and cell permeation. Assuming that cell permeation is the rate-limiting step in PHE degradation, as discussed in Chapter IV, the difference between $q_{\max}$ and q_e for PHE must be attributed to biosorption. Despite the difference in the governing processes, and assuming that biosorption is invariable, q_e is an adequate indicator of biomass activity. As discussed by Button (1985), the transport capacity of microorganisms is inducible and it is a reflection of the physiological state.

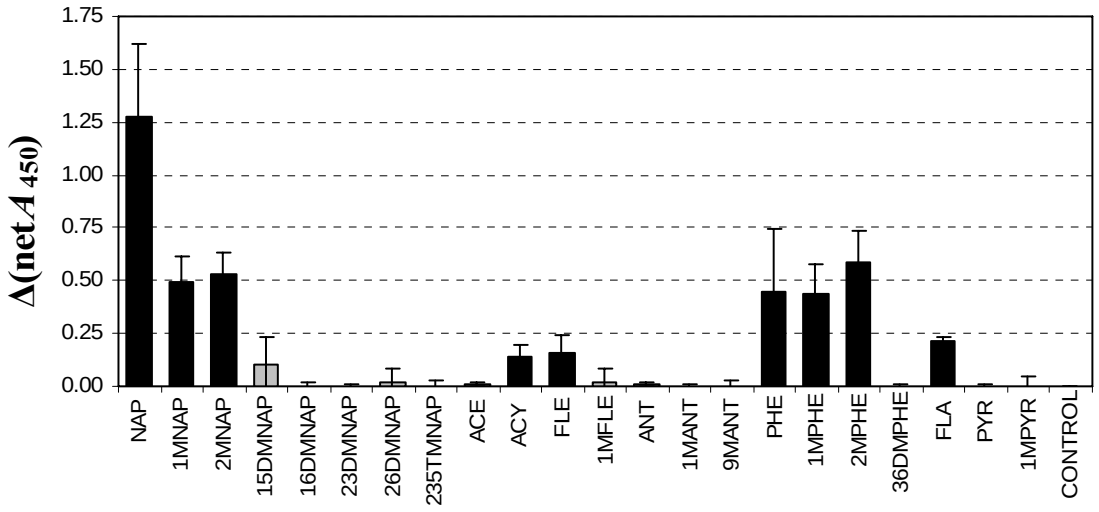

Fig. 3.5. Quantification of growth of strain EPA505 on 22 PAHs using the respiration indicator WST-1. Δ(net A_{450}) denotes the difference in net absorbance of WST-1 formazan at 6 h. Black columns show positive growth, while grey columns negative growth, based on one-tail *t*-test. The error bars represent the margins of error at the 95% confidence level.

Growth experiment

Of the 22 PAHs tested, 9 supported growth as determined by the WST-1 assay (Fig. 3.5). These included NAP and the two monomethylated homologues, PHE and two monomethylated homologues, ACY, FLE, and FLA. Based on these results, 13 PAHs in this study were degraded cometabolically. The fact that FLA, a four-ring PAH, can support growth of strain EPA505 was verified. It was also found that NAP supported the highest growth and that methylation inhibited or prevented growth. For instance, none of the di- or trimethylnaphthalenes supported growth and the same was found for the dimethylphenanthrene. The results of this study agree with the results of Johnsen et al. (2002) for ANT and PYR; however, it was found that PHE supported higher growth than FLA and not the opposite. This is consistent with the findings of Ho et al. (2000) who used visible color change and changes in absorbance as a measure of growth. The results of this study are also in agreement with the results of Story et al. (2004) for five PAHs (PHE, NAP, FLA, ACE, and PYR), but not for ANT and FLE. Differences between the

results of this study and the results of Johnsen et al. (2002) and Story et al. (2004) is possibly attributed to the induction of strain EPA505 by FLA in consistency with the biokinetic experiments. No significant correlations were found between Δ(net A_{450}) and any of the biokinetic parameters, which means that the ability of PAHs to support growth of strain EPA505 is not related to biodegradation kinetics.

This study reports reliable experimental coefficients describing biodegradability of unsubstituted and methylated PAHs by *Sphingomonas paucimobilis* strain EPA505. The strain was able to degrade all PAHs of interest. The considerable variability in the observed kinetic and growth parameters signifies the influence of chemical structure on PAH biodegradability. The data can be used in modeling biodegradability of simple PAH mixtures (Chapter V) and as the training set for the development of QSBRs (Chapter IV). QSBRs can give insight into the fundamental molecular properties and processes that govern biodegradation and reduce the need for experimental biodegradability studies.

CHAPTER IV
DEVELOPMENT OF QUANTITATIVE STRUCTURE-BIODEGRADABILITY RELATIONSHIPS FOR UNSUBSTITUTED AND METHYLATED POLYCYCLIC AROMATIC HYDROCARBONS

OVERVIEW

Quantitative structure-biodegradability relationships (QSBRs) were developed for parameters describing biodegradability of polycyclic aromatic hydrocarbons (PAHs) by *Sphingomonas paucimobilis* strain EPA505. The training dataset contained values of the following Monod-type kinetic parameters: the maximal specific biodegradation rate, q_{max}, the affinity coefficient, K_S, and the specific affinity, q_{max}/K_S, as well as values of Δ(net A_{450}), a measure of microbial growth on individual PAHs. The Cerius^2 modeling environment was used to develop the QSBRs. A genetic function approximation (GFA) algorithm generated a set of regression equations between a series of molecular descriptors and a biodegradability parameter. Statistical analysis and validation testing confirmed the validity and predictive power of the final QSBRs. Molecular descriptors related to spatial and topological features were essential in explaining biodegradability. Evaluation of the biodegradability data showed that q_{max} correlated well with transmembrane flux as theoretically estimated by a simple partitioning model, pointing to membrane transport as the rate-determining process in the biodegradation of the majority of tested PAHs. A kinetic experiment in the presence of azide, a membrane protein inhibitor, suggested that the transport mechanism can be either simple or facilitated diffusion, depending on the PAH. A mechanistic interpretation of the developed QSBRs and analogies drawn between the QSBRs and binding and solvation models also suggested membrane binding-and-transport as the limiting process. This study demonstrates the value of QSBR not only as a predictive tool, but also as a method to understand the basic properties and processes that govern biodegradation at the molecular level.

INTRODUCTION

Quantitative structure-activity relationships (QSARs) and other similar models express the effects of molecular structure and properties on the behavior of chemical compounds. As such, they are important in assessing the environmental distribution, fate, and harmfulness of pollutants. The predictive value of QSARs is evident for large and diverse classes of chemicals for which experimental data is limited. In the case of PAHs, models are available for PAH toxicity (Govers et al., 1984; Braga et al., 2000; Marino et al., 2002) and physicochemical properties (Ferreira, 2001; de Lima Ribeiro and Ferreira, 2003; Abraham et al., 2005), but not for biodegradability. The need for QSBRs is apparent considering the importance of microbial degradation in PAH fate in the environment (NRC, 2003).

Attempts to model the biodegradability of a group of homologues based on molecular structure have been made as early as 1966 (Alexander and Lustigman, 1966). However, the number of available QSBRs is low compared to that of other QSARs. Reluctance in developing QSBRs is related to our limited understanding and complexity of the biodegradation process (Damborsky and Schultz, 1997), as well as the variability and inconsistencies in biodegradation data. Advances in molecular simulation, molecular descriptors, and statistical algorithms, and their incorporation in user-friendly software packages has encouraged the development of QSBRs not only as predictive tools, but as a method to understand the basic properties and processes that govern biodegradation at the molecular level. Certainly, biodegradability of pollutants in the environment is not only dependent on chemical structure, but also on environmental conditions, including the presence of microorganisms capable of degrading the pollutants.

The objective of this study was to develop QSBRs describing biodegradability of common PAHs consisting of low-molecular-weight, unsubstituted, and methyl-substituted homologues. Development was based on the dataset generated in Chapter III on the biodegradability of select PAHs by *Sphingomonas paucimobilis* strain EPA505. The dataset contains values of three Monod-type kinetic parameters: the maximal specific degradation rate, q_{max}, the affinity coefficient, K_S, and the specific affinity,

q_{max}/K_S, as well as values of the change in net absorbance at 450 nm due to the reduction of a formazan salt, Δ(net A_{450}), a measure of bacterial growth on individual PAHs. Standard biological equilibrium constants and standard rate coefficients are appropriate for QSAR analysis because they relate to free energy changes of biochemical reactions (Selassie, 2003). Δ(net A_{450}) is also appropriate because it is pertinent to a quantifiable feature of a biochemical reaction, e.g. a stoichiometric coefficient. While QSAR development for Michaelis-type coefficients of enzymatic reactions is common (Carotti et al., 1988; Compadre et al., 1990; Lewis et al., 1998; Ekins et al., 1999; Bundy et al., 2000), the great majority of QSBRs in the literature were built for first-order degradation coefficients. In fact, there is only one study that developed QSBRs for Monod coefficients (Pitter, 1985). Apart from that, QSBRs are often trained on data compiled from different studies, introducing considerable uncertainty due to inherent inconsistencies that greatly reduce the interpretive and predictive power of the models. In this work, a consistent dataset was used to develop four individual QSBRs corresponding to the biodegradability parameters q_{max}, K_S, q_{max}/K_S, and Δ(net A_{450}). The generated models were evaluated on a statistical and mechanistic basis to reveal specific processes governing the biodegradability of PAHs by strain EPA505.

METHODS AND MATERIALS

Development and evaluation of QSBRs

The dataset generated in Chapter III contains values of three Monod-type kinetic coefficients for 20 PAHs. It also contains Δ(net A_{450}) values for 22 PAHs. Explanation of biodegradability parameters and compound abbreviations can be found in Chapter III. The first step in the development of QSBRs involved statistical evaluation and preparation of the data with SPSS 12.0 (Chicago, IL, USA). Structure-activity relationships are more meaningful when built on normally distributed data. Skewness and kurtosis values of the data distributions showed that q_{max}, K_s, and q_{max}/K_S were skewed, which is usual for biological data. Logarithmic transformation was used to normalize the data. Nonzero values of Δ(net A_{450}) were nearly normally distributed

making transformation unnecessary. Standard z-score values of $\log q_{max}$ detected 1MPYR as a univariate outlier ($z < 2.5$).

The Cerius^2 4.9 molecular simulation package (Accelrys Inc., San Diego, CA) was used for QSBR development. Molecules were imported to Cerius^2 as structure SD files. The energy of molecules was minimized using a CFF91 open forcefield that is suitable for aromatic hydrocarbons (Maple et al., 1994). A training set was created by entering the molecular structures and the corresponding biodegradability data to a table. Addition of molecular descriptors to the table involved simultaneous calculation of the descriptor values for each molecule. Quantum mechanical descriptors were calculated by MOPAC7, built in Cerius^2, using the PM3 semi-empirical Hamiltonian (Stewart, 1989). All meaningful descriptors from Descriptor+, a module in Cerius^2, were added to the study table. Descriptor values calculated by Cerius^2 were in agreement with standard values for PAHs from Mackay et al. (1992), Mallard and Linstrom (2000), Jinno Lab (1996), Bjørstedth (1983), and Karcher (1985). Also, when comparison was possible, values coincided with those reported by de Lima Ribeiro and Ferreira (2003). It was found that descriptors calculated by MOPAC7 were more accurate than those calculated by other methods in Cerius^2, e.g., CNDO/2 (Pople and Segal, 1966) for the energy of the highest occupied molecular orbital, and MNDO (Dewar and Thiel, 1977) for the heat of formation. Therefore, descriptor values calculated by an algorithm in addition to MOPAC7 were discarded from the training set. Experimental values of the octanol/water partition coefficient, $\log K_{ow}$, from Howard and Meylan (1997) were used instead of the values calculated by Cerius^2. The final training set contained 41 descriptors from the following categories: conformational, electronic, informational, quantum mechanical, spatial, structural, thermodynamic, and topological. Definitions of these categories and individual descriptors are provided in the manual of Cerius^2 and the references therein (Accelrys Inc., 2004). To create QSBRs, a biodegradability parameter was set as the dependent variable and the 41 molecular descriptors as the independent variables.

QSBRs were created by the GFA algorithm, a genetic function approximation algorithm (Rogers and Hopfinger, 1994) built in the QSAR+ module of Cerius^2. In

principle, the algorithm generated 100 parent equations, containing randomly-chosen descriptors. Regressions were performed on the generated equations and equations were ordered according to their lack-of-fit (*LOF*) score (Friedman, 1991). Crossover operations randomly mixed descriptors from random pairs of parent equations to produce progeny equations. A progeny equation substituted the equation with the highest *LOF* if its *LOF* score was in the top 100, otherwise it was discarded. Crossovers were repeated 20,000 times. Recombination of terms resulted in an improved final population of 100 equations, ordered according to their *LOF* scores. *LOF* of an equation is defined as:

$$LOF = LSE/[1-(c+d\cdot p)/n]^2 \qquad (4.1)$$

where *LSE* is the least square error, *c* is the number of basis functions (linear, quadratic, or spline), *d* is the smoothing parameter, *p* is the number of descriptors in the QSBR, and *n* is the number of observations in the training set. *LOF* is a measure of statistical fit and an indicator of overfitting. The GFA algorithm was preferred over more traditional regression methods because it generates superior equations and reveals relationships that are not directly obvious when descriptors must be pre-selected (Rogers and Hopfinger, 1994). Another advantage of the GFA algorithm is that it permits regression with splines.

Splines are useful when the activity data does not have a linear effect over its entire range or when the data reflects more than one process. Use of spline regression with the Δ(net A_{450}) data is beneficial because it allows use of the whole dataset and not just nonzero values. To develop a QSBR for Δ(net A_{450}), truncated power splines of the form $<D - a>$ were used, where *D* is the value of a descriptor for a specific molecule and *a*, a constant, is the knot of the spline. The spline equals zero if the value of $(D - a)$ is negative; otherwise it equals $(D - a)$.

Preliminary runs of the GFA algorithm were performed to identify multivariate outliers. It was found that for $\log q_{max}$, 1MFLE and 1MPYR were outliers based on their absolute studentized residual values of greater than 3.0 and their Cook's distance of greater than 0.27, resulting from $4/(n - p)$. 1MFLE, with a standardized residual of less

than -2.5, was also identified as a potential outlier for log($1/K_S$). 1MPYR was also a univariate outlier as discussed above. Based on these findings, 1MFLE and 1MPYR were removed from all models except the Δ(net A_{450}) model. In the latter, the leverage value for NAP was high (0.72), but the values of the studentized residual and Cook's distance were normal (0.22 and 0.03, respectively).

The final 100 equations generated by the GFA for each parameter were further evaluated on a statistical basis. Despite the satisfactory statistical capabilities of QSAR+, statistical analyses were performed with SPSS 12.0 except validation. Calculated parameters included the correlation coefficient, R, the coefficient of determination, R^2, and its adjusted value, R^2-adj. The significance of regression equations was tested by the F-test. Overfitting was prevented by satisfying the relationship $n \geq 5p$ (Okey and Stensel, 1996). Multicollinearity was diagnosed using the variance inflation factor, *VIF*, and condition indices, with a cutoff value of 4 and 30, respectively. For condition indices above 30, multicollinearity was spotted by finding two or more descriptors with proportion of variance of 0.5 or higher. The significance of the unstandardized coefficients was tested by the t-test at the 0.05 significance level, and coefficients not statistically different than zero were removed from the equations. Relative explanatory importance of each descriptor in a model was determined by the beta weights and semipartial correlations. Standardized residuals were analyzed for normality using normal probability plots, and for homoscedasticity using residual plots. Residual plots were also used to evaluate the linearity assumption for the models. Influential data points were identified by a series of diagnostic tests, including the studentized residuals, Cook's distances, leverage, and the chi-square statistic of the Mahalanobis distances.

QSBRs were tested for their uncertainties and predictive power using a bootstrap validation test and a randomization test, respectively. The bootstrap test calculated the coefficient of determination, $R^2_{bootstrap}$, and its uncertainty by repeatedly analyzing random samples of the dataset with resampling. Fisher's randomization method tested the assumption that adequate random regressions exist for a parameter. Biodegradability values were randomly re-assigned 19 times (0.05 significance level) and statistical

parameters were calculated each time and compared to the parameters of the nonrandom QSBR. This method tested the validity of both a model and the data on which the model was built.

Investigation of the cell penetration mechanism

A kinetic experiment was conducted to investigate the potential influence of facilitated transport on biodegradation kinetics. The same experimental procedure described in Chapter III was followed. Five PAHs were tested (NAP, 26DMNAP, ANT, 2MPHE, and PYR), representing the whole range of logK_{ow} values observed in Chapter III. PAHs were degraded by *Sphingomonas paucimobilis* strain EPA505 in the presence and absence azide, a membrane protein inhibitor. Duplicate reactors were used for each treatment. Azide was added as sodium salt to a final concentration of 30 mM. At this concentration azide sufficiently inhibits mediated membrane transport but is unlikely to affect short-term enzyme activity (Bugg et al., 2000).

Table 4.1
Statistic and validation parameters of final QSBRs.

							Validation test results		
QSBR	R^2	R^2-adj	F	Sig. F	n	p	$R^2_{bootstrap}$	$n_{R_{rand}<R}$ [a]	$s_{R-R_{rand}}$ [b]
logq_{max}	0.843	0.809	25.0	0.000	18	3	0.84 ± 0.01	19	2.51
log(1/K_s)	0.821	0.797	34.4	0.000	18	2	0.82 ± 0.00	19	2.99
log(q_{max}/K_s)	0.878	0.852	33.6	0.000	18	3	0.88 ± 0.01	19	2.35
Δ(net A_{450})	0.976	0.970	164.4	0.000	22	4	0.98 ± 0.00	19	1.63

[a] Number of R values from 19 random trials that are less than the R value for the nonrandom trial.
[b] Number of standard deviations of the mean R of all random trials to the nonrandom R value.

RESULTS

Final QSBRs are represented by Eq. 4.2 through 4.5 with uncertainties in the unstandardized coefficients representing standard errors. Selected equations were among the top of the GFA equation output for each parameter. For example, Eq. 4.2 had the second lowest *LOF* score among equations generated for logq_{max} and Eq. 4.3 the third

lowest *LOF* score among equations generated for log(1/K_S). In other words, the GFA algorithm successfully converged to valid and useful equations. Table 4.1 summarizes statistical parameters of the QSBRs. Equations are characterized by high coefficients of determination and significance of the *F*-statistic. In addition, equations are not overfitted as indicated by comparison of *p* to *n*, and R^2-adj to R^2. Even valid models with a large number of cases and a small number of independent variables can have poor explanatory and predictive power, especially when the observations are not sufficiently independent of each other. As found by bootstrap, the calculated R^2 is accurate and the probability of it being low is small. Furthermore, the values of the randomization parameters $n_{R_{rand}<R}$ and $s_{R-R_{rand}}$ indicate that at the 95% confidence level there is high likelihood that QSBRs represent a true probability.

$$\log q_{\max}\ (\mu\text{mol mg}^{-1}\ \text{h}^{-1}) = 4.3057(\pm 1.0271) - 0.0063(\pm 0.0008) \cdot \text{PMI-mag} - 6.9874(\pm 1.5383) \cdot \text{Shadow-Yzfrac} + 0.0163(\pm 0.0038) \cdot \text{Jurs-PNSA-1} \quad (4.2)$$

$$\log(1/K_S)\ (\mu\text{mol L}^{-1}) = -11.7796(\pm 1.7250) + 1.9545(\pm 0.2602) \cdot \text{RadOfGyration} + 9.1430(\pm 1.9384) \cdot \text{Shadow-Yzfrac} \quad (4.3)$$

$$\log(q_{\max}/K_S)\ (\text{L mg}^{-1}\ \text{h}^{-1}) = 1.3605(\pm 0.2840) + 0.0090(\pm 0.0011) \cdot \text{Hf\_MOPAC} + 0.6805(\pm 0.0835) \cdot \text{PHI} - 0.3060(\pm 0.0390) \cdot \text{Shadow-Ylength} \quad (4.4)$$

$$\Delta(\text{net } A_{450})\ (\ ) = 0.0440(\pm 0.0202) + 0.3211(\pm 0.0497) \cdot \langle\text{Shadow-Xlength} - 11.469\rangle + 0.0089(\pm 0.0013) \cdot \langle\text{Jurs-PNSA-1} - 98.060\rangle + 0.0485(\pm 0.0023) \cdot \langle 152.195 - \text{MW}\rangle - 0.5823(\pm 0.0600) \cdot \langle\text{HOMO\_MOPAC} + 8.5464\rangle \quad (4.5)$$

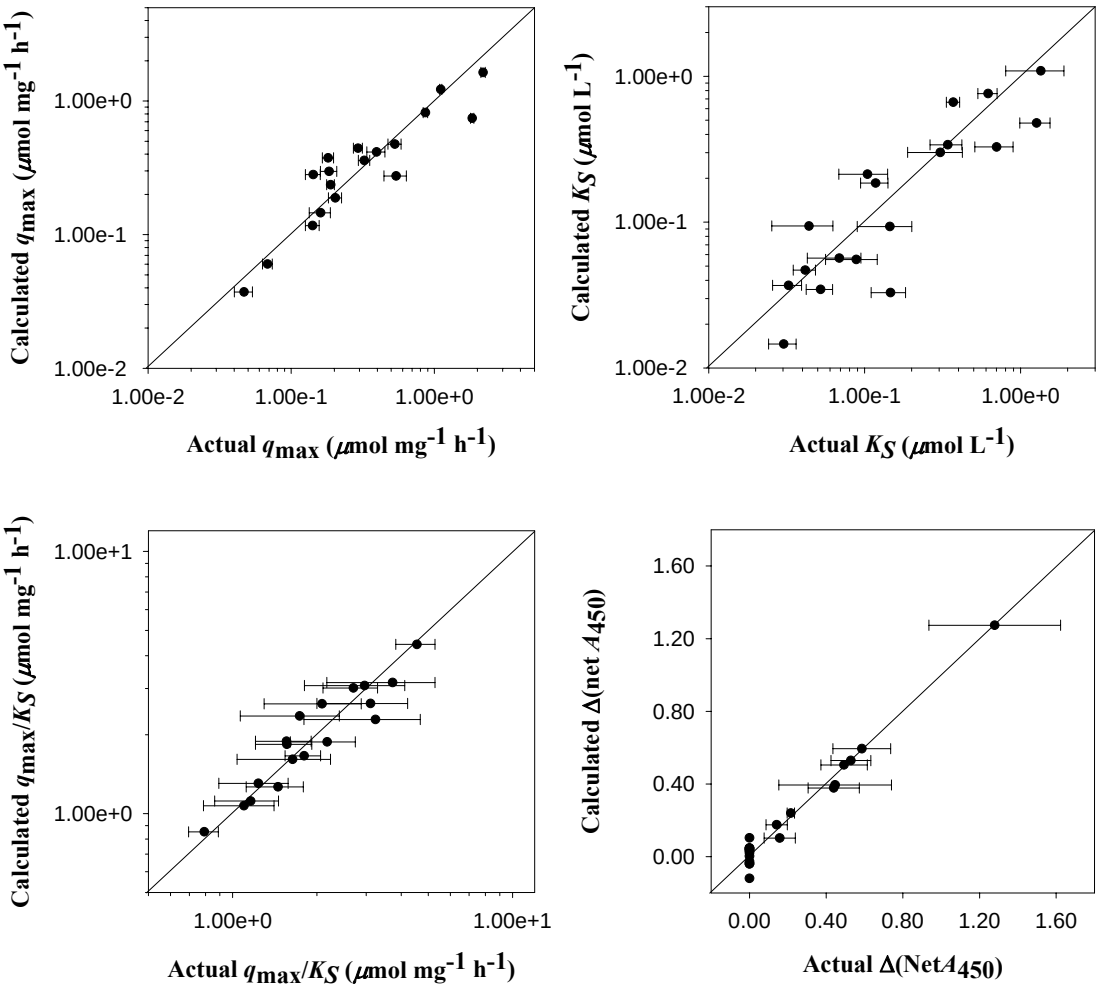

Fig. 4.1. Comparison of measured biodegradability parameters with those calculated by the four QSBRs (Eq. 4.2 through 4.5). Diagonal lines have slope equal to 1. Error bars represent 95% confidence intervals for the experimental values.

A comparison between the actual values of the biodegradability parameters and those calculated by the QSBRs is depicted in Fig. 4.1. Comparison shows good agreement between the experimental and calculated values. Eq. 4.2 though 4.4 confirmed the assumption of linearity and resulted in normally distributed and homoscedastic residuals. Eq. 4.5 resulted in normally distributed standardized residuals for nonzero values of Δ(net A_{450}) but also in heteroscedasticity. The following influential

observations were detected in the QSBRs: 235TMNAP and 2MPHE in the logq_{max} model; PYR in the log($1/K_S$) model; ACY, 36DMPHE, and FLA in the log(q_{max}/K_S) model; and 1MNAP and 9MANT in the Δ(net A_{450}). These observations indicate potential experimental error or peculiarity in the underlying biochemical process or structure-activity relationship. An attempt was made to construct a QSBR for log(q_{max}/K_S) using only the descriptors found for the logq_{max} and log($1/K_S$) models (5 descriptors). The resulting equations were satisfactory, but inferior to Eq. 4.4. To recapitulate, QSBRs were constructed for all four biodegradability parameters; the models are statistically valid and have significant predictive power.

The following definitions apply to the molecular descriptors appearing in Eq. 4.2 through 4.5. PMI-mag is the magnitude of the principle moments of inertia about the principle axes of a molecule. Shadow-Yzfrac is the fraction of the area of the projection of a molecule on the YZ plane divided by the area of the rectangle enclosing the projection of the molecule. Shadow-Xlength and Shadow-Ylength are the lengths of the projection of the molecular shape on the X- and Y-axis, respectively. Jurs-PNSA-1 is the partial negative surface area, i.e., the sum of the solvent-accessible surface areas of all negatively charged atoms (Stanton and Jurs, 1990). RadOfGyration is the radius of gyration. Hf_MOPAC is the heat of formation as calculated by MOPAC7. PHI is the molecular flexibility index (Hall and Kier, 1991). MW is the molecular weight. HOMO_MOPAC is the energy of the highest occupied molecular orbital as calculated by MOPAC7.

Descriptors in the final QSBRs are organized in six categories: spatial, spatial and electronic, electronic, topological, structural, and thermodynamic (Table 4.2). Each descriptor appears in a single QSBR, except Shadow-Yzfrac and Jurs-PNSA-1 appearing in two QSBRs. Despite the apparent exclusivity, the following high correlations exist between descriptors ($r > 0.80$): RadOfGyration with PMI-mag, Shadow-Xlength, PHI, and MW; PMI-mag with Shadow-Xlength; and PMI-mag with MW. Descriptor values in Table 4.2 illustrate the consistent effect (increase or decrease) of methylation on

Table 4.2
Values of molecular descriptors present in the final QSBRs as calculated by QSAR+ (Accelrys Inc., 2004). Compound abbreviations are explained in Chapter III.

	Spatial					Spatial/ Electronic	Electronic	Topo-logical	Structural	Thermo-dynamic
Compound	**PMI-mag** (amu·Å^2)	**RadOf Gyration** (Å)	**Shadow-Xlength** (Å)	**Shadow-Ylength** (Å)	**Shadow-Yzfrac**	**Jurs-PNSA-1**	**HOMO_MOPAC**[a] (eV)	**PHI**	**MW**	**Hf_MOPAC**[a] (kcal/mol)
NAP	121.278	2.632	9.183	7.396	0.739	105.305	-8.616	1.175	128.173	35.888
1MNAP	147.637	2.784	9.581	8.128	0.728	97.818	-8.505	1.392	142.200	31.236
2MNAP	170.227	2.935	10.489	7.747	0.657	97.094	-8.567	1.392	142.200	30.010
15DMNAP	182.491	2.977	10.282	8.669	0.703	85.259	-8.404	1.613	156.227	26.934
23DMNAP	210.146	3.081	10.137	7.555	0.687	92.505	-8.532	1.613	156.227	25.094
26DMNAP	231.400	3.261	11.469	7.844	0.671	87.916	-8.509	1.613	156.227	24.204
235TMNAP	242.262	3.207	10.419	8.251	0.760	81.153	-8.424	1.839	170.254	20.710
ACE	157.495	2.776	9.194	8.303	0.714	81.877	-8.401	1.092	154.211	40.802
ACY	153.273	2.757	9.228	8.579	0.752	112.793	-8.782	0.991	152.195	78.373
FLE	229.969	3.029	11.381	7.461	0.714	104.581	-8.572	1.307	166.222	50.299
1MFLE	274.335	3.198	11.295	7.758	0.726	98.060	-8.564	1.513	180.249	44.968
ANT	296.947	3.260	11.646	7.410	0.737	129.217	-7.979	1.539	178.233	56.085
1MANT	335.705	3.375	11.847	8.291	0.727	121.246	-7.913	1.751	192.260	51.539
9MANT	314.123	3.274	11.611	8.376	0.755	116.416	-7.906	1.751	192.260	53.755
PHE	260.691	3.135	11.697	7.995	0.756	129.217	-8.546	1.539	178.233	50.784
1MPHE	313.154	3.325	12.021	8.532	0.690	120.039	-8.480	1.751	192.260	46.387
2MPHE	341.693	3.457	12.629	8.031	0.662	118.589	-8.537	1.751	192.260	45.017
36DMPHE	383.380	3.581	11.647	9.118	0.724	107.962	-8.399	1.967	206.287	39.453
FLA	284.509	3.122	10.341	9.039	0.757	127.043	-8.440	1.386	202.255	105.502
PYR	290.271	3.180	11.633	9.203	0.771	128.250	-7.977	1.386	202.255	60.201
1MPYR	347.329	3.377	12.036	9.579	0.696	118.831	-7.917	1.579	216.282	55.516

[a] MOPAC descriptors are categorized as Quantum Mechanical by QSAR+. Here, they are categorized based on the molecular quantity they describe.

Table 4.3
Relative explanatory importance of descriptors within each QSBR based on beta weights of unstandardized coefficients and semipartial correlations. Relative importance of "1" is higher than of "2", etc. Correlation signs (+ or −) between the biodegradability parameters and descriptors are provided in parentheses.

	Spatial					Spatial/ Electronic	Electronic	Topo- logical	Structural	Thermo- dynamic
QSBR	**PMI-mag**	**RadOf Gyration**	**Shadow-Xlength**	**Shadow-Ylength**	**Shadow-Yzfrac**	**Jurs-PNSA-1**	**HOMO_MOPAC[a]**	**PHI**	**MW**	**Hf_MOPAC[a]**
$\log q_{max}$	1 (–)				2 (–)	2 (+)				
$\log(1/K_s)$		1 (+)			2 (+)					
$\log(q_{max}/K_s)$				1 (–)				1 (+)		1 (+)
Δ(net A_{450})			3[b]			3[b]	2[b]		1[b]	

[a] MOPAC descriptors are categorized as Quantum Mechanical by QSAR+. Here, they are categorized based on the molecular quantity they describe.
[b] Refers to the spline containing the corresponding descriptor.

descriptor values. Descriptors not conforming to this effect are Shadow-Xlength and Shadow-Yzfrac, signifying the importance of methyl-substituent position for the values of these descriptors.

The relative explanatory importance of the descriptors in each QSBR, based on the values of beta weights and semipartial correlations, is presented in Table 4.3. Results indicate that spatial descriptors, describing the three-dimensional shape of molecules, are essential in explaining biodegradability. In fact, q_{max} and $1/K_S$ are solely explained by spatial descriptors. The molecular flexibility index, PHI, and the heat of formation, Hf_MOPAC, were also important in describing the specific affinity, q_{max}/K_S. Table 4.3 includes the sign of correlation (+ or –) between a biodegradability parameter and a descriptor.

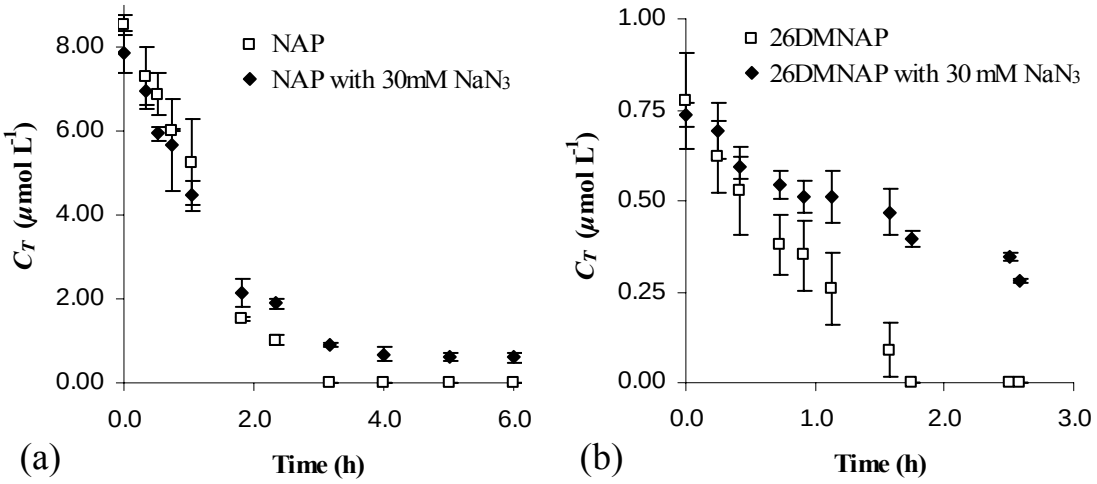

Fig. 4.2. Degradation of naphthalene (a) and 2,6-dimethylnaphthalene (b) in the presence and absence of sodium azide (NaN_3). Azide is an inhibitor of facilitated membrane transport. Each data point represents the mean concentration from two independent batch reactors, while the error bars represent one standard deviation from the mean. Data indicate that facilitated transport may be the limiting mechanism in the degradation of 26DMNAP but not NAP.

The kinetic experiment with azide was used to gain insight into the influence of facilitated membrane transport on biodegradation kinetics. Data on ANT, 2MPHE, and PYR were inconclusive and are not discussed further. The results for NAP and 26DMNAP are illustrated in Fig. 4.2. Each data point represents the mean concentration from two independent batch reactors, while error bars represent one standard deviation from the mean. Fig. 4.2a shows that azide did not affect the kinetics of NAP biodegradation in the first 108 minutes of the experiment; therefore, data beyond this point were excluded from further investigation for both compounds. First-order lines were fitted to the depletion data using least squares regression. At the 0.05 significance level azide caused significant reduction in the degradation coefficient for 26DMNAP but not for NAP.

DISCUSSION

A QSAR is more meaningful when used to describe how variation in chemical structure relates to a specific response, i.e., a chemical property or reaction coordinate. Eq. 4.2 through 4.4 describe the kinetics of the single initial catabolic step and may be considered mechanistically. Kinetics of this step depend on the kinetics of the initial catabolic reaction or any limiting processes preceding it.

Catabolism of PAHs in bacteria starts with the oxygenation of an aromatic ring or alkyl side-chain. In most cases, these reactions are catalyzed by dioxygenases (Gibson and Parales, 2000). A number of studies (Jerina et al., 1984; Dutta et al., 1998; Pinyakong et al., 2004) propose that the initial catabolic reaction in sphingomonads is catalyzed by dioxygenase(s) characterized by relaxed PAH specificity. This is consistent with the detection of PAH dihydroxy metabolites (Ho et al., 2000; Story et al., 2001; Story et al., 2004). There is evidence that the hypothetical dioxygenase is related to naphthalene dioxygenase (NDO). For example, it has been suggested that a gene in *Sphingomonas aromaticivorans* strain F199 encodes for an oxygenase component of naphthalene dioxygenase (Romine et al., 1999b); its enzymatic activity has not yet been confirmed. Dioxygenases participating in the catabolism of aromatic compounds are multicomponent enzyme systems consisting of one or two electron transport proteins

functioning before the oxygenase component (Gibson and Parales, 2000). The electron-transport proteins (e.g., a flavoprotein and a ferredoxin) could become rate-determining in diminishing quantities (Zhou et al., 2002), but in this research the variability in the observed kinetics and the fact that the biomass was induced do not support this possibility. The information presented above indicates that initial enzymatic transformation is uniform in strain EPA505. Is it the rate-determining process?

In a well-mixed aqueous environment, two critical processes precede the biotransformation of organic compounds: cell membrane binding-and-transport, and degradative enzyme binding. Each of these processes could potentially determine the kinetics of biotransformation. For example, a two-stage substrate uptake model that included membrane transport followed by catabolism showed that transporter content can be as influential in determining biodegradation kinetics as the rates of subsequent enzymatic reactions (Button, 1991). There is limited information about the mechanisms contributing to PAH binding and transport across bacterial membranes. It has been traditionally assumed that aromatic compounds, including PAHs, can freely diffuse into bacterial cells (Bateman et al., 1986). More recently, a number of specific outer membrane (OM) proteins have been associated with the regulation of aromatic compound uptake by Gram-negative bacterial cells. Specific permeases catalyze transport of different classes of aromatics (Nikaido, 2003). For example, a protein encoded in the pWW0 TOL plasmid of *Pseudomonas putida* facilitates transport of *m*-xylene (Kasai et al., 2001). Another permease was found to facilitate toluene transport into cells of *Pseudomonas putida* F1 (Wang et al., 1995). The *pbhD* gene in *Sphingomonas paucimobilis* strain EPA505, which is involved in fluoranthene metabolism, is homologous to pyruvate phosphate dikinase (*ppdK*), a gene involved in glucose uptake by prokaryotic and plant cells (Story et al., 2000). It was hypothesized that *pbhD* is associated to the uptake of fluoranthene metabolites released from the cells (Story et al., 2000). If energy expenditure is coupled to membrane transport, then permeases are active carriers. A study by Miyata et al. (2004) presented the first indications of the presence of saturable, energy-dependent transport of PAHs in

mycobacteria. The study concluded that membrane transport, rather than metabolism, was the rate-limiting process in induced cells, although contribution of metabolism could not be ruled-out (Miyata et al., 2004). Despite the significant differences between mycobacteria and sphingomonads (mycobacteria are Gram-positive), both genera are commonly found in PAH-contaminated soils (Mueller et al., 1997). Certain OM proteins function as active efflux pumps that regulate uptake of toxic compounds, including PAHs (Romine at al., 1999a). For instance, Bugg et al. (2000) discovered an active efflux mechanism regulating the uptake of phenanthrene in *Pseudomonas fluorescens* LP6a. The same study suggested that PAH uptake is dominated by simple partitioning and that efflux does not have a significant effect on the rate of phenanthrene biotransformation. This brief literature review shows that a variety of mechanisms are involved in membrane transport of aromatic compounds and that membrane transport can potentially be the rate-limiting mechanism in biodegradation.

A recent study (Bressler and Gray, 2003) used a simple flux model to demonstrate the effect of membrane transport on the biotransformation rate of unsubstituted and alkyl PAHs. The flux equation was of the form:

$$J = k_m (C_L^{out} - C_L^{in}) \tag{4.6}$$

where k_m denotes the permeability of the membrane per unit area, and C_L^{out} and C_L^{in} the extra- and intracellular substrate aqueous concentrations, respectively. The permeability was expressed as:

$$k_m = 0.003 \frac{K_{ow}}{\mathrm{MW}^{1/2}} \qquad (\mathrm{cm\ s^{-1}}) \tag{4.7}$$

where K_{ow} is the octanol/water partition coefficient and MW the molecular weight (Stein, 1967). This equation assumes that, for small molecules, the diffusivity as calculated by the Einstein-Stokes equation is inversely proportional to the square root of molecular weight (Ohki and Spangler, 2005). Assuming that $C_L^{in} \approx 0$ due to intracellular biodegradation and that the maximal flux, $J_{\max}$, occurs when C_L^{out} equals the aqueous solubility, S (mg cm^{-3}), a combination of Eq. 4.5 and 4.6 results in:

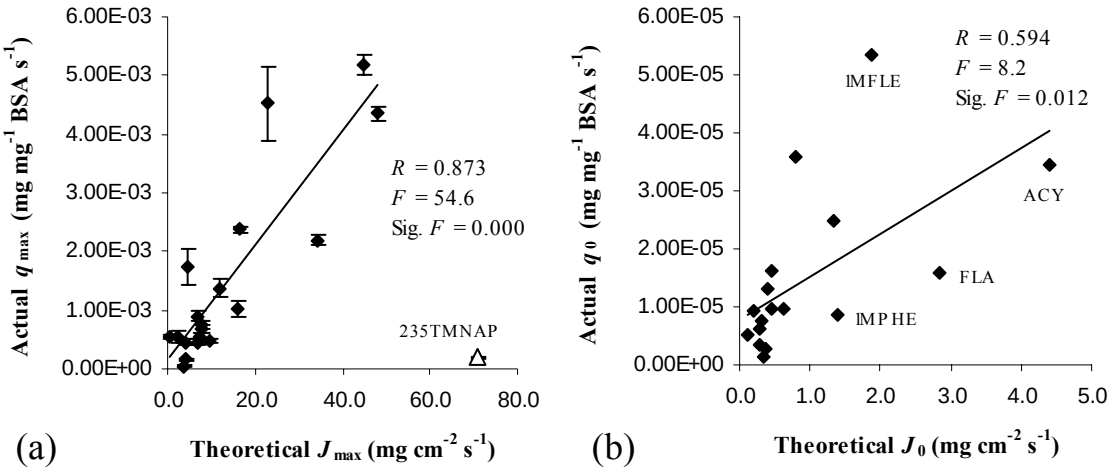

Fig. 4.3. Regressions between theoretical transmembrane flux, as calculated by Eq. 4.8 and 4.9, and the observed specific biodegradation rate for different PAHs. Fig. 4.3a refers to maximal flux and biodegradation rate, while Fig. 4.3b to initial values of the same quantities. 2,3,5-Trimethylnaphthalene is an outlier in (a). Four influence points are identified in (b). Both regressions are statistically significant and illustrative of the potential importance of transport as the rate-determining mechanism in the biotransformation of PAHs by strain EPA505.

$$J_{\max} = 0.003 \frac{K_{ow} S}{\mathrm{MW}^{1/2}} \qquad (\mathrm{mg\ cm^{-2}\ s^{-1}}) \tag{4.8}$$

A regression was performed between the logarithm of the maximal first-order degradation coefficients for seven PAHs and benzene as compiled by Aronson et al. (1998), and the log$J_{\max}$ as calculated by Eq. 4.8 (Bressler and Gray, 2003). The regression suggested that PAH biodegradation rates are related to transmembrane flux as calculated by the physicochemical properties of the PAHs.

Following similar methodology, a regression was performed between $J_{\max}$ and the experimental $q_{\max}$ and another between the specific biodegradation rate at t = 0, q_0, and the theoretical flux at t = 0, J_0, as calculated by the following equation:

$$J_0 = 0.003 \frac{K_{ow} C_L^0}{\mathrm{MW}^{1/2}} \tag{4.9}$$

where C_L^0 is the experimental initial extracellular PAH concentration in the aqueous

phase. Inhibitory compounds, namely 1MNAP, 2MNAP, and 23DMNAP, were excluded from the second regression. Fig. 4.3a depicts a statistically significant relation between J_{max} and q_{max}, suggesting membrane transport as the rate-limiting process. The obvious outlier, 235TMNAP, is located distantly below the regression line, possibly indicating biotransformation rather than transport as the rate-limiting mechanism for this compound. The regression in Fig. 4.3b is not as definitive, yet it is statistically significant. Using the same outlier diagnostics used for QSBR development, the following influence points were detected: ACY, 1MFLE, 1MPHE, and FLA, as identified in the figure. From these, ACY, 1MPHE, and FLA are located below the regression line, suggesting biotransformation as the possible rate-limiting mechanism. From all the influence points identified in Fig. 4.3, 235TMNAP, ACY, and FLA were also identified as influence points in QSBR, indicating possible common causality.

The correlation between q_{max}, a measured quantity, and J_{max} a theoretical quantity, is significant evidence that the rate-limiting step in PAH biodegradation by strain EPA505 is membrane transport. Given the concentration gradient dependence (Eq. 4.6), the transport mechanism is possibly diffusion, simple or facilitated. The experiment with azide showed that azide caused significant reduction in the biodegradation rate of 26DMNAP but not NAP. This finding suggests that facilitated diffusion potentially plays a role in the kinetics of 26DMNAP biodegradation but not NAP, implying that membrane transport is not a uniform process and that it could influence biotransformation kinetics to a different extent depending on the PAH. Given the smaller size and lower hydrophobicity of NAP compared to 26DMNAP, it is possible that NAP diffuses through a transmembrane channel while the larger 26DMNAP requires a permease carrier to catalyze its transport. Both channels and carriers can exhibit saturation kinetics (Saier, 2000); therefore use of the Monod-type model is probably justifiable for both cases.

The evidence indicates that membrane transport is the rate-limiting process in the degradation of PAHs by strain EPA505 and that transport is not a uniform process. In addition, potential outliers were found suggesting enzymatic transformation as the rate-

limiting process. Due to the heterogeneity in the processes determining kinetics, one could argue that Eq. 4.2 through 4.4 are invalid. This argument is reasonable. However, it is not supported by the statistical significance and predictive power of the developed QSBRs, which may be explained by two reasons: (i) the QSBRs are flexible in reflecting different rate-limiting processes; or (ii) there is one common process for most PAHs, while PAHs not conforming or PAHs with a peculiarity appear as outliers. Interpretation and understanding of the molecular descriptors is critical in resolving the enigma.

Spatial descriptors were found to be essential in explaining biodegradation kinetics. The magnitude of the principal moments of inertia (PMI-mag) is a spatial descriptor encoding information about spatial distribution of mass and its rotational properties. It also represents the role of molecular size and volume in occupying the space between water molecules. PMI-mag is negatively correlated with aqueous solubility. Indeed, substitution of PMI-mag by the logarithm of solubility in Eq. 4.2 resulted in slightly better statistics. The equation with PMI-mag (Eq. 4.2) was preferred because experimental solubility values are not available for every possible PAH homologue. The negative coefficient of PMI-mag means that decreasing PMI-mag (or increasing solubility) results in increasing $q_{\max}$, which is consistent with Eq. 4.8. PMI-mag is also highly correlated with the molecular weight, as well as the molecular area, a descriptor related to binding and transport (Accelrys Inc., 2004).

Another spatial descriptor with high explanatory value was the radius of gyration, RadOfGyration. Like PMI-mag, it contains information about the rotational properties of a molecule. It correlates well with $\log K_{ow}$, a measure of hydrophobicity, and the molecular volume, a descriptor related to binding and transport (Accelrys Inc., 2004). The positive coefficient of RadOfGyration in Eq. 4.3 suggests that binding affinity increases with hydrophobicity. The descriptor also correlates with the molecular area, a quantity related to binding (Accelrys Inc., 2004).

Shadow-area shape indices, Shadow-Ylength and Shadow-Yzfrac, are spatial descriptors providing information on the size, shape, and orientation of a molecule. The descriptors are calculated by projecting the molecular shape on the three Cartesian

planes following alignment of the principle moments of inertia with the X, Y, and Z axes (Rohrbaugh and Jurs, 1987). The negative coefficient of Shadow-Ylength in Eq. 4.4 suggests a negative correlation between size and q_{max}/K_S. This observation may be consistent with the observation that in PAHs the percent percutaneous penetration after 24 hours is negatively correlated with the molecular size as described by a shadow index (Moss et al., 2002); however, a direct analogy between the specific affinity and percent penetration after 24 hours cannot be drawn because it is unknown whether the percent penetration reflected kinetics or equilibrium. Shadow-Yzfrac is the fraction of the area of the projection of a molecule on the YZ plane divided by the area of the rectangle enclosing the projection of the molecule. Fractional shadow indices are not commonly used in QSAR modeling. Shadow-Yzfrac appears in both Eq. 4.2 and 4.3, signifying its influence on PAH binding and transport. It is unique in this study because it does not correlate with any other descriptors. It indicates that the position of methyl substituents influences biodegradability. A similar fractional shadow index was among the five descriptors selected to explain estrogen receptor binding for 58,000 chemicals (Hong et al., 2002).

Charged partial surface area (CPSA) descriptors, called "Jurs" in QSAR+, encode spatial and electronic information related to the tendency of molecules to engage in polar interactions (Stanton and Jurs, 1990). Jurs-PNSA-1 is the partial negative surface area, i.e., the sum of the solvent-accessible surface areas of all negatively charged atoms, and it correlates negatively with the desolvation free energy. The positive coefficient of Jurs-PNSA-1 in Eq. 4.2 means that q_{max} increases with increasing values of this descriptor. Jurs-PNSA-1 also correlates with density, a spatial descriptor expressing transport behavior (Accelrys Inc., 2004).

All descriptors analyzed in the previous paragraphs are spatial. Eq. 4.4 for q_{max}/K_S also contains a topological and a thermodynamic descriptor. The molecular flexibility index, PHI, is a topological descriptor characterizing the conformational flexibility of a molecule within a given energy range (Hall and Kier, 1991). Its coefficient in Eq. 4.4 suggests that the specific affinity increases with PHI. Molecular

flexibility has a strong effect on biological activity, particularly binding affinity (Becker et al., 2000). Molecular flexibility, together with hydrophobicity and polar surface area, was important in modeling transport through the blood-brain barrier (Winkler and Burden, 2004). The enthalpy of formation of a molecule from its constituent atoms, Hf, is a thermodynamic descriptor not related to logK_{ow}. Hf positively correlates with the specific affinity and correlates well with density, a quantity describing transport behavior (Accelrys Inc., 2004). Hf was important in explaining biodegradability of substituted benzenes by river bacteria (Lu et al., 2003).

The meaning of the descriptors in Eq. 4.2 through 4.4 agrees with the hypothesis of binding-and-transport as the rate-limiting mechanism. A number of mathematical expressions have been proposed for modeling binding of ligands to proteins and enzymes. A popular expression analyzes the free energy change upon binding, ΔG_{bind}, as a sum of free energy components:

$$\Delta G_{\text{bind}} = \Delta G_{\text{T+R}} + \Delta G_{\text{FLEX}} + \Delta G_{\text{HYD}} + \Delta G_{\text{POLAR}} \qquad (4.10)$$

where $\Delta G_{\text{T+R}}$ is the reduction in translational and rotational energy, ΔG_{FLEX} is the loss in bond flexibility, ΔG_{HYD} is the hydrophobic interaction energy, and ΔG_{POLAR} is the polar energy contribution (Lewis et al., 1998). There is striking similarity between the components of free energy upon binding with the descriptors used in Eq. 4.2 through 4.4. Specifically, $\Delta G_{\text{T+R}}$ can be related to PMI-mag and RadOfGyration. These descriptors express rotational properties of a molecule and also translational properties, given their association with molecular mass. ΔG_{FLEX} can be associated with the molecular flexibility index, PHI. ΔG_{HYD} can be linked to PMI-mag, RadOfGyration, and to a lesser degree to PHI, as well as all the hydrophobicity measures that these descriptors represent. Finally, ΔG_{POLAR} can be related to Jurs-PNSA-1. The analogy between Eq. 4.2 through 4.4 and Eq. 4.10 is strong evidence that binding is associated with the rate-limiting process.

Solute binding involves transfer out of the water phase. Therefore, linear solvation energy relationships (LSERs) could give insight into the mechanisms determining the observed biodegradation kinetics. The generic Abraham solvation

equation for a condensed system is:

$$K = c + eE_s + sS_s + aA_s + bB_s + vV_s \quad (4.11)$$

where K represents a set of solute properties, E_s is the solute excess molar refractivity, S_s is the solute polarizability, A_s and B_s are the overall hydrogen bond acidity and basicity, respectively, V_s is the McGowan volume, and c, e, s, a, b, and v are multiple regression coefficients (Abraham, 1993; Abraham et al., 2004). Unsubstituted and methylated PAHs are weak hydrogen bond bases and tend to engage in hydrogen bonding to any hydrogen bond acids of a system. The values of E_s, S_s, B_s, V_s for the PAHs in this study are provided in Table 4.4.

Table 4.4
Values of solute descriptors of the Abraham solvation equation (Eq. 4.11) (M.H. Abraham, personal communication, April 28, 2005).

Compound	E_s (0.1 L/mol)	S_s	B_s	V_s (0.01 L/mol)
NAP	1.340	0.92	0.20	1.085
1MNAP	1.337	0.94	0.22	1.226
2MNAP	1.304	0.81	0.25	1.226
15DMNAP	1.402	1.05	0.18	1.367
23DMNAP	1.402	0.85	0.28	1.367
26DMNAP	1.347	0.82	0.25	1.367
235TMNAP	1.470	1.00	0.25	1.508
ACE	1.604	1.05	0.22	1.259
ACY	1.750	1.14	0.26	1.216
FLE	1.588	1.06	0.24	1.357
1MFLE	1.588	1.06	0.25	1.497
ANT	2.290	1.34	0.28	1.454
1MANT	2.290	1.30	0.30	1.595
PHE	2.055	1.29	0.29	1.454
1MPHE	2.055	1.25	0.29	1.595
2MPHE	2.055	1.25	0.29	1.595
36DMPHE	2.050	1.29	0.29	1.736
FLA	2.377	1.55	0.24	1.585
PYR	2.808	1.71	0.28	1.585
1MPYR	2.808	1.70	0.26	1.726

A regression was performed between $\log(1/K_S)$ and the solute descriptors of the Abraham equation (Table 4.4). Although K_S expresses the affinity of a receptor for the substrate, it must also include substrate desolvation. The resulting solvation equation is provided below, with uncertainties in unstandardized coefficients representing standard errors:

$$\log(1/K_S)\ (\mu\text{mol L}^{-1}) = -2.1629(\pm 1.1924) + 1.2388(\pm 1.2932) \cdot E_s - 1.2514(\pm 2.2301) \cdot S_s - 2.5393(\pm 5.1947) \cdot B_s + 1.9946(\pm 0.7993) \cdot V_s \quad (4.12)$$

$n = 20$, $R^2 = 0.745$, $F = 11.0$, Sig. $F = 0.000$

For transport of a solute from the water to a lipid-like phase, the *s* and *b* coefficients are always negative while *v* is always positive, which is consistent with the signs of the coefficients in Eq. 4.12. Nevertheless, the regression is problematic basically due to multicollinearity. An alternative equation that uses fewer descriptors is:

$$\log(1/K_S)\ (\mu\text{mol L}^{-1}) = -2.6886(\pm 0.6815) + 0.5241(\pm 0.2426) \cdot E_s + 1.8084(\pm 0.6558) \cdot V_s \quad (4.13)$$

$n = 20$, $R^2 = 0.740$, $F = 24.2$, Sig. $F = 0.000$

Eq. 4.13 is statistically valid and provides insight for a mechanistic understanding of the observed affinity coefficients. It illustrates the significance of solute molecular volume, and therefore, hydrophobicity, in binding of the substrate to the rate-limiting receptor. Two binding processes precede biotransformation: membrane binding and enzyme binding. Which is the limiting one?

Absence of descriptors from Eq. 4.2 through 4.4 can be as meaningful as their presence. Strong evidence that substrate-degradative enzyme interaction is not the rate-determining process is the absence of electronic descriptors related to chemical reactivity. Such descriptors include the energy of the highest occupied molecular orbital, HOMO, the difference in energy between the highest occupied and lowest unoccupied molecular orbitals, HOMO-LUMO gap, and superdelocalizability, Sr. The HOMO energy is commonly used in QSARs as a measure of nucleophilicity and ionization potential. A molecule with high HOMO energy donates electrons more readily than a

molecule with low HOMO energy. Nucloephilicity is important in the biodegradability of PAHs because dioxygenases function by electrophilic addition of activated oxygen. HOMO energy was not present in any of the generated equations sets for q_{max}, K_S, or q_{max}/K_S. In addition, HOMO energy does not correlate with any of the final descriptors for these parameters. Presence of HOMO in the relationship for Δ(net A_{450}) is consistent with the fact that this parameter reflects more than one pathway step including nucleophilic attack by oxygenases at one point in the degradation pathway(s). Another popular electronic descriptor used in quantitative-structure models for biodegradability, toxicity, and physicochemical properties is the HOMO-LUMO gap (Karelson et al., 1996), a measure of chemical stability. This descriptor was manually calculated from the HOMO and LUMO values generated by MOPAC7. HOMO-LUMO gap was not present in any of the generated equations sets for q_{max}, K_S, q_{max}/K_S, or Δ(net A_{450}). Finally, Sr is an index of reactivity of aromatic hydrocarbons that is related to the HOMO energy (Fukui, 1997). Sr was present only in 3 and 5 of the 100 generated equations for q_{max} and K_S, respectively. These equations had relatively high *LOF* scores and were not statistically significant. That enzyme-substrate interaction is probably not the rate-determining step implies that the rate-limiting step is either membrane binding-and-transport or enzyme binding and orientation of the substrate in the active site. The latter is possible (Polgar, 1992; Wang et al., 2001) but unlikely. For example, it was found that although hydroxylation rates of *p*-substituted toluenes by the cytochrome CYP2B4 was adequately described by steric properties (Lewis et al., 1995), addition of HOMO significantly improved the QSAR (Lewis et al., 1998).

Interpretation of Eq. 4.5 requires separate discussion. This equation is different from the other QSBRs in that it does not express a single reaction mechanism but different degradation paths that can be convergent or divergent (Story et al., 2001). For this reason it can not be considered mechanistically, especially because pathways have not been delineated for all PAHs of interest. The fact that Eq. 4.5 cannot be considered mechanistically does not imply invalidity. Spline regression and other nonlinear modeling methods are adaptable to heterogeneities, outliers, discontinuities, and other

anomalies in the data (Eriksson et al., 2003). In addition, despite the fundamental differences between Eq. 4.5 and the other QSBRs, the main difference in descriptor use involves the HOMO energy. The spline containing this descriptor in Eq. 4.5 expresses susceptibility to nucleophilic attack subsequent to the initial oxidation step, given that all PAHs in the degradation study were biotransformed. This nucleophilic attack possibly involves ring cleavage, a prerequisite for growth support.

In this study, QSBRs were developed describing biodegradability of PAHs by *Sphingomonas paucimobilis* strain EPA505. The QSBRs are statistically valid and have significant predictive power. Two approaches were followed, a simple flux model, and interpretation of the generated QSBRs, to investigate the processes determining biodegradation kinetics. Both approaches resulted in similar evidence, based on which it is concluded that, contrary to common belief, membrane binding-and-transport is the rate-determining process in the biodegradation of most of the PAHs tested. It is unknown to what degree PAH binding and transport are distinguishable through the QSBRs and which biomolecules and processes they involve. This study and others with similar findings initiate needed research on membrane binding-and-transport of PAHs that would enhance our understanding of both PAH biodegradability and toxicity mechanisms.

CHAPTER V
MODELING BIODEGRADATION OF BINARY AND TERNARY MIXTURES OF POLYCYCLIC AROMATIC HYDROCARBONS

OVERVIEW

Biodegradation of mixtures of polycyclic aromatic hydrocarbons (PAHs) by *Sphingomonas paucimobilis* strain EPA505 was investigated. The investigation focused on three- and four-ring PAHs, specifically 2-methylphenanthrene, fluoranthene, and pyrene. Biodegradation rates in batch cultivations were measured for the individual compounds and their binary and ternary mixtures. It was observed that kinetics in a mixture were either similar or slower than those observed for the individual PAHs and that kinetics were influenced by the mixture composition and the kinetic properties of the components. A material balance equation containing the Monod kinetic model was numerically fitted to depletion data to estimate extant kinetic parameters for the individual compounds. Similarly, equations containing kinetic-interaction models derived from enzyme kinetics were fitted to the depletion data for the binary and ternary mixtures. Interaction types considered included no-interaction (NI or Monod), pure competitive interaction (CI), non-competitive or mixed-type interaction (NCI/MI), uncompetitive inhibition (UCI), and nonspecific interaction based on pure competition (SKIP). Model fit was evaluated based on statistical and probabilistic criteria and inferences were reached about underlying interaction mechanisms based on model fit. Mixture kinetics were most adequately described by the pure CI model with mutual substrate exclusivity. This model is fully predictive, requiring no additional parameters other than those estimated in the sole-PAH experiments. It was also shown that, for low percent inhibition values and with limited number of data points, competitive interaction kinetics may not be evident, resembling no-interaction kinetics. Despite simplifications, the experiment described in this study is a reasonable starting point for understanding mixture effects and simulating engineered and natural systems.

INTRODUCTION

PAHs are ubiquitous pollutants of significant environmental and toxicological importance (Harvey, 1991). PAHs often occur in complex mixtures containing parent compounds and substituted homologues. Common sources of PAH mixtures include petroleum and creosote. The primary mechanism of PAH removal from the environment is biodegradation (NRC, 2003), also used extensively as a clean-up technology. Therefore, knowledge of biodegradation kinetics in natural and engineered systems is essential in calculating risks from PAH exposure and effectively implementing removal practices. It has been observed that degradation of a PAH in a mixture can be significantly affected by interactions with other mixture components (Guha et al., 1999). Yet the majority of studies on PAH biodegradability have focused either on modeling degradation of individual PAHs or on qualitatively describing interaction effects. A discussion on the current state, recent advances, and potential developments in microbial kinetics of suspended heterotrophic cultures (Kovárová-Kovar and Egli, 1998) signifies the need for a systematic experimental and modeling effort to elucidate the principles of mixed-substrate kinetics and express them quantitatively.

Studies modeling biodegradation of PAH mixtures are limited. Stringfellow and Aitken (1995) observed pure competitive inhibition kinetics in the degradation of binary mixtures of phenanthrene with one of naphthalene, 1-methylnaphthalene, 2-methylnaphthalene, and fluorene by two different pseudomonads. Naphthalene, methylnaphthalenes, and phenanthrene were carbon sources, while fluorene was degraded cometabolically. Guha et al. (1999) studied degradation of binary and ternary mixtures of naphthalene, phenanthrene, and pyrene by an acclimated mixed culture. The pure competitive inhibition model adequately described biodegradation kinetics, especially for the ternary mixture. Knightes (2000) investigated biodegradation of two binary mixtures, naphthalene with 1-methylnaphthalene and naphthalene with phenanthrene, as well as degradation of a complex mixture of nine unsubstituted and methylated PAHs. Biodegradation was achieved by an enriched consortium containing at least two sphingomonads. Despite data scatter, the competitive inhibition model

adequately captured interaction effects. All the above studies assumed that deviations from the Monod behavior were a result of purely competitive interactions. Two of the three studies assumed mutual substrate exclusivity. While these assumptions are reasonable for degradation of mixtures of homologous carbon and energy sources by pure cultures, it is not always valid as shown by studies with phenol, trichlorophenol, and pentachlorophenol (Klečka and Maier, 1988), benzene and toluene (Oh et al., 1994), and benzene, toluene, and phenol (Reardon et al., 2000; Reardon et al., 2002). Depending on the protein(s), transporters or enzymes, determining the kinetics of biodegradation, different interactions may occur between the solutes and single or multiple binding sites.

Biodegradation experiments in this study used pure *Sphingomonas paucimobilis* EPA505 induced with fluoranthene as described in Chapter III. A potent PAH degrader, this strain is commonly found in creosote- and fuel oil-contaminated soils (Mueller et al., 1997). A limited number of studies have investigated degradation of mixtures of PAHs by strain EPA505. Lantz et al. (1997) examined the effects of the concentration of a neutral creosote fraction containing 25 PAHs on the rate and extent of fluoranthene mineralization in the presence of Triton X-100. Luning Prak and Pritchard (2002) measured degradation rates of mixtures of phenanthrene, fluoranthene, and pyrene in the presence of Tween 80. Daugulis and McCracken (2003) evaluated degradation of a mixture of phenanthrene, naphthalene, pyrene, fluoranthene, chrysene, and benzo[a]pyrene in the presence of dodecane. All these studies were conducted under batch conditions and used dispersants to test biodegradation at concentrations above solubility. None of these studies applied kinetic modeling to quantitatively explain interaction effects.

The purpose of this study was to model biodegradation of binary and ternary mixtures of PAHs in batch systems, as a direct extension of the modeling conducted in Chapter III for individual PAHs. 2-Methylphenanthrene (2MPHE), a three-ring substituted PAH, fluoranthene (FLA), and pyrene (PYR), both four-ring PAHs, were used in the investigation. Kinetics were measured for the individual compounds and their

binary and ternary mixtures. The Monod and a series of interaction kinetic models were fitted to the data and inferences were reached about the interaction mechanisms and model applicability based on model fit. Despite simplifications, the experiment described in this study is a reasonable starting point for understanding mixture effects and simulating engineered and natural systems.

METHODS AND MATERIALS

Kinetic model formulation

Kinetic modeling of hyperbolic substrate uptake by a pure culture as a function of substrate concentration is often based on the Monod model. As discussed in Chapter III, the Monod and Andrews models adequately described biotransformation kinetics for 20 individual PAHs by *Sphingomonas paucomobilis* strain EPA505. When a substrate is present in a mixture of homologous compounds, biotransformation kinetics may be affected by interactions between the compounds and receptors, transporters or enzymes. The effect of interactions can be modeled on the basis of enzyme kinetics. It should be noted that there is no generic kinetic model that can alone describe all the possible protein-ligand interactions, especially when the receptor(s) are unknown or uncharacterized. This study attempted to cover the most common interaction types only.

When there is no interaction, kinetics can be described by the Michaelis-Menten model, which is analogous to the Monod model:

$$v_1 = \frac{V_{\max,1} C_{L,1}}{K_1 + C_{L,1}} \tag{5.1}$$

where v_1 (μmol substrate L^{-1} h^{-1}) is the initial velocity of the enzymatic transformation of substrate C_1, V_{max} is the limiting maximal initial velocity (μmol substrate L^{-1} h^{-1}), and $C_{L,1}$ is the concentration of substrate C_1 in the liquid phase. K_1 (μmol/L) is the dissociation constant of the EC_1 complex assuming rapid equilibrium, where E is the enzyme of interest.

An equilibrium system describing interactions among an enzyme E, a substrate C_1, and two alternative reversible substrates, C_2 and C_3, is represented in Fig. 5.1a. The model assumes that the alternative substrates act as inhibitors of the following types:

competitive, noncompetitive, or mixed-type (CI, NCI, or MI). The model also assumes that no direct interactions occur among C_1, C_2, and C_3. Constants K_1, K_2,

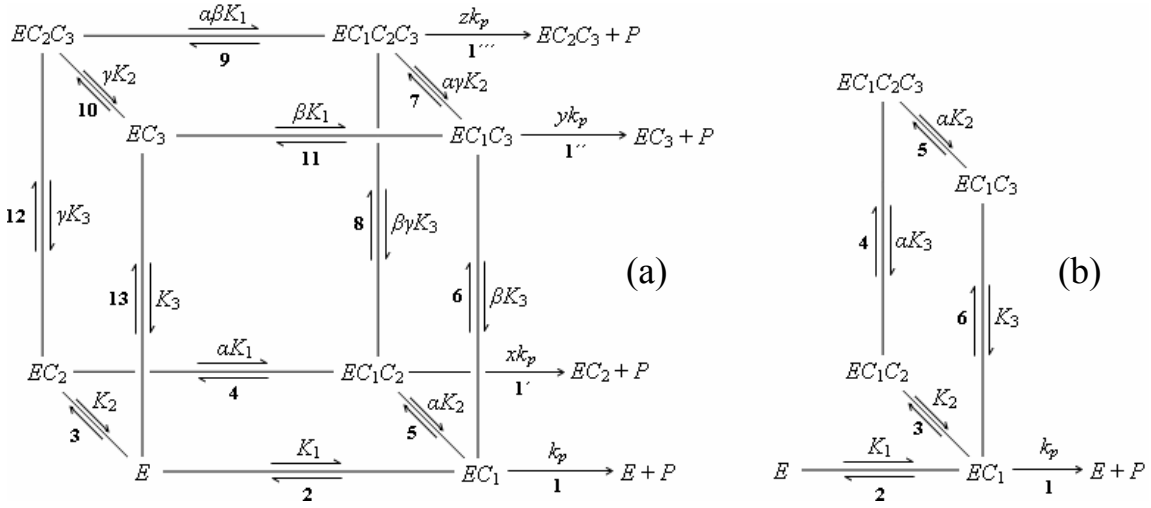

Fig. 5.1. Equilibria among an enzyme E, a substrate C_1, and two reversible inhibitors, C_2 and C_3. If C_2 and C_3 are alternative substrates, interactions can be competitive, noncompetitive, or mixed (a). If C_2 and C_3 are not substrates, inhibition is uncompetitive (b). Both systems assume no independent interactions between C_2 and C_3. Adapted from Keleti and Fajszi (1971), Segel (1975), and Martinez-Irujo et al. (1998).

and K_3 are the dissociation constants of complexes EC_1, EC_2, and EC_3, respectively. Factors α and β describe the relative change in enzyme affinity for C_1 caused by C_2 and C_3, respectively, or, conversely, the relative change in affinity for C_2 and C_3 caused by C_1. Factor γ describes the mutual effect of C_2 and C_3 on binding to E. When $\gamma = 1$, presence of C_2 does not affect binding of C_3 and vice versa, whereas when $\gamma \rightarrow \infty$, binding is mutually exclusive. The rate constant, k_p, describes the rate of dissociation of EC_1 to the reaction product, P, and the pure enzyme. Factors x, y, and z, assuming values between 0 and 1, describe the relative catalytic activity of complexes EC_1C_2, EC_1C_3, and $EC_1C_2C_3$, respectively, in yielding P. Fig. 5.1a includes numbers corresponding to each of the reversible and irreversible reactions for easy reference. Assuming rapid

equilibrium, and $x = y = z = 0$, a kinetic expression of the chemical system is (Martinez-Irujo et al., 1998):

$$v_1 = \frac{V_{\max,1} C_{L,1}}{K_1 + C_{L,1} + \frac{K_1 C_{L,2}}{K_2} + \frac{K_1 C_{L,3}}{K_3} + \frac{C_{L,1} C_{L,2}}{\alpha K_2} + \frac{C_{L,1} C_{L,3}}{\beta K_3} + \frac{K_1 C_{L,2} C_{L,3}}{\gamma K_2 K_3} + \frac{C_{L,1} C_{L,2} C_{L,3}}{\alpha\beta\gamma K_2 K_3}} \tag{5.2}$$

A pure competitive interaction model is described by reactions 1, 2, 3, 12, 10, and 13 in Fig. 5.1a. The corresponding kinetic model (Eq. 5.3) results from Eq. 5.2 when $\alpha, \beta \rightarrow \infty$:

$$v_1 = \frac{V_{\max,1} C_{L,1}}{K_1 + C_{L,1} + \frac{K_1 C_{L,2}}{K_2} + \frac{K_1 C_{L,3}}{K_3} + \frac{K_1 C_{L,2} C_{L,3}}{\gamma K_2 K_3}} \tag{5.3}$$

When $\gamma \rightarrow \infty$, the two alternative substrates are mutually exclusive and reactions 10 and 12 of the above sequence do not occur. When $C_{L,3} = 0$, Eq. 5.3 can be used to describe competitive kinetics between two substrates only, i.e., C_1 and C_2.

Noncompetitive and mixed-type interaction by two different mutually exclusive alternative substrates is described by reactions 1, 2, 3, 4, 5, 6, 11, and 13 in Fig. 5.1a. The kinetic equation for this system stems from Eq. 5.2 when $\gamma \rightarrow \infty$:

$$v_1 = \frac{V_{\max,1} C_{L,1}}{K_1 + C_{L,1} + \frac{K_1 C_{L,2}}{K_2} + \frac{K_1 C_{L,3}}{K_3} + \frac{C_{L,1} C_{L,2}}{\alpha K_2} + \frac{C_{L,1} C_{L,3}}{\beta K_3}} \tag{5.4}$$

Interaction is purely noncompetitive when $\alpha = \beta = 1$, partially mixed when $\alpha = 1$ and $\beta \neq 1$ and vice versa, and completely mixed when $\alpha \neq 1$ and $\beta \neq 1$. When $C_{L,3} = 0$ and $\alpha = 1$, Eq. 5.4 can be used to describe noncompetitive kinetics in the case of two alternative substrates only, i.e., C_1 and C_2. When $\alpha \rightarrow \infty$, reactions 4 and 5 of the above sequence do not occur and Eq. 5.4 becomes:

$$v_1 = \frac{V_{\max,1} C_{L,1}}{K_1 + C_{L,1} + \frac{K_1 C_{L,2}}{K_2} + \frac{K_1 C_{L,3}}{K_3} + \frac{C_{L,1} C_{L,3}}{\beta K_3}} \tag{5.4′}$$

In this case, C_2 acts as competitive, and C_3 as a noncompetitive or mixed-type alternative substrate with respect to C_1 (Segel, 1975). If two pure noncompetitive alternative substrates C_2 and C_3 are nonexclusive, then substituting $\alpha = \beta = 1$ in Eq. 5.2 results in:

$$v_1 = \frac{V_{\max,1} C_{L,1}}{K_1 + C_{L,1} + \frac{K_1 C_{L,2}}{K_2} + \frac{K_1 C_{L,3}}{K_3} + \frac{K_1 C_{L,2} C_{L,3}}{\gamma K_2 K_3} + \frac{C_{L,1} C_{L,2}}{K_2} + \frac{C_{L,1} C_{L,3}}{K_3} + \frac{C_{L,1} C_{L,2} C_{L,3}}{\gamma K_2 K_3}} \quad (5.5)$$

which corresponds to all the reactions in Fig. 5.1a except reactions 1′, 1′′, and 1′′′.

Uncompetitive inhibition differs from the cases discussed above in that C_2 and C_3 are inhibitors and not alternative substrates, i.e., they do not bind directly to the free enzyme but to EC_1 yielding inactive complexes. Uncompetitive inhibition by two inhibitors is represented by Fig. 5.1b. Assuming rapid equilibrium, the velocity equation for uncompetitive inhibition is described by (Segel, 1975):

$$v_1 = \frac{V_{\max,1} C_{L,1}}{K_1 + C_{L,1} + \frac{C_{L,1} C_{L,2}}{K_2} + \frac{C_{L,1} C_{L,3}}{K_3} + \frac{C_{L,1} C_{L,2} C_{L,3}}{a K_2 K_3}} \quad (5.6)$$

In the presence of one inhibitor only, the same equation applies by setting $C_{L,3} = 0$.

Assuming that interactions are pertinent to a common rate-limiting protein, i.e., a degradative enzyme or a membrane transporter, Eq. 5.1 through 5.6 can be adapted to describe kinetics of microbial uptake of a substrate present in a mixture of homologues. Specifically, v_1 can be substituted by q_1, the specific uptake rate (μmol substrate mg biomass $^{-1}$ h^{-1}); analogously, $V_{\max}$ can be substituted by $q_{\max}$, the maximal specific uptake rate, whose values were estimated in Chapter III for different PAHs. If the modeled compounds are substrates to a rate-limiting enzyme or transporter, the dissociation constants can be substituted by the substrate affinity coefficients, K_S, whose values were also estimated in Chapter III. In the case of uncompetitive inhibition the dissociation constants K_2 and K_3 cannot be substituted by the affinity coefficients because C_2 and C_3 are not substrates (to be precise, substitution is possible only if the dissociation of inhibitor C_i from EC_1C_i is the rate-limiting step in the transformation of C_i). Therefore, in uncompetitive inhibition K_2 and K_3 must be treated as fitting parameters.

A material balance equation for a batch process with instantaneous partitioning to the biomass and first-order abiotic losses is:

$$-\frac{1}{1+XK_{b,i}}\frac{dC_{T,i}}{dt} = q_i X + k_{a,i} t \tag{5.7}$$

where $C_{T,i}$ is the total concentration of C_i in a liquid sample containing suspended cells, X is the biomass concentration (mg/L), $K_{b,i}$ is the equilibrium partition coefficient for the sorption of C_i to the biomass, $k_{a,i}$ (h^{-1}) is the first-order abiotic loss coefficient for C_i, and t is time. In Eq. 5.7, q_i is expressed in terms of $C_{T,i}$ according to:

$$C_{L,i} = \frac{C_{T,i}}{1 + XK_{b,i}} \tag{5.8}$$

A discussion of the underlying assumptions and applicability of Eq. 5.7 and 5.8 can be found in Chapter III. Modified versions of Eq. 5.1 through 5.6, expressed in terms of microbial kinetics, can be incorporated into Eq. 5.7 yielding the following kinetic models: no-interaction (NI), pure competitive interaction (CI), noncompetitive or mixed-typed interaction (NCI or MI), and uncompetitive inhibition (UCI).

Adjustments to the classic interaction models described above have been proposed to explain deviations from theoretical behavior. Substituting K_2/K_1 with I_2 and K_3/K_1 with I_3 in Eq. 5.3, the microbial kinetic equivalent of pure competitive interaction with mutually exclusive substrates is:

$$q_1 = \frac{q_{\max,1} C_{L,1}}{K_1 + C_{L,1} + I_2 C_{L,2} + I_3 C_{L,3}} \tag{5.9}$$

Despite the theoretical basis of this model, Yoon et al. (1977) suggested that I_2 and I_3 should be treated as unknown parameters to account for cases in which the growth rate in a mixture is greater than the growth rate on either of the individual substrates. This unspecified interaction model, named SKIP for sum kinetics with interaction parameters (Reardon et al., 2000), accurately described kinetics of degradation of monoaromatic hydrocarbons by pure and mixed bacterial cultures (Reardon et al., 2000; Reardon et al., 2002) and is evaluated in this study.

Selection of PAHs for mixture experiments

PAHs were selected from the set of compounds examined in Chapter III for kinetic behavior. Selection was based on a number of considerations. PAHs causing substrate inhibition, namely 1-methylnaphthalene, 2-methylnaphthalene, and 2,3-dimethylnaphthalene, were not desirable because of possible interference between substrate inhibition and other forms of interactions or inhibition. Given that the kinetic models introduced above describe simultaneous interactions, PAHs were sought that would be biodegraded simultaneously. At high substrate concentrations, diauxic or sequential utilization is often observed, although this condition should not be applicable to PAHs due to their low solubilities. It has been suggested that substrates exhibiting low to medium maximal specific uptake rates are utilized simultaneously (Kovárová-Kovar and Egli, 1998). In Chapter III, q_{max} values ranged from 0.01 ± 0.01 for 1-methylpyrene to 2.19 ± 0.07 for 2-methylnaphthalene, both in units of μmol mg^{-1} BSA h^{-1}. To ensure simultaneous biodegradation, compounds were sought exhibiting low to medium q_{max} values. This criterion was also appealing because the slower kinetics would permit simultaneous sampling of multiple reactors, establishing a common time-step that would simplify numerical modeling. To satisfy the above requirements, 2-methylphenanthrene (2MPHE), fluoranthene (FLA), and pyrene (PYR) were selected. In the tested concentration ranges, the selected compounds are not inhibitory, are degraded according to the Monod model, and exhibit low to medium q_{max} (see Table 5.1 below and Table 3.1). In addition, 2MPHE, FLA, and PYR exhibit similar physicochemical properties and J_{max}, the theoretical maximal transmembrane flux as defined in Chapter IV, indicating that biodegradation kinetics for these compounds are determined by a common kinetic mechanism, possibly related to a permease carrier. According to Chapter III, 2MPHE and FLA can support growth of strain EPA505, while PYR cannot.

Chemicals

2-Methylphenanthrene (2MPHE) was purchased from Ultra Scientific (North Kingstown, RI). Fluoranthene (FLA) and pyrene (PYR) were purchased from Avocado Research Chemicals (Heysham, England). PAHs were of the highest purity available,

which was greater than 99%. The internal standard for PAH quantification via gas chromatography was a 1:1 mix of 20016 and GRH-IS standards purchased from Absolute Standards, Inc. (Hamden, CT) and AccuStandard, Inc. (New Haven, CT), respectively. A protein assay was used for the quantification of biomass as bovine serum albumin (BSA) according to the method of Bradford (1976). The protein assay kit was purchased from Bio-Rad (Hercules, CA).

Table 5.1
Best estimates of kinetic parameters describing the biodegradation of 2-methylphenanthrene (2MPHE), fluoranthene (FLA), and pyrene (PYR) individually by strain EPA505. Uncertainty is expressed as the margin of error at the 95% confidence level. Values in parentheses, estimated in Chapter III, are provided for comparison.

Comp.	**Sol.**[a] (μmol/L)	C_T^0 (μmol/L)	q_{max} (μmol mg^{-1} h^{-1})	K_S (μmol/L)	q_{max}/K_S (L mg^{-1} h^{-1})
2MPHE	1.46	0.45 ± 0.00 (0.61 ± 0.02)	0.42 ± 0.04 (0.54 ± 0.10)	0.18 ± 0.03 (0.15 ± 0.06)	2.45 ± 0.54 (3.73 ± 1.56)
FLA	1.29	0.74 ± 0.02 (0.70 ± 0.02)	0.22 ± 0.03 (0.20 ± 0.02)	0.07 ± 0.03 (0.07 ± 0.03)	3.08 ± 1.38 (2.96 ± 1.16)
PYR	0.67	0.37 ± 0.01 (0.34 ± 0.01)	0.15 ± 0.02 (0.16 ± 0.03)	0.14 ± 0.03 (0.15 ± 0.04)	1.08 ± 0.28 (1.10 ± 0.31)

[a] Aqueous solubility values taken from Howard and Meylan (1997) and converted into μmol/L.

Pure culture

Sphingomonas paucimobilis DSM 7526 (strain EPA505) was purchased from DSMZ (Braunschweig, Germany). Cells were induced on FLA as described in Chapter III. To grow biomass for the biokinetic experiment, cryopreserved cells were added to nutrient broth supplemented with 0.4 g/L glucose and incubated for 36 h at 30 ºC (Ye et al., 1996). Biomass was washed three times with Bushnell-Haas broth and the concentrated inoculum was added to batch reactors to initiate biodegradation immediately after measurement of its concentration.

Batch biokinetic experiment

An experiment was conducted to measure biodegradation kinetics of 2MPHE, FLA, and PYR individually, in binary mixtures (2MPHE-FLA, 2MPHE-PYR, and FLA-PYR), and in the ternary mixture (2MPHE-FLA-PYR). Kinetics of the individual compounds provided parameter estimates used to model biodegradation kinetics in the mixtures. Kinetics in the binary mixtures allowed inference about the interaction types without the complexity introduced by the larger mixture. The experiment was conducted under extant conditions as defined by Grady et al. (1996) and discussed in Chapter III. A detailed protocol for the biokinetic experiment can be found in Chapter III. In brief, duplicate 250 mL serum-bottle reactors containing 150 mL of a PAH solution in Bushnell-Haas broth, a total of 14 reactors, received approximately 1.5 mL of the concentrated biomass to achieve $X \approx 3.0$ mg BSA/L. Ten 7-mL samples were taken from each reactor at designated sampling times. Sampling events coincided for all bioreactors establishing a common time-step and total depletion time that would simplify numerical modeling for parameter estimation. To accomplish that, preliminary experiments were conducted to determine appropriate initial concentrations for each PAH, designed to be the same in every treatment. In all cases, initial concentrations were below the corresponding aqueous solubility values (Table 5.1) and satisfied the extant-kinetic conditions.

Samples collected from each batch reactor were added to 16-mL screw cap tubes with Teflon-coated caps containing 3 mL dichloromethane (DCM) for liquid extraction and then shaken on a rotary shaker for at least 4 h. One (1.0) mL of the DCM extract was removed with a glass pipette and added to an autosampler vial with 10 μL internal standard for gas chromatography/mass spectrometry (GC/MS) analysis. A 2.5-mL sample was taken from each reactor at the beginning and at the end of each run for biomass quantification as BSA. Experiments were conducted at 22 °C. As found in Chapter III, degradation by autoclaved cells was not appreciable for 2MPHE, FLA, and PYR, and every other PAH; therefore, no killed-control treatments were tested in this experiment.

Analytical procedures

Measurements of PAH concentration were conducted with GC/MS on an HP 5890 Series II chromatograph interfaced with a HP 5972 mass selective detector (Agilent Technologies Inc., Palo Alto, CA). The type of the column was HP-5MS ((5%-Phenyl)-Methylpolysiloxane, 0.25 mm × 30 m × 0.25 μm, J&W Scientific (Palo Alto, CA)). The following temperature program was used: 60 ºC, 8.0ºC/min for 30 min to 300 ºC. The mass spectrometer was operated in the selective ion mode (SIM). The quantitation limit of the method was 0.001 mg/L. Biomass measurements were conducted with an HP 8452 UV-Visible spectrophotometer (Agilent Technologies Inc., Palo Alto, CA) measuring the absorbance of BSA at 595 nm.

Model fitting and evaluation of fit

Degradation data were used as input to different interaction models to draw inferences about the underlying interaction mechanisms based on the model fit. The integrated form of Eq. 5.7 containing the microbial kinetic equivalent of one of Eq. 5.1, 5.2, and 5.6, or Eq. 5.9 was fitted to the depletion data using nonlinear regression, specifically, minimizing the sum of squared errors, *SSE*, based on *n* observations:

$$SSE_i = \sum_{j=0}^{n-1} (C_{T,i}^j - \hat{C}_{T,i}^j)^2 \tag{5.10}$$

where $C_{T,i}^j$ is the observed total concentration of substrate *i* in the *j*th sample and $\hat{C}_{T,i}^j$ is the corresponding concentration predicted by the model. Simultaneous integration of the kinetic equation over a series of time steps corresponding to the sampling events was accomplished by a fourth-order Runge-Kutta numerical algorithm. In modeling degradation of individual PAHs, the fitting parameters were C_T^0, $q_{\max}$, and K_S. Best estimates of $q_{\max}$ and K_S were used in modeling degradation of mixtures, when applicable. In modeling mixture kinetics, the fitting parameters were one or more of the following, depending on the model: C_T^0, α, β, γ, K_2, K_3, I_2, and I_3. Uncertainties in the best estimates, expressed as the margins of error at the 95% confidence level, $E_{95\%}$, were calculated using the method of Smith et al. (1998). In brief, the method used the mean

square fitting error, s^2, and the inverse of a $p \times p$ matrix containing sensitivity coefficients quantifying the sensitivity of fit to changes in the best estimate of a parameter. Overall, $E_{95\%}$ depended on *SSE* and the total degrees of freedom, df = $n - p$, where n is the numbers of observations and p is the number of fitting parameters. The value of p varies depending on the interaction type. For example, for binary-mixture modeling with uncompetitive inhibition, the fitting parameters are C_T^0 and K_2; therefore, $p = 2$. When using the microbial kinetic equivalent of Eq. 5.2, the value of p is not as apparent because this equation encompasses different interaction types. For example, for binary-mixture modeling, if interaction is purely competitive, $\alpha \rightarrow \infty$ and $p = 1$ due to C_T^0. Similarly, if interaction is partially mixed, $\alpha = 1$ and $p = 1$ due to C_T^0; finally, if interaction is completely mixed, α is different than ∞ and 1, and $p = 2$ due to C_T^0 and α. Best estimates of $q_{\max}$ and K_S used in modeling mixture kinetics were allowed to vary within their 95% confidence intervals without removing any degrees of freedom. The value of df was critical because it affected model fit and significance. Fit models with $p = 1$, i.e., due to C_T^0 only, were considered ideal because they were fully predictive, using no additional kinetic parameters except those estimated in the individual-PAH experiments.

To evaluate model fit, the adjusted pseudo-coefficient of determination was used, defined as (Kvålseth, 1985):

$$R_{adj}^2 = 1 - \frac{n}{n-p}\frac{SSE}{SST} \tag{5.11}$$

where *SST* is the total sum of squares corrected for the mean. The overall significance of the model was tested by the significance of the *F* value, Sig. *F*. Homoscedasticity, an assumption of nonlinear regression, was evaluated using residual plots. When there was evidence of heteroscedasticity, *H*, graphical evaluation was formalized by the modified Park test (Park, 1966), which tests the hypothesis that b_1 in the following regression equation is zero, i.e., there is no heteroscedasticity:

$$\ln(C_{T,i} - \hat{C}_{T,i})^2 = b_0 + b_1 \ln \hat{C}_{T,i} + r_i \tag{5.12}$$

where b_0 and b_1 are regression coefficients and r_i is a residual term. In case the errors were homoscedastic for one reactor and heteroscedastic for the duplicate reactor, the Park test was applied to the combined errors from both reactors. Models with $R^2_{adj} > 0.99$ were not considered for heteroscedasticity. Models with heteroscedastic errors were considered non-ideal. A non-hypothesis-testing approach was implemented to compare the fit of different models to the same data because not all the models used were nested. Even when two models are nested, certain hypothesis tests are not applicable. For example, when comparing the fit of two models, one containing Eq. 5.5 and the other the nested Eq. 5.3, use of the extra-sum-of-squares F test is not possible because the null model and the alternative model would have the same degrees of freedom. The Akaike Information Criterion (*AIC*) (Akaike, 1973) is often used to compare the fit of multiple, nested or non-nested models. This technique, based on information theory rather than statistical significance, can reveal which model is more likely the fittest and quantify how much more likely. A corrected value of the criterion (AIC_c) is calculated as (Motulsky and Christopoulos, 2003):

$$AIC_c = n \cdot \ln\left(\frac{SSE}{n}\right) + 2(p+1) + \frac{2(p+1)(p+2)}{n-p-2} \tag{5.13}$$

The model with the lowest AIC_c value is more likely the fittest. When comparing model fit on the same dataset, the order of AIC_c values usually coincides with the order of the significance values of the F-statistic. In addition, AIC_c allows comparison on a probabilistic basis. In a pair of models, the probability P_{AIC_c} of the model with the lower AIC_c being fitter than the model with the higher AIC_c is given by the following equation (adapted from Motulsky and Christopoulos, 2003):

$$P_{AIC_c} = \frac{1}{1+e^{-0.5|\Delta AIC_c|}} \tag{5.14}$$

where $|\Delta AIC_c|$ is the absolute difference in AIC_c values between the two models. A zero difference results in a probability of 0.5; absolute differences of 6 and 9 result in probabilities of 0.95 and 0.99, respectively. To summarize, model selection was based

on the values of R^2_{adj}, AIC_c, information on heteroscedasticity, and logical deductions from Table 5.2 as described in the following section.

RESULTS AND DISCUSSION

Data show that degradation of 2MPHE, FLA, and PYR in mixtures occurred simultaneously without the evidence of diauxic response. The effects of the presence of other PAHs on the degradation rates varied as shown in Fig. 5.2. For example, the rate of 2MPHE degradation decreased considerably in the presence of FLA (Fig. 5.2a). On the other hand, the rate of FLA degradation did not change noticeably in the presence of PYR (Fig. 5.2b). 2MPHE and FLA reduced the PYR degradation rate to a different extent (Fig. 5.2c), presumably due to the different K_S values of these compounds (Table 5.1). Degradation of PYR in the presence of FLA proceeded at a slow rate until depletion of FLA (Fig. 5.2d); after that point, the rate increased to a level similar to the one observed for PYR alone. Exactly the same behavior has been observed elsewhere (Luning Prak and Pritchard, 2002). To summarize, it was observed that kinetics in a mixture were either similar or slower than those observed for the individual PAHs. Kinetics were influenced by the mixture composition and the kinetic properties of the components.

The first step in explaining mixture kinetics involved estimation of Monod parameters for the individual 2MPHE, FLA, and PYR. Best estimates of the maximal specific uptake rate, $q_{\max}$, the substrate affinity coefficients, K_S, and the specific affinity, $q_{\max}/K_S$ are presented in Table 5.1. Values were consistent with those estimated in Chapter III, also presented in parentheses in the table. 2MPHE exhibited a $q_{\max}$ of 0.42 ± 0.04, followed by FLA and PYR, with values of 0.14 ± 0.03 and 0.07 ± 0.03, respectively, all expressed in μmol mg^{-1} BSA h^{-1}. Statistically, 2MPHE and PYR exhibited the same K_S of 0.18 ± 0.03 and 0.14 ± 0.03, respectively, while FLA exhibited a lower value, 0.07 ± 0.03, all in μmol/L. Uncertainties in the estimates are expressed as the margins of error at the 95% confidence level. When applicable, these estimates, allowed to vary within their confidence intervals, were used to model kinetics in the binary and ternary mixtures.

Table 5.2
Evaluation of model fit in modeling biodegradation of a PAH (2MPHE, FLA, or PYR, underlined in the left column) in binary and ternary mixtures with the other two PAHs. Numbers represent mean values calculated from duplicate reactors.

Mixture	Model	R^2_{adj}	F	Sig. F	AIC_c	df	H	Remarks
2MPHE + FLA	**NI**	0.784	46.4	5.1E-04	-30.8	6	yes	
	CI	0.998	3331.7	2.5E-09	-63.1	6	no	$K_{S,1}/K_{S,2} = 3.40 \pm 2.18$
	UCI	0.996	911.9	3.9E-07	-53.4	5	no	$K_2 = 0.10 \pm 0.01$ μmol/L
	SKIP	0.997	1371.0	1.7E-07	-56.1	5	no	$I_2 = 2.85 \pm 0.25$
2MPHE + PYR	**NI**	1.000	60061.2	6.3E-09	-60.7	5	no	
	CI	0.999	5541.4	7.1E-08	-48.5	5	no	$K_{S,1}/K_{S,2} = 0.84 \pm 0.27$
	UCI	1.000	25119.1	1.1E-06	-46.1	4	no	$K_2 = 1.00 \pm 0.19$ μmol/L
	SKIP	1.000	23752.6	1.2E-06	-45.7	4	no	$I_2 = 0$ (reduces to NI)
FLA + 2MPHE	**NI**	0.998	3116.4	5.7E-08	-49.2	5	no	
	CI	0.996	1542.3	2.7E-07	-45.2	5	no	$K_{S,1}/K_{S,2} = 0.26 \pm 0.12$
	UCI	0.998	1481.5	2.4E-06	-40.2	4	no	$K_2 = 0.95 \pm 0.28$ μmol/L
	SKIP	0.997	1246.5	3.6E-06	-39.2	4	no	$I_2 = 0$ (reduces to NI)
FLA + PYR	**NI**	0.996	2446.4	7.0E-10	-63.1	8	no	
	CI	0.996	1988.4	8.0E-10	-61.6	8	no	$K_{S,1}/K_{S,2} = 0.28 \pm 0.18$
	UCI	0.996	1062.9	3.7E-08	-57.9	7	no	$K_2 \rightarrow \infty$ (reduces to NI)
	SKIP	0.996	1062.9	3.7E-08	-57.9	7	no	$I_2 = 0$ (reduces to NI)
PYR + 2MPHE	**NI**	0.972	319.4	1.1E-06	-62.0	8	yes	
	CI[a]	0.992	1758.9	2.4E-08	-74.7	8	no	$K_{S,1}/K_{S,2} = 0.68 \pm 0.26$
	UCI	0.992	854.9	5.8E-07	-70.3	7	no	$K_2 = 0.15 \pm 0.04$ μmol/L
	SKIP	0.992	866.9	4.0E-07	-70.6	7	yes	$I_2 = 1.10 \pm 0.28$
PYR + FLA	**NI**	0.658	50.2	6.8E-05	-44.9	9	no	
	CI	0.989	907.1	2.9E-10	-79.2	9	no	$K_{S,1}/K_{S,2} = 3.16 \pm 2.97$
	UCI	0.986	347.2	1.7E-08	-73.5	8	no	$K_2 = 0.06 \pm 0.01$ μmol/L
	SKIP	0.988	404.6	1.1E-08	-75.0	8	no	$I_2 = 3.30 \pm 0.67$
2MPHE + FLA + PYR	**NI**	0.937	146.6	6.1E-06	-43.1	7	yes	
	CI	0.991	929.0	1.3E-08	-60.3	7	no	$\gamma \rightarrow \infty$ $K_{S,1}/K_{S,2} = 2.39 \pm 1.36$ $K_{S,1}/K_{S,3} = 0.84 \pm 0.38$
	UCI	-	-	-	-	-	-	unstable solution
	SKIP	0.990	280.0	7.0E-06	-45.9	5	yes	$I_2 = 2.20 \pm 1.04$; $I_3 = 0$
FLA + 2MPHE + PYR	**NI**	0.993	1413.3	1.8E-06	-48.8	6	no	
	CI	0.946	109.5	2.8E-04	-34.4	6	yes	$\gamma \rightarrow \infty$ $K_{S,1}/K_{S,2} = 0.23 \pm 0.12$ $K_{S,1}/K_{S,3} = 0.35 \pm 0.18$
	UCI	0.989	313.5	7.7E-04	-18.3	4	no	$K_2, K_3 \rightarrow \infty$ (reduces to NI)
	SKIP	0.989	314.0	7.7E-04	-18.3	4	no	$I_2, I_3 = 0$ (reduces to NI)
PYR + 2MPHE + FLA	**NI**	0.866	80.6	1.8E-05	-56.5	9	yes	
	CI	0.985	698.4	2.9E-09	-84.7	9	no	$\gamma \rightarrow \infty$ $K_{S,1}/K_{S,2} = 0.72 \pm 0.27$ $K_{S,1}/K_{S,3} = 3.20 \pm 2.63$
	UCI	-	-	-	-	-	-	unstable solution
	SKIP	0.992	389.2	4.5E-07	-74.3	7	no	$I_2 = 0.76 \pm 0.44$ $I_3 = 3.34 \pm 1.30$

[a] The algorithm containing the CI/NCI/MI model initially converged to NCI kinetics ($\alpha = 1.35 \pm 0.85$) with SSE = 6.98E-04 μmol^2 L^{-2}. However, the CI-type kinetics with SSE = 7.98E-04 μmol^2 L^{-2} was preferred because it yielded a lower average AIC_c (-74.7 versus –70.5 for NCI) due to the lower df.

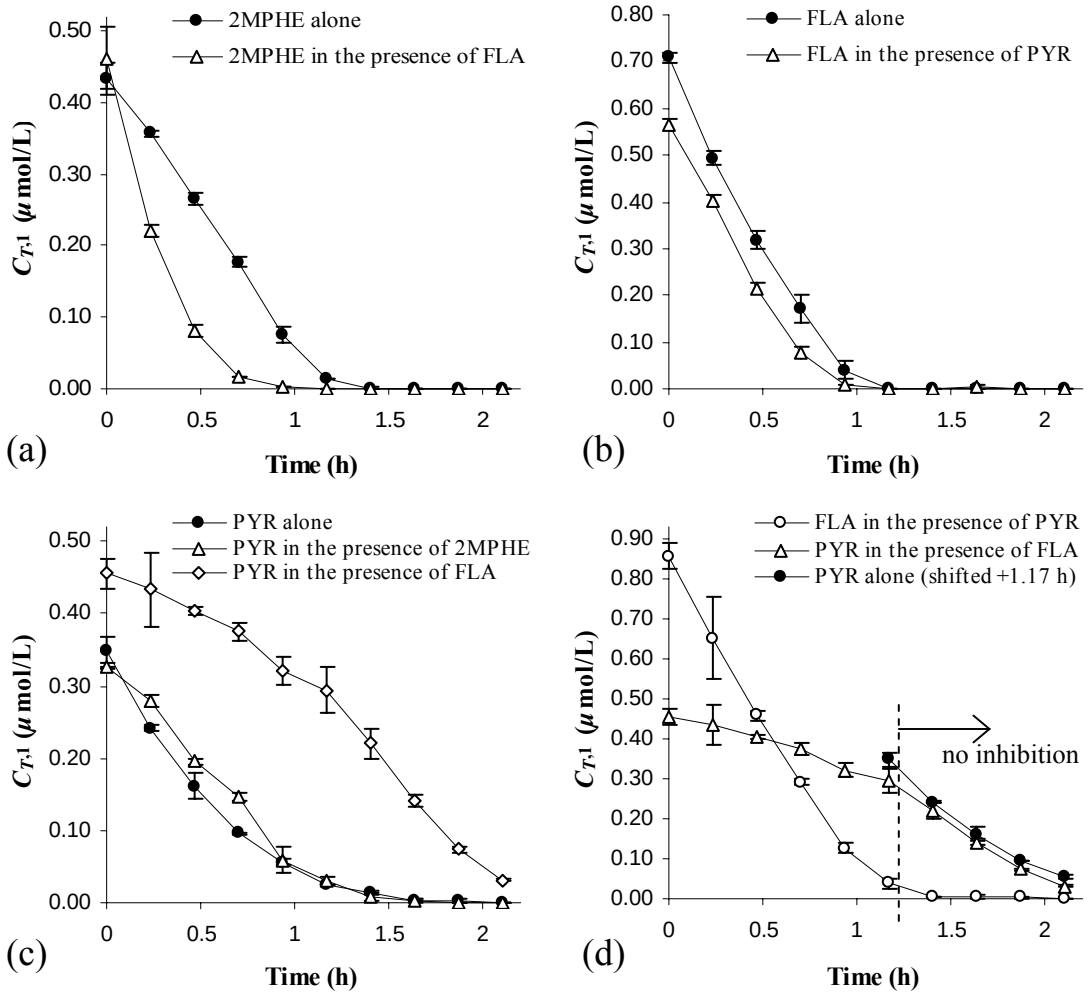

Fig. 5.2. Illustration of mixture effects in the biodegradation of 2MPHE, FLA, and PYR by *Sphingomonas paucimobilis* strain EPA505. Data points represent mean concentrations from duplicate batch reactors. Error bars represent one standard deviation from the mean.

Modeling degradation in the three binary mixtures provided the basis of understanding interaction effects. Fig. 5.3 illustrates fitting of the four models under investigation to the data of PYR degradation in the presence of FLA. Fit was excellent for the CI model, the UCI model, and the SKIP model (Fig. 5.3b through 5.3d). In addition, errors were homoscedastic for all models. Based on probability as calculated by the AIC_c, the correct model is CI, followed by SKIP and UCI. Specifically, there is

90% probability that the CI model (Fig. 5.3b) is the correct one over the SKIP model (Fig. 5.3d). Estimates for the duplicate reactor were analogous; specifically, an 89% probability was found by which the CI model is the right one over the SKIP model.

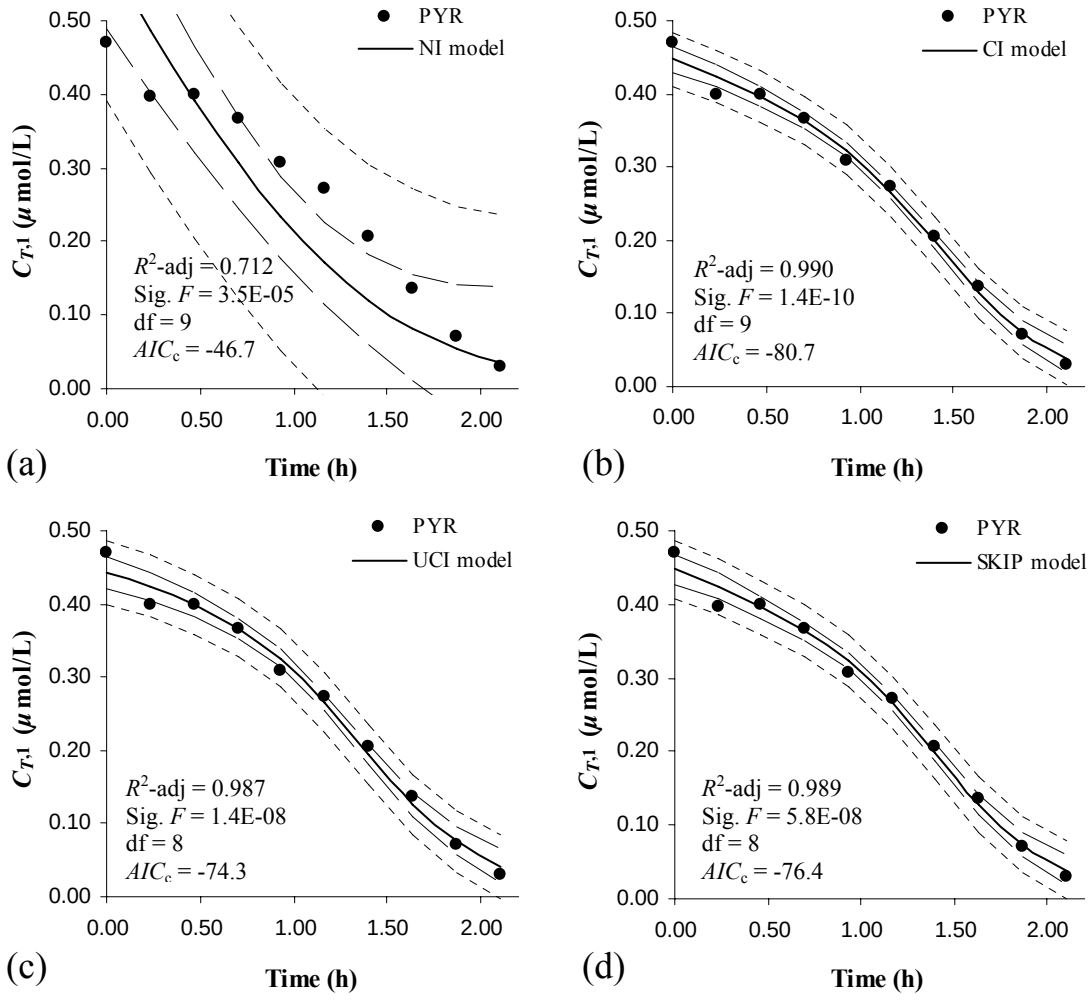

Fig. 5.3. Evaluation of model fit (——) to data of PYR (●) biodegradation in the presence of FLA. Data was acquired from one of duplicate batch reactors. Each model describes a different interaction mechanism: no-interaction Monod (a), pure competitive interaction (b), uncompetitive interaction (c), and nonspecific-interaction kinetics with interaction parameters (d). Long dashes (— —) and short dashes (--) represent the 95% confidence and prediction bands, respectively. Based on the corrected value of the Akaike Information Criterion (AIC_c), there is 89.6% probability that the CI model (b) is the right one compared to the SKIP model (d).

Simulations were also performed for the other binary cases and the results are presented in Table 5.2 with values representing mean values for the duplicate reactors. Based on the AIC_c scores, low being best fit, degradation of 2MPHE in the presence of FLA, PYR in the presence of 2MPHE, and PYR in the presence of FLA were most adequately explained by pure CI kinetics. This was also supported by the I_2 values of the SKIP model being statistically equal to the $K_{S,1}/K_{S,2}$ values of the CI model (Table 5.2). In other words, the unspecified-interaction SKIP model also converged to CI kinetics. Purely competitive interaction requires that the complimentary cases also exhibit CI kinetics. However, for the three complimentary binary cases, i.e., FLA in the presence of 2MPHE, 2MPHE in the presence of PYR, and FLA in the presence of PYR, the fittest model was the NI (Monod) with CI following (Table 5.2). This is paradoxical, considering that CI and NI can never be equivalent algebraically because the $K_{S,1}/K_{S,2}$ ratio is always positive. The inconsistency can be explained in terms of the percent inhibition, $I_{\%}$, defined as the relative change in specific uptake rate due to inhibition. For a binary case, $I_{\%}$ is calculated as follows:

$$I_{\%} = 100\left(1 - \frac{q_1^{inh}}{q_1^{uninh}}\right) = 100\frac{C_{L,2}}{C_{L,2} + K_{S,2}\left(1 + \frac{C_{L,1}}{K_{S,1}}\right)} \tag{5.15}$$

where q_1^{uninh} is the initial uptake rate of substrate C_1 at $C_{L,1}$, and q_1^{inh} is the initial uptake rate of substrate C_1 at $C_{L,1}$ in the presence of $C_{L,2}$. An analogous relationship can be written for ternary cases. The percent inhibition assuming CI kinetics was computed for all binary and ternary cases and the results are presented in. Cases are grouped in two categories, one with high $I_{\%}$ values and the other one with low. Not surprisingly, cases exhibiting CI kinetics also exhibited high $I_{\%}$, while those exhibiting lack of interaction, low $I_{\%}$. A one-tailed *t*-test at the 0.05 significance level showed that the average $I_{\%}$ of the first group was significantly greater than that of the second group. Therefore, the data suggests that interactions may occur without being evident, due to low $I_{\%}$. According to Eq. 5.15, $I_{\%}$ is low for binary cases when one or more of the following conditions occur: $K_{S,2} >> C_{L,2}$, $C_{L,1} >> C_{L,2}$, or $K_{S,2} >> K_{S,1}$. In this study, the low $I_{\%}$ observed in the three

binary cases was a combined result of the latter two conditions, especially the last. As can be seen in Table 5.2, the two cases with the lowest $K_{S,1}/K_{S,2}$ ratios, FLA in the presence of 2MPHE, and FLA in the presence of PYR, exhibited NI kinetics. On the contrary, the two cases with the highest $K_{S,1}/K_{S,2}$ ratios, 2MPHE in the presence of FLA, and PYR in the presence of FLA, exhibited CI kinetics. Given the finding of CI kinetics as well as the experimental design, i.e., the choice of compounds and initial concentrations, competitive inhibition of FLA degradation would have been more evident had more samples per reactor been taken. Then, the algorithm with the CI model would better capture the curvature in the depletion curve caused by inhibition instead of causing the solution curve to lay straight between data points. To summarize, it is proposed that the kinetics of degradation of the binary mixtures of 2MPHE, FLA, and PYR were determined by pure competitive interactions.

A similar study of naphthalene, phenanthrene, and pyrene degradation found that kinetics observed in binary mixtures did not significantly differ from those observed for the individual compounds, despite the fact that competitive interactions were observed in the degradation of the ternary mixture (Guha et al., 1999). Given that the initial PAH concentrations were just below solubility, it was concluded that "if substrate interactions [in the binary mixtures] were operative they probably would have been evident" and that "substrate interactions in binary PAH mixtures are not likely to be significant in contamination scenarios in the environment under aerobic conditions" (Guha et al., 1999). This proposition is not supported by the data of this dissertation, which show clear evidence of competitive interactions especially in cases with high $I_{\%}$. Using the C_T^0 and K_S values reported by Guha et al. (1999), it was found that $I_{\%}$ was relatively low in their binary experiments; for example, $I_{\%}$ for naphthalene degradation was 34% in the presence of phenanthrene and 27% in the presence of pyrene, without taking into account biosorption that would lower $I_{\%}$ even further. $I_{\%}$ for naphthalene in the ternary mixture, assuming mutually exclusive substrates, was considerably higher (48%). This finding is consistent with the proposition that mixtures of competitive substrates may show limited or no evidence of interaction at lower $I_{\%}$ values.

Table 5.3
Percent inhibition, $I_{\%}$, assuming pure competitive interaction (CI) between mutually exclusive substrates. The first group contains cases exhibiting pure CI according to Table 5.2. The second group contains the complimentary cases exhibiting no-interaction kinetics (NI) and not CI as expected. The inconsistency is attributed to the significantly lower $I_{\%}$ values in the second group.

Case	Apparent interaction type	Mean $I_{\%}$[a]	s[b]
2MPHE + FLA	pure CI	71.5	1.9
PYR + 2MPHE	pure CI	48.2	0.4
PYR + FLA	pure CI	83.2	5.0
2MPHE + FLA + PYR	pure CI	64.0	1.6
PYR + 2MPHE + FLA	pure CI	83.5	5.4
FLA + 2MPHE	NI (Monod)	15.7	0.8
2MPHE + PYR	NI (Monod)	21.3	0.4
FLA + PYR	NI (Monod)	9.6	0.1
FLA + 2MPHE + PYR	NI (Monod)	26.1	0.5

[a] Mean calculated from the two duplicate reactors.
[b] Standard deviation from the mean.

The pure CI kinetics found in the degradation of the binary mixtures of 2MPHE, FLA, and PYR in this study pointed to CI kinetics for the ternary mixture. Indeed, degradation of 2MPHE in the presence of FLA and PYR, and PYR in the presence of 2MPHE and FLA were most adequately described by the pure CI model with $\gamma \rightarrow \infty$ (Table 5.2). Mutual substrate exclusivity ($\gamma \rightarrow \infty$) is consistent with the hypothesis of a permease carrier as the enzyme responsible for the observed interaction kinetics and interactions. In the case of FLA degradation in the presence of 2MPHE and PYR, the NI model was apparently the best, followed by the CI model. This discrepancy is again attributed to the low $I_{\%}$ value as shown in Table 5.3. Without exception, $K_{S,1}/K_{S,2}$ values calculated for the binary cases were verified in the ternary cases (Table 5.2). For example, the $K_{S,1}/K_{S,2}$ found for the degradation of PYR in the presence of 2MPHE and FLA was statistically equal to the $K_{S,1}/K_{S,2}$ value for the degradation of PYR in the

presence of 2MPHE (0.72 ± 0.27 and 0.68 ± 0.26, respectively). Similarly, the $K_{S,1}/K_{S,3}$ for the ternary case was statistically equal to the $K_{S,1}/K_{S,2}$ for the degradation of PYR in the presence of FLA (and 3.20 ± 2.63 and 3.16 ± 2.97, respectively). Fitting of the CI model to the biodegradation data for the three binary and the single ternary mixture is

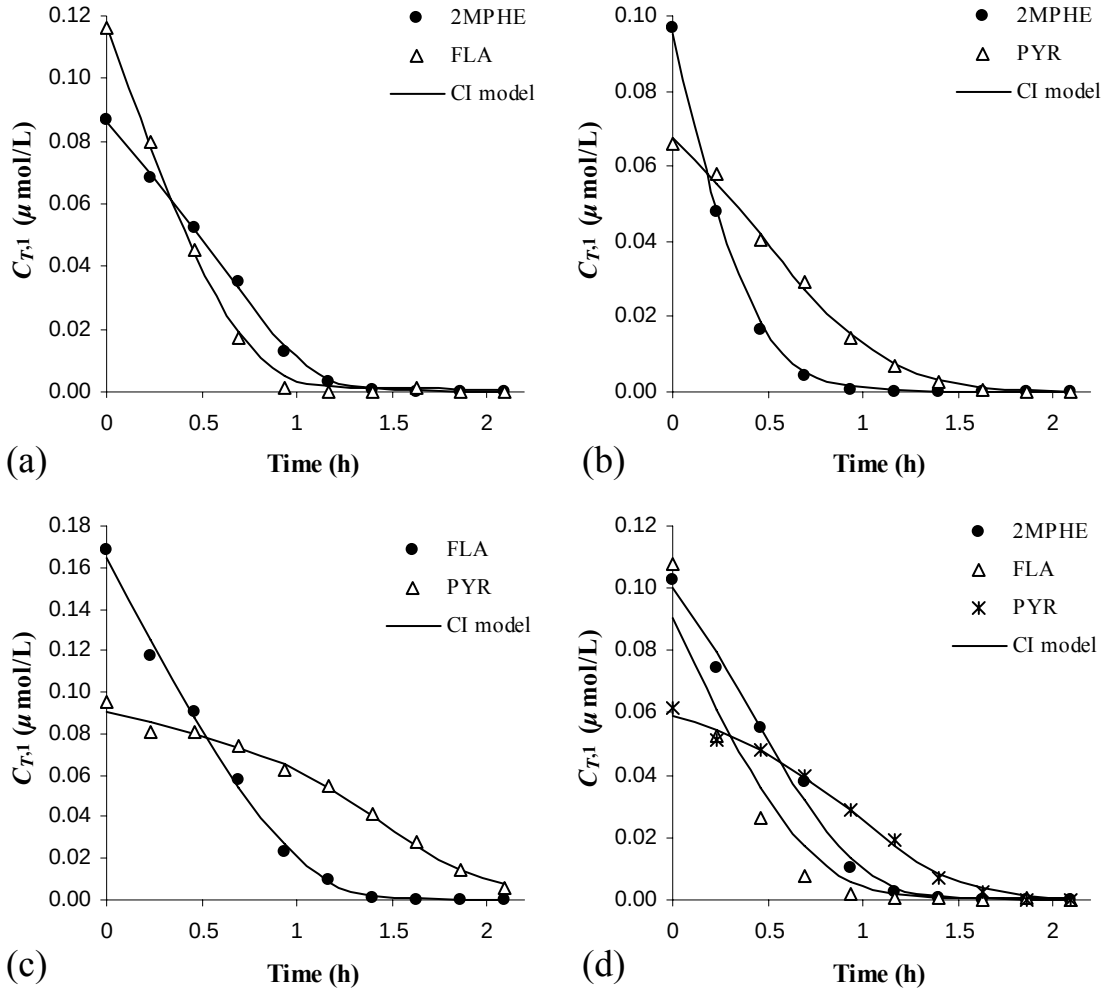

Fig. 5.4. Fitting of the pure competitive interaction model (CI) to depletion data of binary (a, b, and c) and ternary (d) mixtures of 2MPHE, FLA, and PYR. In every case, the model describes pure competitive interactions by exclusive alternative substrates. From the four interaction models tested (NI, CI/NCI/MI, UCI, and SKIP), the CI model most adequately described biodegradation in mixtures. Presented data was acquired from one of duplicate batch reactors.

illustrated in Fig. 5.4. The agreement between the experimental and predicted curves is excellent except for the FLA degradation in the ternary mixture for reasons discussed above. Model statistics can be found in Table 5.2. To summarize, it was found that the kinetics of degradation of both binary and ternary mixtures of 2MPHE, FLA, and PYR by strain EPA505 are determined by purely competitive interactions with mutual substrate exclusivity.

The occurrence of competitive interactions suggests that transformation kinetics are determined by a common mechanism, possibly membrane binding and transport as proposed in Chapter IV. In addition, mutual substrate exclusivity implies that 2MPHE, FLA, and PYR are alternative ligands to a common binding site. The finding of CI kinetics is consistent with the hypothesis that "competitive metabolism may be common phenomenon among PAH-degrading organisms" based on the observation of CI in physiologically diverse microorganisms (Stringfellow and Aitken, 1995). A pure CI model with mutually exclusive alternative substrates is fully predictive, requiring no additional parameters other than those estimated in sole-PAH experiments. From this perspective, the SKIP model was not useful in simulating the data other than for verification of pure CI kinetics. The SKIP model may also be useful in cases where kinetics cannot be explained mechanistically. Assuming that competitive interactions are common in the biodegradation of PAHs by *Sphingomonas paucimobilis* strain EPA505, then parameters calculated in Chapter III and those estimated by the qualitative structure-biodegradability relationships (QSBRs) of Chapter IV would be valuable in describing biodegradation of a wide range of PAH mixtures by the strain.

The finding of pure CI kinetics for mixtures of 2MPHE, FLA, and PYR does not rule out other types of interaction for different PAH mixtures. Therefore, additional testing of homologous and heterologous PAH mixtures is required for determining occurrence and types of interactions. Testing should involve binary as well as complex PAH mixtures. Although derivation of the pure CI model is easy for any number of mutually exclusive components, derivation of models with uniform or mixed forms of interaction is cumbersome for large mixtures. A graphical method for analysis of

interactions among multiple substrates/inhibitors can be found in Asante-Appiah and Chan (1996). Given that the effects of an occurring interaction are not always detectable, as seen in this study, selection of test compounds and their initial concentrations should be such as to increase the degree of anticipated interactions. Finally, experiments with mixed cultures will indicate whether similar interactions can be expected in natural or engineered systems.

CHAPTER VI
SUMMARY AND CONCLUSION

Polycyclic aromatic hydrocarbons (PAHs) are ubiquitous environmental pollutants of significant public health and environmental concern. Knowledge of physicochemical behavior, bioavailability, and fate of PAHs is necessary for accurate exposure assessment and implementation of effective detoxification strategies for wastes and contaminated sites. This research trained models for the physicochemical properties and biodegradability of common PAHs. The following paragraphs summarize the findings and conclusions of this research.

Chapter II described the development of linear free energy relationships (LFERs) predicting physicochemical properties of PAHs based on chromatographic retention data. LFERs accurately estimated the liquid aqueous solubilities, $S_{w,L}$, octanol/water partition coefficients, K_{ow}, liquid vapor pressures, $P_{v,L}$, and Henry's law constants, H_c, for methylated naphthalenes. Given the compound diversity in the reference set, developed LFERs can be used to estimate properties of various PAHs, including unsubstituted and methylated forms with possibly up to five aromatic rings. The developed LFERs give an insight into how structural characteristics influence physicochemical properties. Results showed that $S_{w,L}$ and $P_{v,L}$ decrease with the number of methyl substituents, while K_{ow} increases. No relation was evident between H_c and the number of substituents. It was determined that GC retention data is not applicable to the estimation of physicochemical properties involving liquid phases only, i.e., $S_{w,L}$, and K_{ow}. GC column hydrophobicity did not have an apparent effect on the accuracy of $P_{v,L}$ estimates for methylated naphthalenes. The low $S_{w,L}$ and high K_{ow} values for highly methylated naphthalenes suggest that these compounds occur at low concentrations in water and have a high bioaccumulation potential. The EPIWIN software was found useful in providing order-of-magnitude predictions of physicochemical properties in the absence of experimental data. The next logical step in this research should be the evaluation of the validity of the LFERs for larger unsubstituted and alkylated PAHs.

Validation should involve comparison with literature values, comparison with estimates of the Abraham equation (Abraham et al., 2005), and randomization tests.

Chapter III discussed measurements of extant kinetic parameters describing degradation of individual PAHs by *Sphingomonas paucimobilis* strain EPA505. The bacterium rapidly degraded all 20 PAHs tested. The ability of strain EPA505 to metabolize a wide range of PAHs may be indicative of loose specificity of initial dioxygenases or related to the existence of glutathione-*S*-transferase activity. Of the 22 PAHs tested, only 9 supported bacterial growth while the rest were degraded cometabolically. The potency of strain EPA505 and its ubiquity in PAH-contaminated environments demonstrates the need to fully delineate its PAH catabolic pathways and better understand its ecological role. The Monod or Andrews model successfully simulated the experimental kinetic data. The following parameters were generated for each PAH: the maximal specific uptake rate, q_{max}, the affinity coefficient, K_S, the specific affinity, q_{max}/K_S, and the difference in the net absorbance at 450 nm, Δ(net A_{450}). The significant variability in the observed kinetic and growth parameters is indicative of the influence of substrate chemical structure on PAH biodegradability. Generated kinetic and growth parameters are essential for modeling biodegradability of simple PAH mixtures by strain EPA505 and as consistent training sets for the development of quantitative structure-biodegradability relationships (QSBRs). Continuation of this research should involve the following steps: (i) quantification of biodegradability of larger PAHs using dispersants or analytical techniques that can accurate determine low liquid-phase concentrations; (ii) comparison between the characteristic time of biosorption to the characteristic time of biodegradation and evaluation of the validity of the instantaneous-biosorption assumption; (iii) measurement of the Andrews inhibition coefficients using higher initial concentrations; (iv) identification of the major metabolites in PAH biodegradation by strain EPA505; and (v) measurement of kinetic parameters for microbial consortia from PAH-contaminated soils.

Chapter IV focused on the development of QSBRs for each of the kinetic and growth parameters from Chapter III. Statistical analysis and validation testing confirmed

the explanatory and predictive power of the QSBRs. The genetic function approximation (GFA) algorithm was particularly useful in creating valid models and revealing important molecular descriptors without requiring descriptor pre-selection. Molecular descriptors related to spatial and topological molecular features were essential in explaining biodegradation kinetics. A wealth of evidence was presented suggesting membrane binding-and-transport as the rate-determining step in PAH biodegradation by strain EPA505. It included: the presence and explanatory importance of spatial descriptors related to binding and transport; the correlation of q_{max} with the theoretical transmembrane flux, J_{max}; the absence of electronic descriptors related to reactivity from the QSBRs; the similarity between the components of the theoretical free energy upon binding, ΔG_{bind}, with the descriptors present in the QSBRs; and the signs of the coefficients of the Abraham solvation equation for $K_{S,}$ which were consistent with the hypothesis of transport to a lipid-like phase. The kinetic experiment with azide indicated that the purported rate-limiting transport mechanism can be either simple or facilitated diffusion depending on the PAH. Chapter IV demonstrated the value of QSBR not only as a predictive tool, but also as a method to understand the basic properties and processes that govern biodegradation at the molecular level. Further investigation is needed to validate the hypothesis of the rate-determining process. Investigation should include kinetic experiments with whole cells, cell extracts, and permeabilized cells, and comparison of the kinetics from the different systems. Finally, the applicability of QSBRs should be tested for PAH biodegradation by mixed cultures.

Chapter V focused on the kinetics of PAH mixture biodegradation by strain EPA505. Degradation of 2MPHE, FLA, and PYR in their binary and ternary mixtures occurred simultaneously without the evidence of diauxic effects. Extant kinetics observed in the binary and ternary mixtures were generally slower than those observed for the individual compounds, suggesting the presence of antagonistic interactions. Among different interaction models, the pure competitive interaction model with mutual substrate exclusivity most adequately simulated mixture kinetics. It was shown that competitive interactions may not always be detectable at low percent inhibition, $I_{\%}$,

values; therefore, it is suggested that selection of test compounds and their initial concentrations be such as to increase the degree of anticipated interactions as quantified by $I_{\%}$. Occurrence of competitive interactions suggested that transformation kinetics were determined by a common kinetic mechanism, possibly membrane binding or transport, as proposed in Chapter IV. Mutual substrate exclusivity implied that tested PAHs behaved as alternative ligands to a common binding site. Competitive interactions are consistent with the hypothesis that competitive metabolism is common among PAH-degrading microorganisms. Additional testing of homologous and heterologous PAH mixtures is required for verification of the hypothesis. Testing should also include mixed microbial cultures.

The contribution of this research is multifaceted. Findings such as physicochemical property values can be directly used in the risk assessment/management methodology. Values of biokinetic coefficients can be directly used in modeling degradation of wastes containing single PAHs or simple PAH mixtures. They can also provide indications of relative degradation rates that are likely to be observed in the environment or engineered systems. The greatest contribution of this research is believed to be the development of models describing properties and behavior of PAHs on a quantitative and mechanistic basis. The approach followed in this research can serve as a template for the investigation of relevant processes, e.g., toxicokinetics, and the characterization of other complex mixtures of environmental importance.

REFERENCES

Abraham, M.H., 1993. Scales of solute hydrogen-bonding: Their construction and application to physicochemical and biochemical processes. Chem. Soc. Rev. 22, 73 – 83.

Abraham, M.H., Ibrahim, A., Zissimos, A.M., 2004. Determination of sets of solute descriptors from chromatographic measurements. J. Chromatogr. A, 1037, 29-47.

Abraham, M.H., Autenrieth, R., Dimitriou-Christidis, P., 2005. The estimation of physicochemical properties of methyl and other alkyl naphthalenes. J. Environ. Monit. 7, 445-449.

Accelrys Inc., 2004. Cerius^2 Modeling Environment, Release 4.9. Accelrys Inc., San Diego. Available from: <http://www.accelrys.com/>.

Akaike, H., 1973, Information theory and an extension of the maximum likelihood principle. In: Fitting Models to Biological Data Using Linear and Nonlinear Regression. A Practical Guide to Curve Fitting. GraphPad Software Inc., San Diego. Available from: <http://www.graphpad.com/manuals/prism4/RegressionBook.pdf>.

Alexander, M., Lustigman, B.K., 1966. Effect of chemical structure on microbial degradation of substituted benzenes. J. Agric. Food Chem. 14, 410-413.

Allamandola, L.J., Sandford, S.A., Wopenka, B., 1987. Interstellar polycyclic aromatic hydrocarbons and carbon in interplanetary dust particles and meteorites. Science 237, 56–59.

Andrews, J.F., 1968. A mathematical model for the continuous culture of microorganisms utilizing inhibitory substrates. Biotechnol. Bioeng. 10, 707-723.

Aronson, D., Citra, M., Shuler, K., Printup, H., Howard, P.H., 1998. Aerobic Biodegradation of Organic Chemicals in Environmental Media: A Summary of Field and Laboratory Studies. Environmental Science Center, Syracuse Research Corporation. Available from: <http://www.syrres.com/pdfs/AERBIO.pdf>.

Asante-Appiah, E., Chan, W.-C., 1996. Analysis of the interactions between an enzyme and multiple inhibitors using combination plots. Biochem. J. 320, 17-26.

Atlas, R.M., 1995. Bioremediation of petroleum pollutants. Int. Biodeter. Biodegr. 35, 317-327.

ATSDR (Agency for Toxic Substances and Disease Registry), 1994. HAZDAT Database. Available from: <http://www.atsdr.cdc.gov/hazdat.html>.

ATSDR (Agency for Toxic Substances and Disease Registry), 1995. Toxicological Profile for Polycyclic Aromatic Hydrocarbons. U.S. Department of Health and Human Services. Available from: <http://www.atsdr.cdc.gov/toxprofiles/tp69.pdf>.

ATSDR (Agency for Toxic Substances and Disease Registry), 1997. ToxFAQs for Wood Creosote, Coal Tar Creosote, Coal Tar, Coal Tar Pitch, and Coal Tar Pitch Volatiles. U.S. Department of Health and Human Services. Available from: <http://www.atsdr.cdc.gov/tfacts85.html>.

ATSDR (Agency for Toxic Substances and Disease Registry), 2003. 2003 CERCLA Priority List of Hazardous Substances. U.S. Department of Health and Human Services. Available from: <http://www.atsdr.cdc.gov/clist.html>.

Barkay, T., Navon-Venezia, S., Ron, E.Z., Rosenberg, E., 1999. Enhancement of solubilization and biodegradation of polyaromatic hydrocarbons by the bioemulsifier Alasan. Appl. Environ. Microbiol. 65, 2697-2702.

Bateman, J.N., Speer, B., Feduik, L., Hartline, R.A., 1986. Naphthalene association and uptake in *Pseudomonas putida*. J. Bacteriol. 166, 155-161.

Becker, O.M., Yaakov, L., Ravitz, O., 2000. Flexibility, conformation spaces, and bioactivity. J. Phys. Chem. 104, 2123-2135.

Bernstein, M.P., Dworkin, J.P., Sandford, S.A., Allamandola, L.J., 2002. Ultraviolet irradiation of the polycyclic aromatic hydrocarbon (PAH) naphthalene in H_2O. Implications for meteorites and biogenesis. Adv. Space Res. 30, 1501-1508.

Bjørstedth, A., 1983. Handbook of Polycyclic Aromatic Hydrocarbons. Marcel Dekker Inc., New York, NY.

Bradford, M.M, 1976. A rapid and sensitive method for the quantitation of microgram quantities of protein using the principle of protein-dye binding. Anal. Biochem. 72, 248–254.

Braga, R.S., Barone, P.M.V.B., Galvao, D.S., 2000. Identifying carcinogenic activity of methylated and non-methylated polycyclic aromatic hydrocarbons (PAHs) through electronic and topological indices. Braz. J. Phys. 30, 560-568.

Bressler, D.C., Gray, M.R., 2003. Transport and reaction process in bioremediation of organic contaminants. 1: Review of bacterial degradation and transport. International Journal of Chemical Reactor Engineering 1, Review R3. Available from: <http://www.bepress.com/ijcre/vol1/R3>.

Bugg, T., Foght, J.M., Pickard, M.A., Gray, M.R., 2000. Uptake and active efflux of polycyclic aromatic hydrocarbons by *Pseudomonas fluorescens* LP6a. Appl. Environ. Microbiol. 66, 5387-5392.

Bundy, J.G., Durham, D.G., Paton, G.I., Campbell, C.D., 2000. Investigating the specificity of regulators of degradation of hydrocarbons and hydrocarbon-based compounds using structure-activity relationships. Biodegradation 11, 37-47.

Button, D.K., 1985. Kinetics of nutrient-limited transport and microbial growth. Microbiol. Rev. 49, 270-297.

Button, D.K., 1991. Biochemical basis for whole-cell uptake kinetics: Specific affinity, oligotrophic capacity, and the meaning of the Michaelis constant. Appl. Environ. Microbiol. 57, 2033-2038.

Carotti, A., Raguseo, C., Klein, T.E., Langridge, R., Hansch, C., 1988. QSAR analysis of the subtilisin hydrolysis of x-phenyl hippurates. II. A study of subtilisin BPN'. Chem.-Biol. Interact. 67, 171-184.

Coates, J.D., Woodward, J., Allen, J., Philp, P., Lovley, D.R., 1997. Anaerobic degradation of polycyclic aromatic hydrocarbons and alkanes in petroleum-contaminated marine harbor sediments. Appl. Environ. Microbiol. 63, 3589-3593.

Compadre, C.M., Hansch, C., Klein, T.E., Langridge, R., 1990. The structure-activity relationship of the papain hydrolysis of *n*-benzoylglycine esters. Biochim. Biophys. Acta 1038, 158-163.

Dabestani, R., Ivanov, I.N., 1999. A compilation of physical, spectroscopic, and photophysical properties of polycyclic aromatic hydrocarbons. Photochem. Photobiol. 70, 10-34.

Damborsky, J., Schultz, T.W., 1997. Comparison of the QSAR models for toxicity and biodegradability of anilines and phenols. Chemosphere 34, 429-446.

Daubert, T.E., Danner, R.P., 1989. Physical and Thermodynamic Properties of Pure Chemicals: Data Compilation. Hemisphere Publishing Co., New York, NY.

Daugulis, A.J., McCracken, C.M., 2003. Microbial degradation of high and low molecular weight polyaromatic hydrocarbons in a two-phase partitioning bioreactor by two strains of *Sphingomonas* sp. Biotechnol. Lett. 25, 1441-1444.

Dewar, M.J.S., Thiel, W., 1977. Ground states of molecules. 38: The MNDO method: Approximations and parameters. J. Am. Chem. Soc. 99, 4899-4907.

van den Dool, H., Kratz, P.D., 1963. A generalization of the retention index system including linear temperature programmed gas-liquid partition chromatography. J. Chromatogr. 2, 463-471.

Dunnivant, F.M., Elzerman, A.W., Jurs, P.C., Hasan, M.N., 1992. Quantitative structure-property relationships for aqueous solubilities and Henry's law constants of polychlorinated biphenyls. Environ. Sci. Technol. 26, 1567-1573.

Dutta, T.K., Selifonov, S.A., Gunsalus, I.C., 1998. Oxidation of methyl-substituted naphthalenes: Pathways in a versatile *Sphingomonas paucimobilis* strain. Appl. Environ. Microbiol. 64, 1884-1889.

Eisenthal, R., and Danson, M.J. (Eds.), 1992. Enzyme Assay: A Practical Approach. IRL Press, Oxford, UK.

Ekins, S., Bravi, G., Ring, B.J., Gillespie, T.A., Gillespie, J.S., Vandenbranden, M., Wrighton, S.A., Wikel, J.H., 1999. Three-dimensional quantitative structure

activity relationship analyses of substrates for CYP2B6. J. Pharmacol. Exp. Ther. 288, 21-29.

Ellis, T.G., Barbeau, D.S., Smets,B.F., Grady, C.P.L.Jr., 1996. Respirometric technique for determination of extant kinetic parameters describing biodegradation. Water Environ. Res. 68, 917-926.

Eriksson, L., Jaworska, J., Worth, A.P., Cronin, M.T., McDowell, R.M., Gramatica, P., 2003. Methods for reliability and uncertainty assessment and for applicability evaluations of classification- and regression-based QSARs. Environ. Health Persp. 111, 1361-1375.

Ferreira, M.M.C., 2001. Polycyclic aromatic hydrocarbons: A QSPR study. Chemosphere 44, 125-146.

Fetzer, J.C., 2000. Large (C >= 24) Polycyclic Aromatic Hydrocarbons: Chemistry and Analysis. John Wiley & Sons, New York, NY.

Finizio, A., Vighi, M., Sandroni, D., 1997. Determination of *n*-octanol/water partition coefficient (K_{ow}) of pesticide: Critical review and comparison of methods. Chemosphere 34, 131-161.

Fischer, R.G., Wittlinger, R., Ballschmiter, K., 1992. Retention-index based vapor pressure estimation for polychlorobiphenyl (PCB) by gas chromatography. Fresenius J. Anal. Chem. 342, 421-425.

Friedman, J.H., 1991. Multivariate adaptive regression splines (with discussion). Ann. Statistics 19, 1-141.

Fukui, K., 1997. Frontier Orbitals and Reaction Paths: Selected Papers of Kenichi Fukui. World Scientific, Singapore, Singapore.

Gibson, D.T., Parales, R.E., 2000. Review: Aromatic hydrocarbon dioxygenases in environmental biotechnology. Curr. Opin. Biotech. 11, 236-243.

Govers H., Ruepert C., Aiking H., 1984. Quantitative structure-activity relationships for polycyclic aromatic hydrocarbons: Correlation between molecular connectivity, physico-chemical properties, bioconcentration and toxicity in *Daphnia pulex*. Chemosphere 13, 227-236.

Grady, C.P.L.Jr., Smets, B.F., Barbeau, D.S., 1996. Variability in kinetic parameter estimates: A review of possible causes and a proposed terminology. Water Res. 30, 742-748.

Guha, S., Peters, C.A., Jaffé, P.R., 1999. Multisubstrate biodegradation kinetics of naphthalene, phenanthrene, and pyrene mixtures. Biotechnol. Bioeng. 65, 491-499.

Hall, L.H., Kier, L.B., 1991. The molecular connectivity chi indexes and kappa shape indexes in structure-property modeling. In: Cerius^2 Modeling Environment, Release 4.9. Accelrys Inc., San Diego. Available from: <http://www.accelrys.com/>.

Hansch, C., Fujita, T., 1964. ρ-σ-π Analysis: A method for the correlation of biological activity and chemical structure. J. Am. Chem. Soc. 86,1616-1626.

Hansch, C., Leo, A., 1995. Exploring QSAR: Fundamentals and Applications in Chemistry and Biology. ACS Professional Reference Book, American Chemical Society, Washington, DC.

Harvey, R.G., 1991. Polycyclic Aromatic Hydrocarbons: Chemistry and Carcinogenicity. Cambridge University Press, Cambridge, UK.

Harvey, R.G., 1997. Polycyclic Aromatic Hydrocarbons. Wiley VCH, New York, NY.

Healy, F.P., 1980. Slope of the Monod equation as an indicator of an advantage in nutrient competition. Microbial Ecol. 5, 281-286.

Herbes, S.E., Schwall L.R., 1978. Microbial transformations of PAHs in pristine and petroleum contaminated sediments. Appl. Environ. Microbiol. 35, 306-316.

Ho, Y., Jackson, M., Yang, Y., Mueller, J.G., Pritchard, P.H., 2000. Characterization of fluoranthene- and pyrene-degrading bacteria isolated from PAH-contaminated soils and sediments. J. Ind. Microbiol. Biot. 24, 100-112.

Hodgeson, J.W., Bashe, W.J., Baker, T.V., 1990. Method 550.1: Determination of Polycyclic Aromatic Hydrocarbons in Drinking Water by Liquid-Solid Extraction and HPLC with Coupled Ultraviolet and Fluorescence Detection. U.S. EPA, Office of Research and Development. Available from:

<http://www.dec.state.ak.us/eh/docs/lab/dw/Chem/organics/550.1.pdf>.

Hong, H., Tong, W., Fang, H., Shi, L., Xie, Q., Wu, J., Perkins, R., Walker, J.D., Branham, W., Sheehan, D.M., 2002. Prediction of estrogen receptor binding for 58,000 chemicals using an integrated system of a tree-based model with structural alerts. Environ. Health Persp. 110, 29-36.

Howard, P.H., Meylan, W.M., 1997. Handbook of Physical Properties of Organic Chemicals. Lewis Publishers, Boca Raton, FL.

IARC (International Agency for Research on Cancer), 1987. IARC Monographs on the Evaluation of Carcinogenic Risks to Humans: Overall Evaluations of Carcinogenicity. Supplement 7. IARC, Lyon, France.

Jerina, D.M., Van Balderen, P.J., Yagi, H., Gibson, D.T., Mahadevan, V., Neese, A.S., Koreeda, M., Sharma N.D., Boyd, D.R., 1984. Synthesis and absolute configuration of the bacterial cis - 1,2 and cis - 10,11 dihydrodiol metabolites of benz[a]anthracene formed by a strain of *Beijerinkia*. J. Org. Chem. 49, 3621–3628.

Jinno Lab, 1996. Polycyclic Aromatic Hydrocarbons (PAHs): Data Base in Alphabetical Order. Available from: <http://chrom.tutms.tut.ac.jp/JINNO/DATABASE/00alphabet.html>.

Johnsen, A.R., Hausner, M., Schell, A., Wuertz, S., 2000. Evaluation of fluorescently labeled lectins for noninvasive localization of extracellular polymeric substances in *Sphingomonas* biofilms. Appl. Environ. Microbiol. 66, 3487-3491.

Johnsen, A.R., Bendixen, K., Karlson, U., 2002. Detection of microbial growth on polycyclic aromatic hydrocarbons in microtiter plates by using the respiration indicator WST-1. Appl. Environ. Microbiol. 68, 2683-2689.

Johnsen, A.R., 2004. Protocol: Microplate Test for Growth on PAHs. Available from: <http://www2.dmu.dk/1_Viden/2_Miljoe-tilstand/3_jord/4_microtitermethods/PAHmicrotitre04_02_22.pdf>.

Kaliszan, R., 1987. Quantitative Structure-Chromatographic Retention Relationships. John Wiley & Sons, New York, NY.

Karcher, W., Fordham, R., Dubois, J.J., Glaude, P.G.J.M., Ligthart, J.A.M., 1985. Spectral Atlas of Polycyclic Aromatic Compounds: Including Data on Occurrence and Biological Activity. D. Reidel Pub. Co. for the Commission of the European Communities, Dordrecht, The Netherlands.

Karelson, M., Lobanov, V.S., Katritzky, A.R., 1996. Quantum-chemical descriptors in QSAR/QSPR studies. Chem. Rev. 96, 1027–1043.

Karickhoff, S.W., Brown, D.S., 1979. Determination of Octanol/Water Distribution Coefficients, Water Solubilities, and Sediment/Water Partition Coefficients for Hydrophobic Organic Pollutants. U.S. EPA Report No. EPA-660/4-79/032.

Kasai, Y., Inoue, J., Harayama, S., 2001. The TOL plasmid pWW0 *xylN* gene product from *Pseudomonas putida* is involved in m-xylene uptake. J. Bacteriol. 183, 6662-6666.

Keleti, T., Fajszi, Cs., 1972. The system of double inhibitors. Math. Biosci. 12, 197-215.

Klečka, G.M. Maier, W.J., 1988. Kinetics of microbial growth on mixtures of pentachlorophenol and chlorinated aromatic compounds. Biotechnol. Bioeng. 31, 328-335.

Knightes, C.D., 2000. Mechanisms governing sole-substrate and multi-substrate biodegradation kinetics of polycyclic aromatic hydrocarbons. Doctoral Dissertation, Princeton University, Princeton, NJ.

Knightes, C.D., Peters, C.A., 2000. Statistical analysis of nonlinear parameter estimation for Monod biodegradation kinetics using bivariate data. Biotechnol. Bioeng. 69, 160-170.

Koutek, B., Cvačka, J., Streinz, L., Vrkočová, P., Doubský, J., Šimonová, H., Feltl, L., Svoboda, V., 2001. Comparison of methods employing gas chromatography retention data to determine vapour pressures at 298 K. J. Chromatogr. A 923, 137-152.

Kovárová-Kovar, K., Egli, T., 1998. Growth kinetics of suspended microbial cells: From single-substrate-controlled growth to mixed-substrate kinetics. Microbiol. Mol. Biol. Rev. 62, 646-666.

Kurz, J., Ballschmiter, K., 1999. Vapour pressures, aqueous solubilities, Henry's law constants, partition coefficients between gas/water (K_{gw}), *n*-octanol/water (K_{ow}) and gas/*n*-octanol (K_{go}) of 106 polychlorinated diphenyl ethers (PCDE). Chemosphere 38, 573-586.

Kvålseth, T.O., 1985. Cautionary note about R^2. Am. Stat. 39, 279-285.

LaGrega, M.D., Buckingham P.L., Evans, J.C., 2001. Hazardous Waste Management, McGraw Hill, New York, NY.

Lantz, S.E., Montgomery, M.T.,Schultz, W.W., Pritchard, P.H., Spargo, B.J., Mueller, J.G., 1997. Constituents of an organic wood preservative that inhibit the fluoranthene-degrading activity of *Sphingomonas paucimobilis* strain EPA505. Environ. Sci. Technol. 31, 3573-3580.

Leahy, J.G., Colwell, R.R., 1990. Microbial degradation of hydrocarbons in the environment. Microbiol. Rev. 54, 305-315.

Ledesma, E.B., Wornat, M.J., 2000. QSRR prediction of chromatographic retention of ethynyl-substituted PAH from semiempirically computed solute descriptors. Anal. Chem. 72, 5437-5443.

Lewis, D.F.V., Ioannides, C., Parke, D.V., 1995. A quantitative structure-activity relationship study on a series of ten *para*-substituted toluenes binding to cytochrome P4502B4 (CYP2B4) and also their hydroxylation rates. Biochem. Pharm. 50, 619-625.

Lewis, D.F.V., Eddershaw, P.J., Dickins, M., Tarbit, M.H., Gordfard, P.S., 1998. Structural determinants of cytochrome P450 substrate specificity, binding affinity and catalytic rate. Chem. Biol. Interact. 115, 175-199.

de Lima Ribeiro, F.A., Ferreira, M.M.C., 2003. QSPR models of boiling point, octanol-water partition coefficient and retention time index of polycyclic aromatic hydrocarbons. J. Mol. Struct. 663, 109-126.

Lloyd-Jones, G., Lau, P.C.K., 1997. Glutathione S-transferase-encoding gene as a potential probe for environmental bacterial isolates capable of degrading polycyclic aromatic hydrocarbons. Appl. Environ. Microbiol. 63, 3286-3290.

Lu, G.H., Wang, C., Bao, G.Z., 2003. Quantitative structure-biodegradation relationship study for biodegradation rates of substituted benzenes by river bacteria. Environ. Toxicol. Chem. 22, 272-275.

Luning Prak, D.J., Pritchard, P.H., 2002. Degradation of polycyclic aromatic hydrocarbons dissolved in Tween 80 surfactant solutions by *Sphingomonas paucimobilis* EPA 505. Can. J. Microbiol. 48, 151-158.

Luthy, R.G., Dzombak, D.A., Peters, C.A., Roy, S.B., Ramaswami, A., Nakles, D.V., Nott, B.R., 1994. Remediating tar-contaminated soils at manufactured gas plant sites: Technological challenges. Environ. Sci. Technol. 28, 266A-276A.

Mackay, D., Shiu, W.Y., Ma, K.C., 1992. Illustrated Handbook of Physical-Chemical Properties and Environmental Fate for Organic Chemicals. Lewis Publishers, Chelsea, MI.

Mallard, W. G., Linstrom, P. J., 2000. NIST Chemistry WebBook, NIST Standard Reference Database 69. National Institute of Standards and Technology, Gaithersburg. Available from: <http://webbook.nist.gov>.

Maple, J.R., Hwang, M.-J., Stockfisch, T.P., Dinur, U., Waldman, M., Ewig, C.S., Hagler, A.T., 1994. Derivation of class II force fields: 1. Methodology and quantum force field for the alkyl functional group and alkane molecules. J. Comput. Chem. 15, 162-182.

Marino, D.J.G., Peruzzo, P.J., Castro, E.A., Toropov, A.A., 2002. QSAR carcinogenic study of methylated polycyclic aromatic hydrocarbons based on topological descriptors derived from distance matrices and correlation weights of local graph invariants. Internet Electronic Journal of Molecular Design 1, 115-133. Available from: <http://www.biochempress.com>.

Martinez-Irujo, J.J., Villahermosa, M.L., Mercapide, J., Cabodevilla, J.F., Santiago, E., 1998. Analysis of the combined effect of two linear inhibitors on a single enzyme. Biochem. J. 329, 689-698.

Meylan, W.M., Howard, P.H., 1991. Bond contribution method for estimating Henry's law constants. Environ. Toxicol. Chem. 10, 1283-1293.

Meylan, W.M., Howard, P.H., 1994. Validation of Water Solubility Estimation Methods Using Log K_{ow} for Application in PCGEMS & EPI. Prepared for U.S. Environmental Protection Agency; Syracuse Research Corporation, Environmental Science Center, Syracuse, NY.

Meylan, W.M., Howard, P.H., 1995. Atom/fragment contribution method for estimating octanol-water partition coefficients. J. Pharm. Sci. 84, 83-92.

Meylan, W.M., Howard, P.H., Boethling, R.S., 1996. Improved method for estimating water solubility from octanol/water partition coefficient. Environ. Toxicol. Chem. 15, 100-106.

Miyata, N., Iwahori, K., Foght, J.M., Gray, M.R., 2004. Saturable, energy-dependent uptake of phenanthrene in aqueous phase by *Mycobacterium* sp. strain RJGII-135. Appl. Environ. Microbiol. 70, 363-369.

Moss, G.P., Dearden, J.C., Patel, H., Cronin, M.T.D., 2002. Review: Quantitative structure–permeability relationships (QSPRs) for percutaneous absorption. Toxicol. In Vitro 16, 299-317.

Motulsky, H.J., Christopoulos, A., 2003. Fitting Models to Biological Data Using Linear and Nonlinear Regression: A Practical Guide to Curve Fitting. GraphPad Software Inc., San Diego. Available from: <http://www.graphpad.com/manuals/prism4/RegressionBook.pdf>.

Mueller, J.G., Chapman, P.J., Pritchard, P.H., 1989. Action of a fluoranthene-utilizing bacterial community on polycyclic aromatic hydrocarbon components of creosote. Appl. Environ. Microbiol. 55, 3085-3090.

Mueller, J.G., Chapman, P.J., Blattmann, B.O., Pritchard, P.H., 1990. Isolation and characterization of a fluoranthene-utilizing strain of *Pseudomonas paucimobilis*. Appl. Environ. Microbiol. 56, 1079-1086.

Mueller, J.G., Devereux, R., Santavy, D.L., Lantz, S.E., Willis, S.G., Pritchard, P.H., 1997. Phylogenetic and physiological comparisons of PAH-degrading bacteria from geographically diverse soils. Anton. Leeuw. Int. J. G. 71, 329-343.

Nikaido, H. 2003. Molecular basis of bacterial outer membrane permeability revisited. Microbiol. Mol. Biol. Rev. 67, 593-656.

NRC (National Research Council), 1983. Risk Assessment in the Federal Government: Managing the Process. National Academy Press, Washington, DC.

NRC (National Research Council), 2003. Oil in the Sea III: Inputs, Fates, and Effects. National Academy Press, Washington, DC.

Oh, Y.-S., Shareefdeen, Z., Baltzis, B.C., Bartha, R., 1994. Interactions between benzene, toluene, and p-xylene (BTX) during their biodegradation. Biotechnol. Bioeng. 44, 533-538.

Ohki, S., Spangler, R.A., 2005. Passive and facilitated diffusion. In: Yeagle P.L. (Ed.). The Structure of Biological Membranes. CRC Press, Boca Raton, FL.

Okey, R.W., Stensel, H.D., 1996. A QSAR biodegradability model: A QSBR. Water Res. 30, 2206-2214.

Park, R.E., 1966. Estimation with heteroscedastic error terms. Econometrica 34, 888-896.

Peijnenburg, W.J.G.M., Damborsky, J. (Eds.) 1996. Biodegradability Prediction: Proceedings of the NATO Advanced Research Workshop on QSAR Biodegradation II - QSARs for Biotransformation and Biodegradation, Luhacovice, Czech Republic, May 2-3 1996. Kluwer Academic Publishers, Dordrecht, The Netherlands.

Pinyakong, O., Habe, H., Kouzuma, A., Nojiri, H., Yamane, H., Omori, T., 2004 Isolation and characterization of genes encoding polycyclic aromatic hydrocarbon dioxygenase from acenaphthene and acenaphthylene degrading *Sphingomonas* sp. strain A4. FEMS Microbiol. Lett. 238, 297-305.

Pitter, P., 1985. Correlation of microbial degradation rates with the chemical structure. Acta Hydrochim. Hydrobiol. 13, 453-460.

Polgar, L., 1992. Prolyl endopeptidase catalysis: A physical rather than a chemical step is rate-limiting. Biochem J. 283, 647-648.

Pople, J.A., Segal, G.A., 1966. CNDO, 2.Version, C. J.Chem.Phys. 44, 3289-3296.

Prausnitz, J.M., Lichtenthaler, R.N., de Azevedo, E.G., 1986. Molecular Thermodynamics of Fluid-Phase Equilibria. Prentice Hall, Inc., Englewood Cliffs, NJ.

Reardon, K.F., Mosteller, D.C., Bull Rogers, J.D., 2000. Biodegradation kinetics of benzene, toluene, and phenol as single and mixed substrates for *Pseudomonas putida* F1. Biotechnol. Bioeng. 69, 385-400.

Reardon, K.F., Mosteller, D.C., Bull Rogers, J.D., DuTeau, N.M., Kim, K.-H., 2002. Biodegradation kinetics of aromatic hydrocarbon mixtures by pure and mixed bacterial cultures. Environ. Health Persp. 110, 1005-1011.

Robinson, J.A., 1985. Determining microbial kinetic parameters using non-linear regression analysis: Advantages and limitations in microbial ecology. Adv. Microb. Ecol. 8, 61-114.

Rogers, D., Hopfinger, A. J., 1994. Application of genetic function approximation to quantitative structure-activity relationships and quantitative structure-property relationships. J. Chem. Inf. Comput. Sci., 34, 854-866.

Rohrbaugh, R.H. Jurs, P.C., 1987. Descriptions of molecular shape applied in studies of structure/activity and structure/property relationships. Anal. Chim. Acta 199, 99-109.

Romine, M.F., Fredrickson, J.K., Li, S.-M.W., 1999a. Induction of aromatic catabolic activity in *Sphingomonas aromaticivorans* strain F199. J. Ind. Microbiol. Biot. 23, 303–313.

Romine, M.F., Stillwell, L.C., Wong, K.-K., Thurston, S.J., Sisk, E.C., Sensen, C., Gaasterland, T., Fredrickson, J.K., Saffer, J.D., 1999b. Complete sequence of a 184-kilobase catabolic plasmid from *Sphingomonas aromaticivorans* F199. J. Bacteriol., 181, 1585-1602.

Saier, M.H.Jr., 2000. A functional-phylogenetic classification system for transmembrane solute transporters. Microbiol. Mol. Biol. Rev. 64, 354-411.

Segel, I.H., 1975. Enzyme Kinetics: Behavior and Analysis of Rapid Equilibrium and Steady State Enzyme Systems. Wiley, New York, NY.

Selassie, C.D., 2003. History of Quantitative Structure-Activity Relationships. In: Abraham, D.J. (Ed.). Burger's Medicinal Chemistry and Drug Discovery: Volume 1: Drug Discovery. Wiley, Hoboken, NJ.

Siddiqi, M.A., Yuan, Z., Honey, S.A., Kumar, S., Sikka, H.C., 2002. Metabolism of PAHs and methyl-substituted PAHs by *Sphingomonas paucimobilis* strain EPA 505. Polycycl. Aromat. Comp. 22, 621-630.

Sikkema, J., de Bont, J.A., Poolman, B. 1994. Interactions of cyclic hydrocarbons with biological membranes. J. Biol. Chem. 269, 8022-8028.

Smith, L.H., Kitanidis, P.K., McCarty, P.L., 1997. Numerical modeling and uncertainties in rate coefficients for methane utilization and TCE cometabolism by a methane-oxidizing mixed culture. Biotechnol. Bioeng. 53, 320-331.

Smith, L.H., McCarty, P.L., Kitanidis, P.K., 1998. Spreadsheet method for evaluation of biochemical reaction rate coefficients and their uncertainties by weighted nonlinear least-squares analysis of the integrated Monod equation. Appl. Environ. Microbiol. 64, 2044-2055.

Snow, N.H., 1996. Determination of free-energy relationships using gas chromatography. J. Chem. Educ. 73, 592-597.

SRC (Syracuse Research Corporation), 2005. PhysProp Database: SRC PhysProp Database. Available from: <http://esc.syrres.com/interkow/>.

SRI International, 1992. Directory of Chemical Producers: United States of America. SRI International, Menlo Park, CA.

Stanton, D.T., Jurs, P.C., 1990. Development and use of charged partial surface area structural descriptors in computer-assisted quantitative structure-property relationship studies. Anal. Chem. 62, 2323-2329.

Stein, W.D., 1967. The movement of molecules across cell membranes. In: Transport and Reaction Process in Bioremediation of Organic Contaminants: 1. Review of Bacterial Degradation and Transport. International Journal of Chemical Reactor Engineering 1, Review R3. Available from: <http://www.bepress.com/ijcre/vol1/R3>.

Stewart, J.J., 1989. Optimization of parameters for semi-empirical methods I-method. J. Comput. Chem. 10, 209-220.

Story, S.P., Parker, S.H., Kline, J.D., Tzeng, T.J., Mueller, J.G., Kline, E.L., 2000. Identification of four structural genes and two putative promoters necessary for utilization of naphthalene, phenanthrene, and fluoranthene by *Sphingomonas paucimobilis* var. EPA505. Gene 260, 155-169.

Story S.P., Parker, S.H., Hayasaka, S.S., Riley, M.B., Kline, E.L., 2001. Convergent and divergent points in catabolic pathways involved in utilization of fluoranthene, naphthalene, anthracene, and phenanthrene by *Sphingomonas paucimobilis* var. EPA505. J. Ind. Microbiol. Biot. 26, 369-382.

Story, S.P., Kline, E.L., Hughes, T.A., Riley, M.B., Hayasaka, S.S., 2004. Degradation of aromatic hydrocarbons by *Sphingomonas paucimobilis* strain EPA505. Arch. Environ. Contam. Toxicol. 47, 168-176.

Stringfellow, W.T., Aitken, M.D., 1995. Competitive metabolism of naphthalene, methylnaphthalenes, and fluorene by phenanthrene-degrading pseudomonads. Appl. Environ. Microbiol. 61, 357-362.

Stringfellow, W.T., Alvarez-Cohen, L., 1999. Evaluating the relationship between the sorption of PAHs to bacterial biomass and biodegradation. Water Res. 33, 2535-2544.

UMBBD (The University of Minnesota Biocatalysis/Biodegradation Database), 2005. Microbial Biocatalytic Reactions and Biodegradation Pathways Primarily for Xenobiotic, Chemical Compounds. Available from: <http://www.labmed.umn.edu/>.

U.S. EPA (Environmental Protection Agency), 2000. Deposition of Air Pollutants to the Great Waters. Third Report to the Congress. U.S. EPA Report No. EPA-453/R-00-005.

U.S. EPA (U.S. Environmental Protection Agency), SRC (Environmental Science Center), 2000. EPIWIN - Estimates Physical / Chemical Properties and Fate Based on Chemical Structure, version 3.10. Available from:

<http://www.epa.gov/opptintr/exposure/docs/EPISuitedl.htm>.

U.S. EPA (U.S. Environmental Protection Agency), 2005. IRIS Database for Risk Assessment. Available from: <http://www.epa.gov/iris/subst/>.

van Aarssen, B.G.K., Bastow, T.P., Alexander, R., Kagi R.I., 1999. Distributions of methylated naphthalenes in crude oils: Indicators of maturity, biodegradation and mixing. Org. Geochem. 30, 1213-1227.

Veith, G.D., Morris, R.T., 1978. A Rapid Method for Estimating LogP for Organic Chemicals. U.S. EPA Report No. EPA-600/3-78-049.

Veith, G.D., DeFoe, D.L., Bergstedt, B.V., 1979. Measuring and estimating the bioconcentration factors of chemicals in fish. J. Fish. Res. Board Can. 36, 1040-1048.

Wang, L.-H., Tsai, A.-L., Hsu, P.-Y., 2001. Substrate binding is the rate-limiting step in thromboxane synthase catalysis. J. Biol. Chem. 276, 14737–14743.

Wang, Y., Rawlings, M., Gibson, T.D., Labbé, D., Bergeron, H., Brousseau, R., Lau, P.C.K., 1995. Identification of a membrane protein and a truncated LysR-type regulator associated with the toluene degradation pathway in *Pseudomonas putida* F1. Mol. Gen. Genet. 246, 570-579.

Wang, Y.H., Wong, P.K., 2002. Mathematical relationships between vapor pressure, water solubility, Henry's law constant, *n*-octanol/water partition coefficient and gas chromatographic retention index of polychlorinated-dibenzo-dioxins. Water Res. 36, 350-355.

Weis, L.M, Rummel, A.M., Masten, S.J., Trosko, J.E., Upham, B.L., 1998. Bay or baylike regions of polycyclic aromatic hydrocarbons were potent inhibitors of gap junctional intercellular communication. Environ. Health Persp. 106, 17-22.

WHO (World Health Organization), 1998. Selected Non-heterocyclic Polycyclic Aromatic Hydrocarbons: Environmental Health Criteria, No. 202. World Health Organization Publications. Available from: <http://www.inchem.org/documents/ehc/ehc/ehc202.htm>.

Williams, A., 2003. Free-Energy Relationships in Organic and Bio-Organic Chemistry. The Royal Society of Chemistry, Cambridge, UK.

Willumsen, P.A., Arvin, E., 1999. Kinetics of surfactant-solubilized fluoranthene by *Sphingomonas paucimobilis*. Environ. Sci. Technol. 33, 2571-2578.

Wilson, A.S., Davis, C.D., Williams, D.P., Buckpitt, A.R., Pirmohamed, M., Park, B.K., 1996. Characterization of the toxic metabolite(s) of naphthalene. Toxicology 114, 233-242.

Winkler, D.A., Burden, F.R., 2004. Modelling blood–brain barrier partitioning using Bayesian neural nets. J. Mol. Graph. Model. 22, 499-505.

Wysocki, J., 2001. What drives a separation – the stationary phase or the mobile phase? LCGC 19, 1150-1159. Available from: <http://www.lcgcmag.com/lcgc/article/articleDetail.jsp?id=2674>.

Ye, D., Siddiqi, M.A., Maccubbin, A.E., Kumar, S., Sikka, H.C., 1996. Degradation of polynuclear aromatic hydrocarbons by *Sphingomonas paucimobilis*. Environ. Sci. Technol. 30, 136-142.

Yoon, H., Klinzing, G., Blanch, H.W., 1977. Competition for mixed substrates by microbial populations. Biotechnol. Bioeng. 19, 1193-1210.

Youngblood, W.W., Blumer, M., 1975. Polycyclic aromatic hydrocarbons in the environment: Homologous series in soils and recent marine sediments. Geochim. Cosmochim. Acta 39, 1303-1314.

Zhou, N.Y., Al-Dulayymi, J., Baird, M.S., Williams, P.A., 2002. Salicylate 5-hydroxylase from *Ralstonia* sp. strain U2: A monooxygenase with close relationships to and shared electron transport proteins with naphthalene dioxygenase. J. Bacteriol. 184, 1547-1555.

VITA

Name: Petros Dimitriou-Christidis

Address: Environmental Engineering Division
Department of Civil Engineering
WERC Room 205
Texas A&M University
College Station, Texas 77843-3136

E-mail Address: petrisdim@yahoo.com

Education: B.S., Environment, 1998
University of the Aegean

M.S., Environmental Engineering, 2000
University of California, Berkeley

Ph.D., Civil Engineering, 2005
Texas A&M University